EG&G Idaho, Inc.

(LTR)

Report No. LO-14-80-069

Date: June 19, 1980

RELEASED BY LOFT CDCS

USNRC - P394

INTERNAL TECHNICAL REPORT

Title: L2-6 FUEL PREPRESSURIZATION AND INITIAL CONDITIONS

Organization:

Author: J. D. Burtt

Checked By: M.L. Russell

Approved By: S.A. Naff

EG&G Idaho, Inc.

FORM EG&G-229
(Rev. 01-80)

LOFT TECHNICAL REPORT

Title	LTR No.
L2-6 Fuel Prepressurization and Initial Conditions	LO-14-80-069
Author: J. D. Burtt JDBurtt Performing Organization	Released By LOFT CDCS Date June 19, 1980
LOFT Review and Approval mcR L.A. Neff IFB Mgr. LEPD Acting Mgr.	Project System Engineer M.L. Russell

DISPOSITION OF RECOMMENDATIONS

Based upon the analysis presented in this document, the L2 Series Experiment Operating Specification will be revised to reflect the changes recommended herein.

RECOMMENDATIONS

To obtain the objectives of LOFT LOCE L2-6, the fuel pressurization should be changed from 2.4 MPa to 4.0 MPa. After LOCE L2-5 is conducted, an evaluation of the experimental data should be conducted to determine what power level and hardware conditions should be used in the L2-6 test to cause permanent cladding deformation.

1. INTRODUCTION

One of the major objectives of LOFT LOCE L2-6 is to study the system response to a large primary system rupture when fuel deformation occurs. The original test plan called for fuel which was prepressurized to a typical beginning-of-life pressure, 2.4 MPa, and initial test conditions identical to the conditions used in LOCE L2-3.[1] Based upon L2-3 data, analysis indicates that for these conditions, no fuel deformation can be expected.

2. ANALYSIS

Evaluation of the L2-3 data, substituting prepressurized fuel for the nonpressurized actually used, showed that no fuel deformation would have occurred. Appendix A documents this analysis. As this analysis was equivalent to the previous plans for L2-6, further studies were initiated to determine the conditions which would result in permanent cladding deformation.

A parallel analysis was performed for LOCE L2-5 to determine what could be expected from this test based upon what was learned from L2-3. L2-5 differs from L2-3 in that it assumes a loss of offsite power resulting in ECC delay and primary pump coastdown. This revised L2-5 analysis (Appendix B) showed no early rewet in the hottest portion of the core. As this would make L2-5 a more severe core transient, a preliminary recommendation for L2-6 would be to use L2-5 test conditions and assumptions. (This is, of course, dependent upon the actual test results from L2-5).

Using these L2-5 conditions as the base case starting point (case 1) a parametric study which varied initial fuel prepressurization and power level was performed. The 6 calculations and their variations are listed in Table 1.

TABLE 1. L2-6 ANALYSIS MATRIX*

Case	Fuel Prepressurization	Power Level
1	0.1 MPa	39.4 kW/m
2	2.4 MPa	39.4 kW/m
3	4.0 MPa	39.4 kW/m
4	0.1 MPa	52.4 kW/m
5	2.4 MPa	52.4 kW/m
6	4.0 MPa	52.4 kW/m

* All other initial conditions held constant at L2-5 values.

Appendix C documents this study. As discussed in depth in the appendix, there is little chance of deformation for the 0.1 or 2.4 MPa pressurization level either power level. The 4.0 MPa prepressurization, which represents typical end-of-life pressure levels, showed different results. At the 39.4 kW/m power level (case 3) the hoop strain on the cladding showed the beginnings of plastic deformation (creep or ballooning). As the codes are generally conservative these conditions may not, in fact, cause the deformation required to meet the L2-6 objectives. (Again, L2-5 test data are necessary to determine this conclusion more accurately.) Case 6 indicates that at the higher values of both power and pressurization levels, the fuel should deform enough to meet the goals of the test.

3. CONCLUSIONS

In order to meet the objectives of L2-6 the experiment should be performed with an initial fuel prepressurization of 4.0 MPa. After LOCE L2-5 is conducted, experimental data will be available which will permit establishing the linear heat generation rate and hardware conditions that will ensure permanent cladding deformation.

4. REFERENCES

1. P. A. Harris, T. K. Samuels, H. C. Welland, LOFT Experiment Operating Specification - Power Ascension Test Series L2, Revision 2, July 1978.

APPENDIX A

ESTIMATES ON CONDITIONS LEADING TO CLADDING BURST IN THE LOFT FUEL

EG&G Idaho

INTEROFFICE CORRESPONDENCE

date July 30, 1979

to S. A. Naff

from S. T. Kelppe *Seppo Kelppe*

subject ESTIMATES ON CONDITIONS LEADING TO CLADDING BURST IN THE LOFT FUEL - STK-1-79

Ref: D. L. Hagrman, "Code Development and Analysis Program/ Cladding Mechanical Limits (CMLIMT)," CDAP-TR-056, May 1979

During a light water reactor (LWR) loss-of-coolant accident (LOCA) or Loss-of-Fluid Test (LOFT) loss-of-coolant experiment (LOCE) a potential exists for the cladding to balloon and fail by bursting for pressurized fuel rods. Due to elevated cladding temperatures, the plasticity limit of the cladding is lowered and the rod internal gas pressure may exceed the external pressure by an amount sufficient enough to cause outward plastic flow of the cladding. The problem is especially important for high rod pressurization. In the following letter, a rough estimate is given for the cladding temperature and pressure conditions required for burst failure of a pressurized water reactor (PWR) (15 X 15) fuel.

Most of the existing rod burst test data correlate the average hoop stresses (pressures) or average tube strains at burst to the applied temperatures and usually a large scatter is observed. On the other hand, if the tangential component of the true local stress is compared to the true stress at burst a failure criterion with considerably small scatter results (see Reference). To apply the failure criterion, the deformation distribution in the cladding needs to be predicted. In a general case, this will require considering the local temperature, stress, and deformation histories in a three-dimensional treatment. This, in turn, may not be possible without a sophisticated clad mechanical behavior model.

To get a rough estimate of average burst stress for the cases where performing a detailed clad deformation analysis is not possible, the following equ tion is recommended which correlates the "typical engineering burst stress" to the clad temperature (see Reference):

$$\log_{10}(S) = 8.42 + 2.78 \cdot 10^{-3}T - 4.87 \cdot 10^{-6}T^2 + 1.49 \cdot 10^{-9}T^3 \quad (1)$$

where S is typical engineering hoop stress at burst (MPa) and T is temperature at rupture (K). The burst stress of Equation (1) is shown in Figure 1, attached.

With assumptions of one dimensional stress state and thin walled cylinder the pressure difference across the cladding (ΔP) which causes the cladding to burst is given by

$$\Delta P = \frac{2t}{D} \cdot S \quad (2)$$

where D is cladding (inner) diameter, t is cladding thickness, and S is hoop stress of Equation (1).

Figure 2, attached, depicts this differential pressure versus cladding temperature. Negative ΔP means here an inside pressure which exceeds the outer pressure and thus tensile hoop stress in the cladding.

If experimentally achieved clad temperature/system pressure data are to be compared with the pressure difference obtained above, information on the rod inside pressure is needed. For initial calculations, simplifying assumptions were made in order to hand calculate internal rod pressures.

To estimate the rod inside pressure analytically, the fuel rod plenum, pellet/cladding gap, and pellet dishing volume were considered. Volumes and temperatures for these gas volumes are summarized below.

1. Plenum - 4.76 cm^3, 623 K (upper plenum cladding temperature).

2. Pellet-Cladding Gap - 2.36 cm^3, equal to cladding temperature.

3. Pellet Dishes - 2.23 cm^3, 1370 K (average fuel steady state temperature).

The pellet cracks and open prosity were neglected in this simplified approach. These parameters are modeled with the more detailed fuel behavior codes, FRAP-S and FRAP-T.

Burst limit curves obtained with the assumptions above have been calculated for several rod initial prepressures and are shown in Figure 3, attached. For comparison, L2-3 test data and Olsen data for unprepressurized rod buckling are included. Rod with atmospheric filling pressure does not burst at temperatures below or equal to 1700 K.

To test the sensitivity of the deduced burst limit on the above assumptions to estimate internal pressure, the 2.4 MPa curve was re-evaluated with 200 K higher plenum temperature (823 K). This curve is included in Figure 3. It is seen that the above simplifying assumptions affect the estimated burst temperature above 6 MPa; however, these results show that even with uncertainty in the assumptions to estimate internal rod pressure, a 2.4 MPa pressurized rod during L2-3 would not have experienced ballooning. However, for highly pressurized rods (4 MPa or above), the simplified method utilized may be inadequate.

A more accurate method would be to utilize FRAP-T to predict the cladding pressure loading and temperatures and then to compare these with the burst criteria shown in Figure 2. The thermal-hydraulic conditions for L2-3 were utilized to evaluate the response of pressurized rods. The results are shown in Figure 4, attached, and indicate no cladding burst failures even for rods with cold prepressurization as high as 5.8 MPa.

It is recommended that the more refined MAPTRO failure limit (CMLIMT) be utilized with detailed FRAP-T calculations to estimate cladding burst failures for LOFT tests.

mim

Attachments:
As stated

cc: V. T. Berta
M. P. Bohn
M. L. Carboneau
E. W. Coryell
W. E. Driskell
L. P. Leach
M. L. Russell
T. K. Samuels
E. L. Tolman BLT
J. R. White
Central File
S. T. Kelppe File

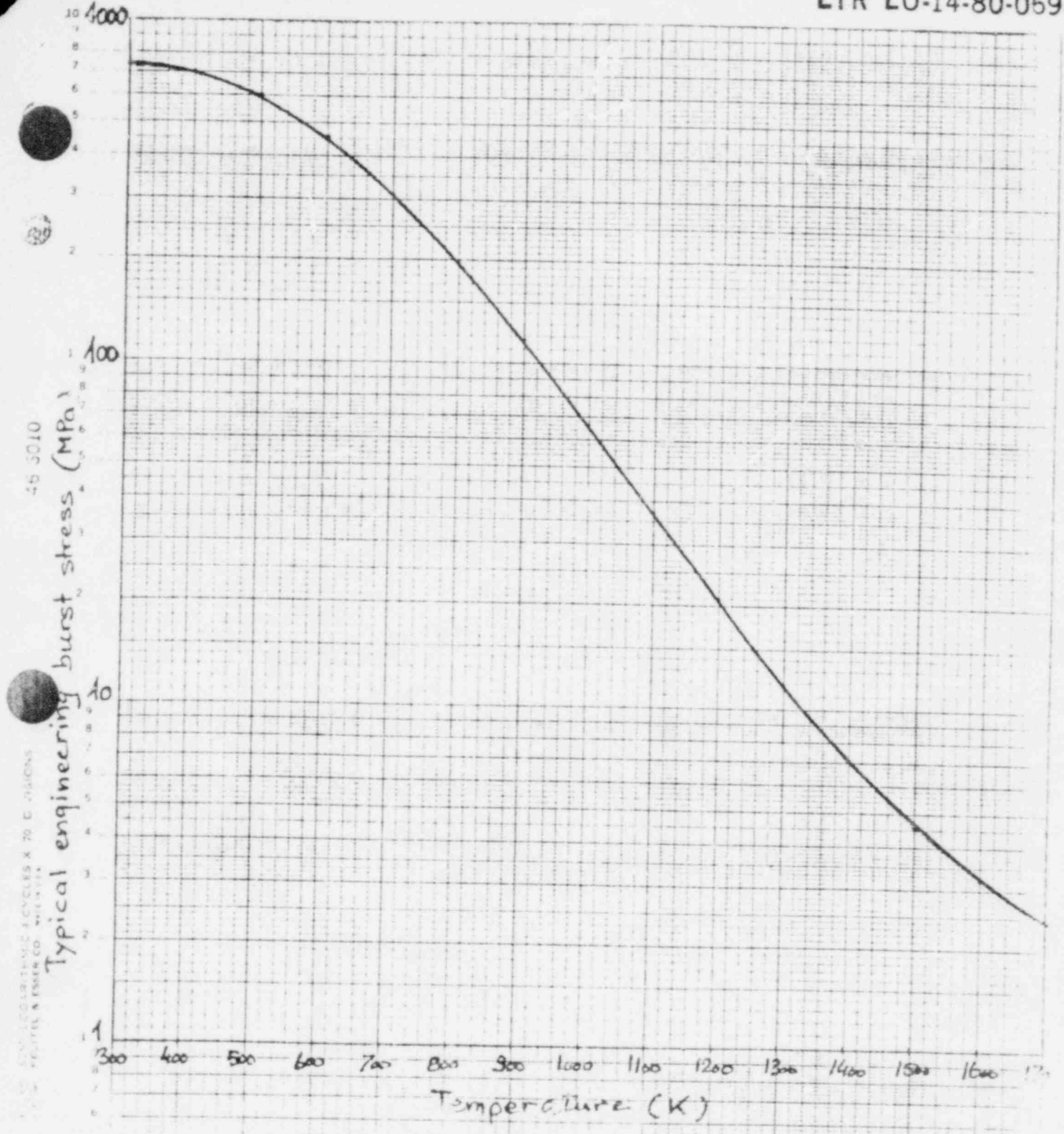

Fig 1. Typical engineering burst stress (S, eq 1) vs. temperature

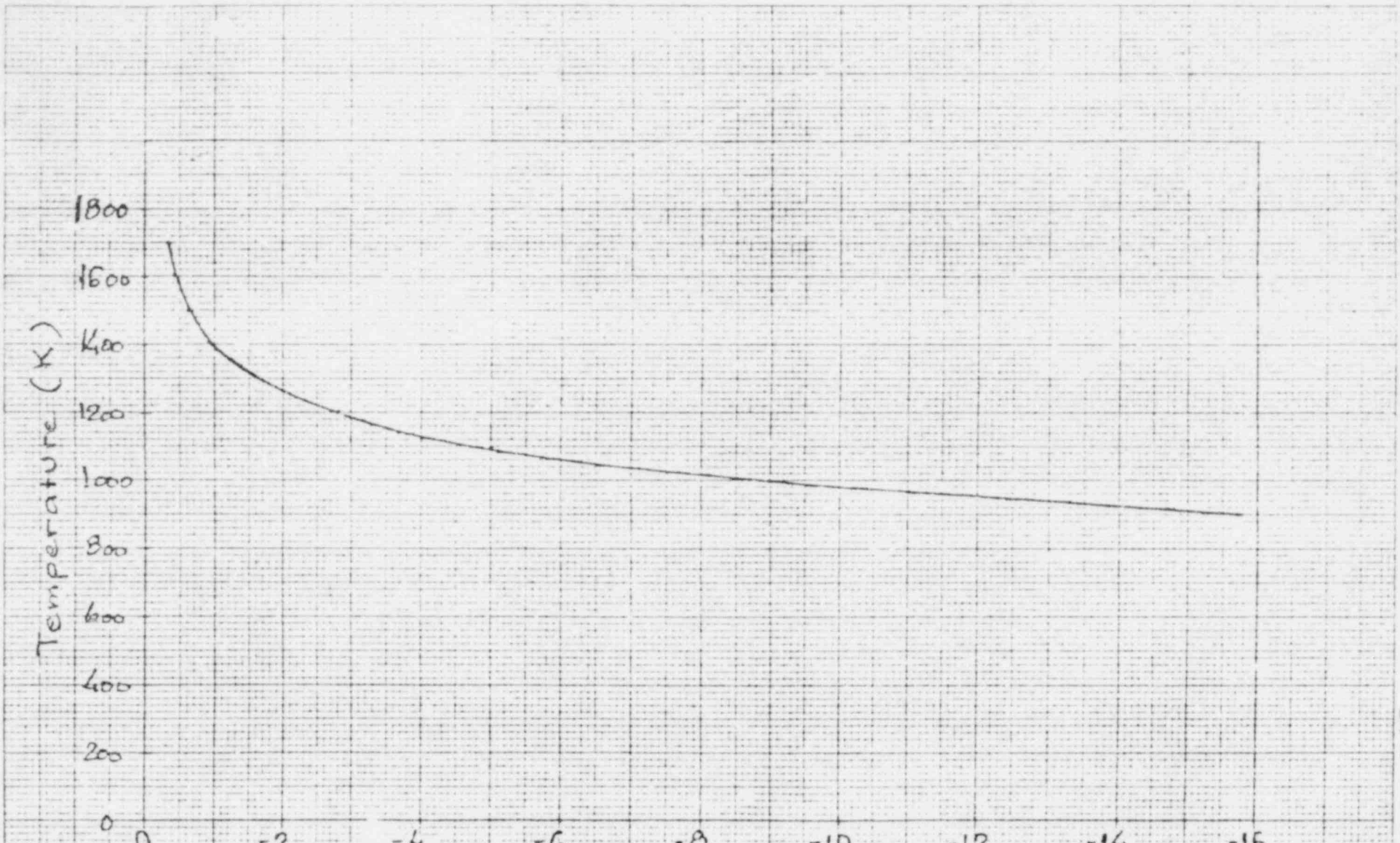

Fig 2. Cladding burst temperature vs. differential pressure over cl.

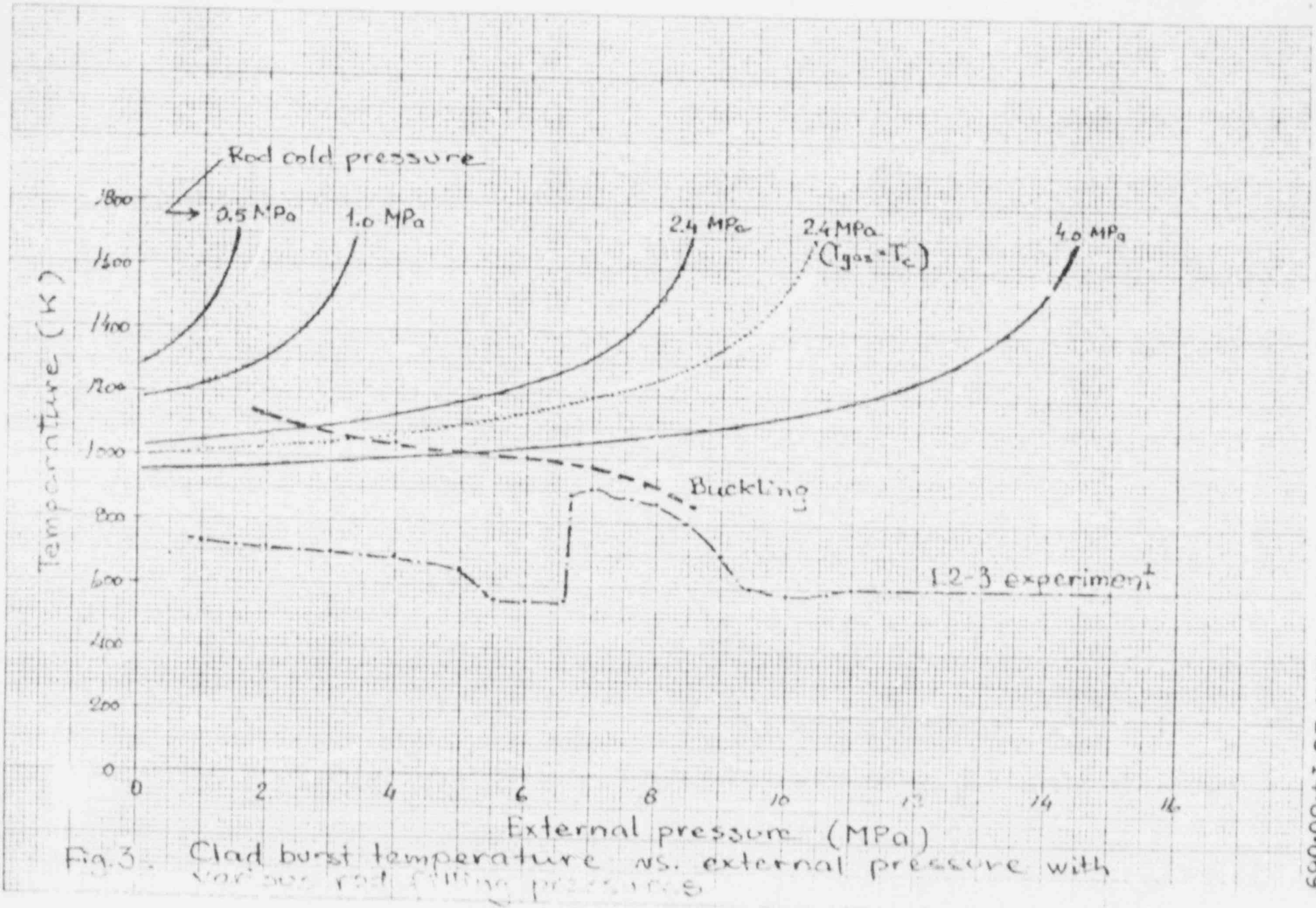

Fig.3. Clad burst temperature vs. external pressure with various rod filling pressures

LTR LO-14-80-069

FIGURE 4. SIMULATED RESPONSE OF PRESSURIZED RODS DURING LOFT TEST L2-3.

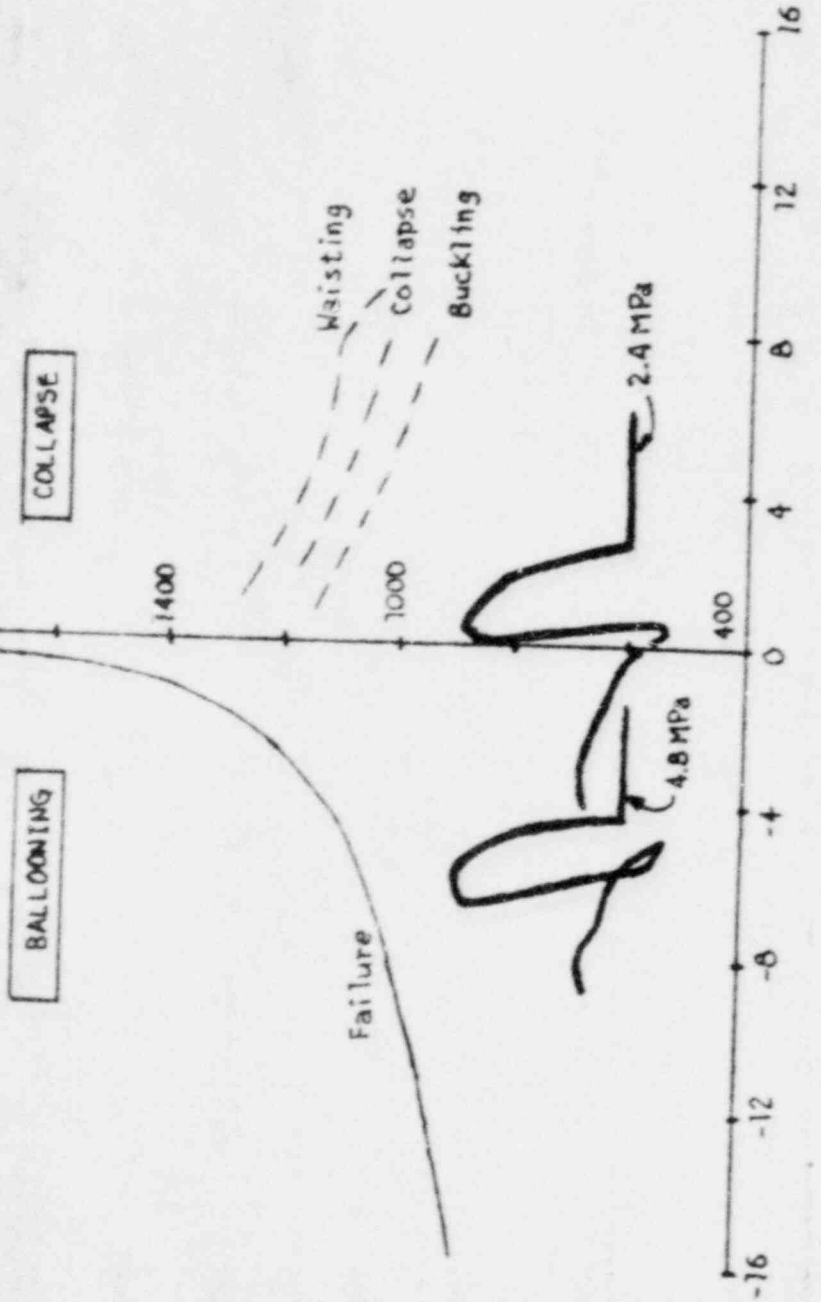

APPENDIX B

PRELIMINARY PREDICTION FOR LOFT LOCE L2-5

EG&G Idaho

LTR LO-14-80-069

INTEROFFICE CORRESPONDENCE

date July 11, 1979

to S. A. Naff

from J. R. White

subject PRELIMINARY PREDICTION FOR LOFT LOCE L2-5 - JRW-17-79

Attached is a report whith documents a preliminary L2-5 calculation performed by C. D. Keeler. The analysis was performed using the same code version (RELAP4/MOD6 with Biasi's CHF correlation) that successfully predicted the early rewet behavior we observed in L2-3.

No early rewet is predicted to occur in L2-5, however, rewetting is predicted to occur later in the transient after accumulator injection begins. It is concluded from this analysis that L2-5 will be a significantly different transient than L2-3 and L2-2 due to the differences in core flow behavior, which in turn are due to differences in intact loop cold leg and broken loop hot leg flows.

Your questions and comments are invited.

mim

Attachment:
As stated

cc: V. T. Berta
C. D. Keeler
L. P. Leach
M. L. Russell
T. K. Samuels
E. L. Tolman
J. R. White File
Central File

PRELIMINARY LOCE L2-5 EXPERIMENT PREDICTION

A preliminary analysis using RELAP/MOD6 was performed to predict the results of Loss-of-Fluid Test (LOFT) Loss-of-Coolant Experiment (LOCE) L2-5. LOCE L2-5 is designed to simulate a 200% (100% of the break area in each leg) double-ended shear in the cold leg of a large four-loop PWR. LOCE L2-5 is almost identical to LOCE L2-3 with the exception that loss of site power coincident with break initiation is assumed for LOCE L2-5, which requires that the primary coolant pumps coast down, and HPIS and LPIS flows be delayed until after the emergency diesel is delivering power. In LOCE L2-5 flows from HPIS and LPIS are set to initiate at 22.0 and 35.0 s respectively, and the pump simulator in the broken loop is in high resistance configuration, simulating a locked rotor pump.

The initial conditions used in the LOCE L2-5 analysis were identical to those of LOCE L2-3, shown in Table 1.

Table 1

LOFT SYSTEM INITIAL CONDITIONS FOR LOCE L2-5

Calculated Core Power[a] (MW)	MLHGR (kW/m)	Hot Leg Temperature (K)	Differential Temperature (K)	Cold Leg Temperature (K)	Calculated Primary Coolant Flow[a] (kg/s)
36.9	39.4	591.5	35.8	555.7	185.8

a. The calculated core power and calculated core flow are based on a total peaking factor of 2.45. The actual core power and core flow will be based on peaking factor measurements done prior to the experiment.

The LOCE L2-5 system analysis was completed to 40 s of blowdown time. Conditions in the system at 40 s showed that reflood would begin at approximately 46 s. Since the hottest rod was predicted to quench before the start of core reflood, a RELAP/MOD6 reflood analysis was not performed. The major event times for L2-3 and L2-5 RELAP4/MOD6 experiment predictions (EP) may be seen in Table 2.

Table 2

L2-3 AND L2-5 MAJOR EVENT TIMES

Event	L2-3 EP Event Time (s)	L2-5 EP (prelim) Event Time (s)
Test Initiation	0.	0.
Pump Trip	none	0.5
HPIS Flow Initiation	15.2	22.0
Accumulator Flow Initiation	15.6	17.3
LPIS Flow Initiation	28.0	35.0
End of Blowdown/Refill	44.0	46. (estimated)
Accumulator empties	59.0	61. (estimated)

Figures 1 through 8 show comparison plots of L2-3 experiment predictions and predictions from the preliminary L2-5 analysis. Figures 1 and 2 show system pressure response in the pressurizer and intact loop hot leg respectively. The pressure traces from both runs essentially overlay until the pressurizer empties. From that point on the slower depressurization of L2-5 may be seen; the slower depressurization being due to a lower hot leg break flow, caused by the increased pump simulator resistance in L2-5.

Pump speed is shown in Figure 3. For L2-5 the pumps are tripped, and start coasting down at 0.5 s, the coastdown being modeled using a variable-inertia pump model. Flow in the intact loop cold leg just downstream of the pumps is shown in Figure 4. Due to flashing in the pump suction, which started coming into play at 5 s, the flow rates are very similar for L2-3 and L2-5 after approximately 6 s. However, the difference in flow between L2-3 and L2-5 from 2 - 6 s is significant. Analysis of L2-2 and L2-3 test data showed that early rewets in the core were due to more intact loop cold leg flow entering the reactor vessel inlet annulus than was leaving the inlet annulus through the broken loop cold leg during the first 6 s of blowdown. This mass of water flowed down the downcomer and up through the core, cooling the fuel rods and causing them to rewet at approximately 6 s.

This behavior was not seen in the L2-5 prediction due to the pump trip at 0.5 s, and a resulting lower intact loop cold leg flow from 2 to 6 s. Since the intact loop cold leg flow essentially equaled the broken loop cold leg break flow during this time period, there was no early rewet of the core predicted for L2-5. Figure 5 shows core inlet flow, which is essentially stagnant for L2-5 from 3 to 16 s.

Figure 6 shows the broken loop hot leg break flow, which was lower than in L2-3 due to the increased number of orifice plates in the pump simulator in L2-5. Figure 7 shows broken loop cold leg break flow, which was essentially the same for both L2-3 and L2-5. Figure 8 shows LPIS flow, which was delayed until 35 s in L2-5.

Figures 9 through 20 show predicted cladding temperatures on the hottest rod in the core for three different analyses: (1) the L2-3 experiment prediction, (2) a post-test L2-3 analysis using the Biasi CHF correlation, and (3) the preliminary L2-5 analysis, which also used the Biasi CHF correlation. The Biasi CHF correlation has been found to give good agreement with L2-2 and L2-3 data in predicting the early rewets which occurred in those experiments.

The hottest rod in the core is modeled by 12 axially-stacked heat slabs of equal length; heat slabs 1 and 12 being at the bottom and top of the rod, respectively. Figures 9 through 20 show predicted cladding temperatures for each of these 12 sections of the hottest rod for both the L2-5 and the two L2-3 predictions.

In the L2-5 analysis the hottest rod did not rewet at approximately 6 s as it did in L2-3 due to the pump coasting down. However, the analysis showed that flow through the core was sufficient during the blowdown phase to rewet the majority of the heat slabs modeling the hottest rod by 35 s. When the hot pin analysis was terminated at 35 s, only heat slabs 3 and 4 had not yet rewet. It is likely that these slabs would also rewet by the time reflood would start at approximately 46 s.

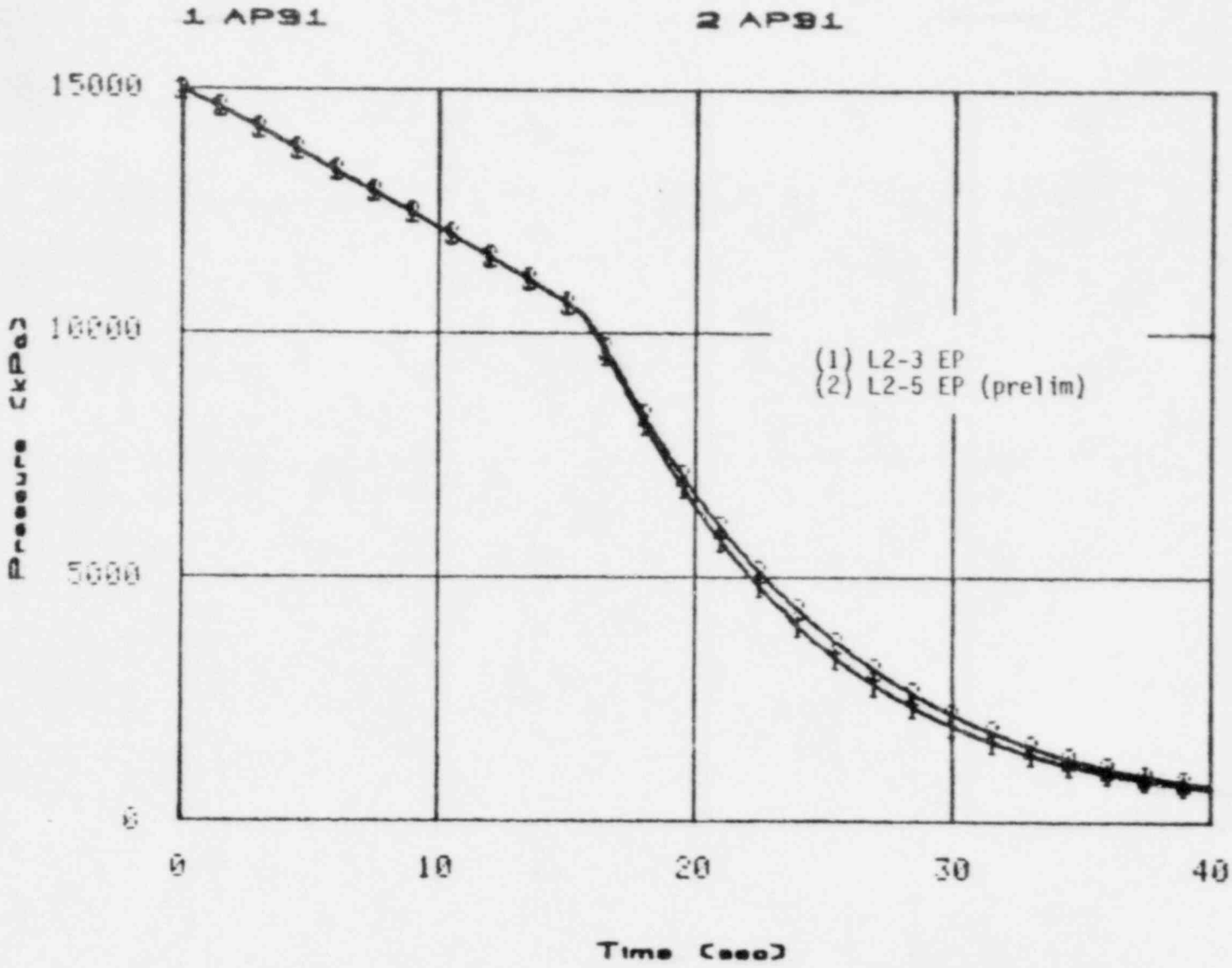

Fig. 1 Pressurizer Pressure; Comparison of L2-3 EP and preliminary L2-5 EP

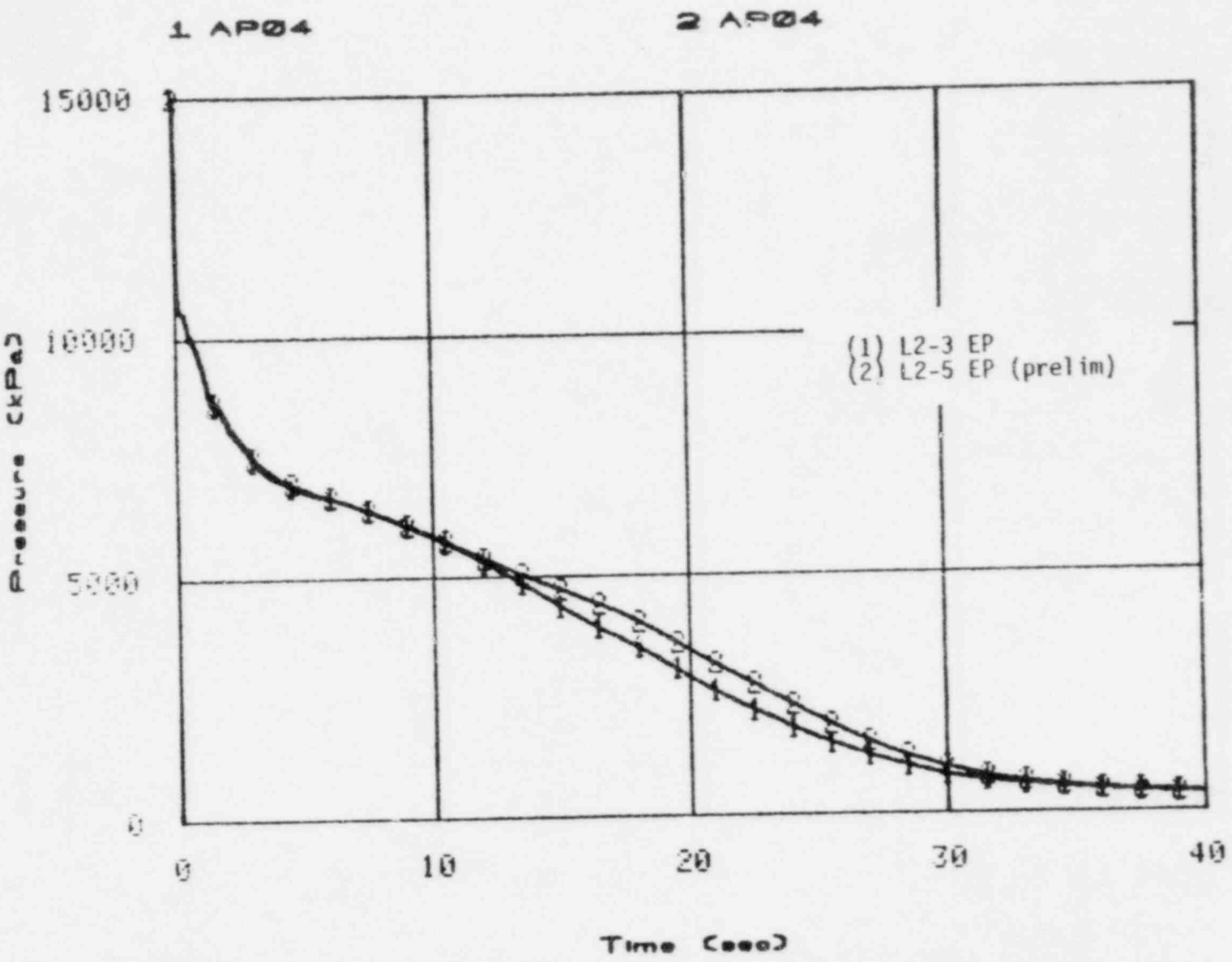

Fig. 2 Pressure--Intact Loop Hot Leg; Comparison of L2-3 EP and preliminary L2-5 EP

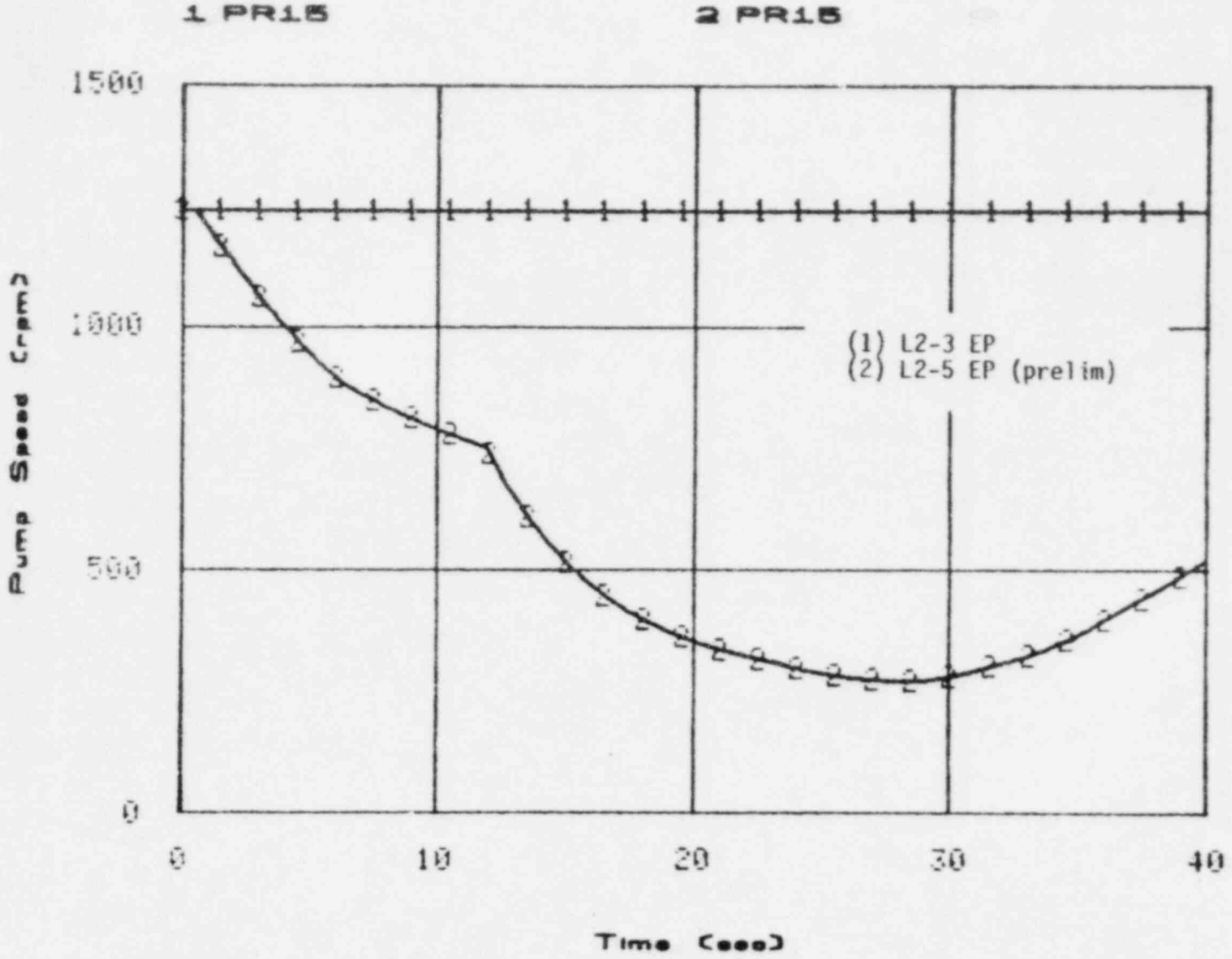

Fig. 3 Pump Speed; Comparison of L2-3 EP and preliminary L2-5 EP

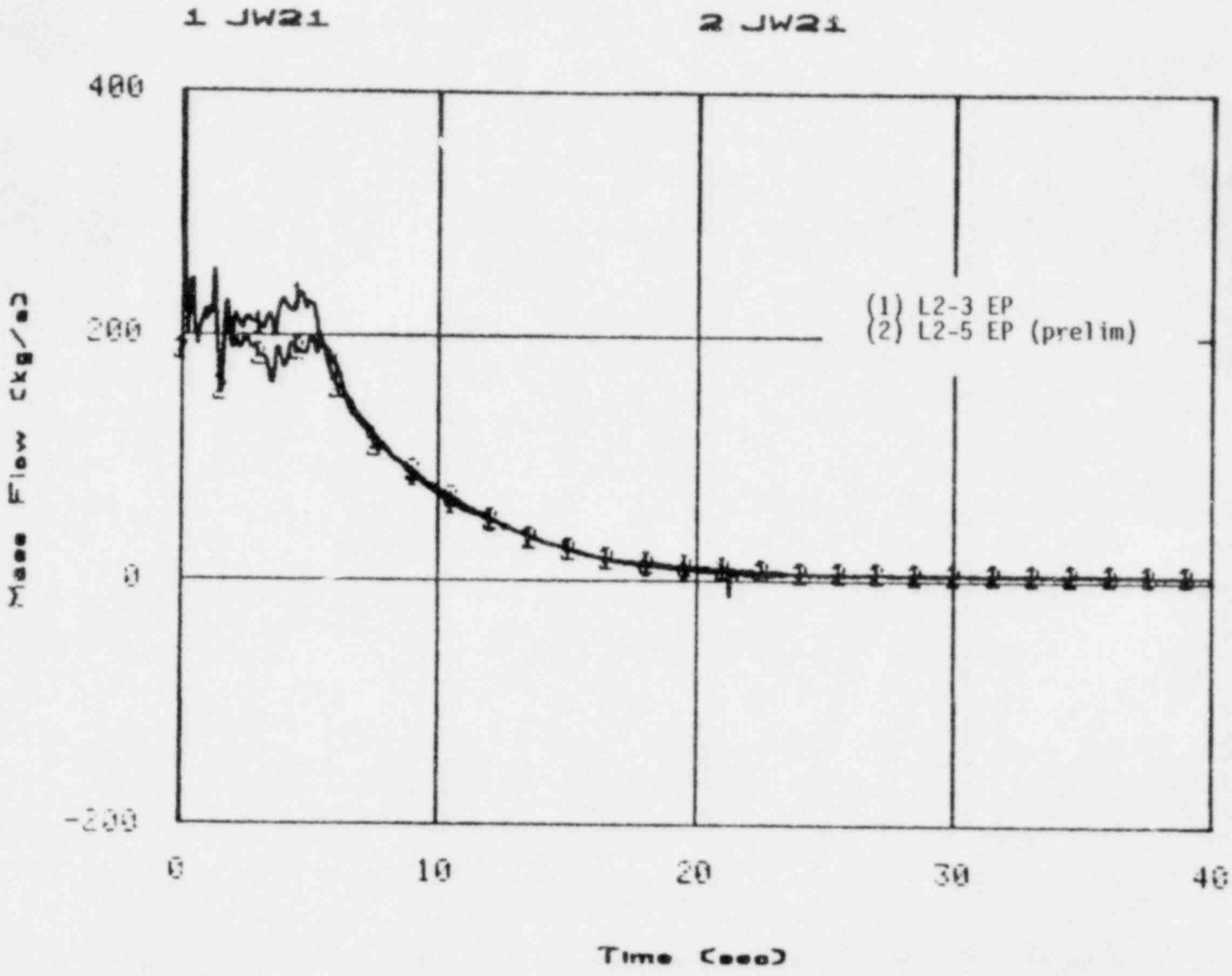

Fig. 4 Intact Loop Cold Leg Flow Rate: Comparison of L2-3 EP and preliminary L2-5 EP (location PC-1)

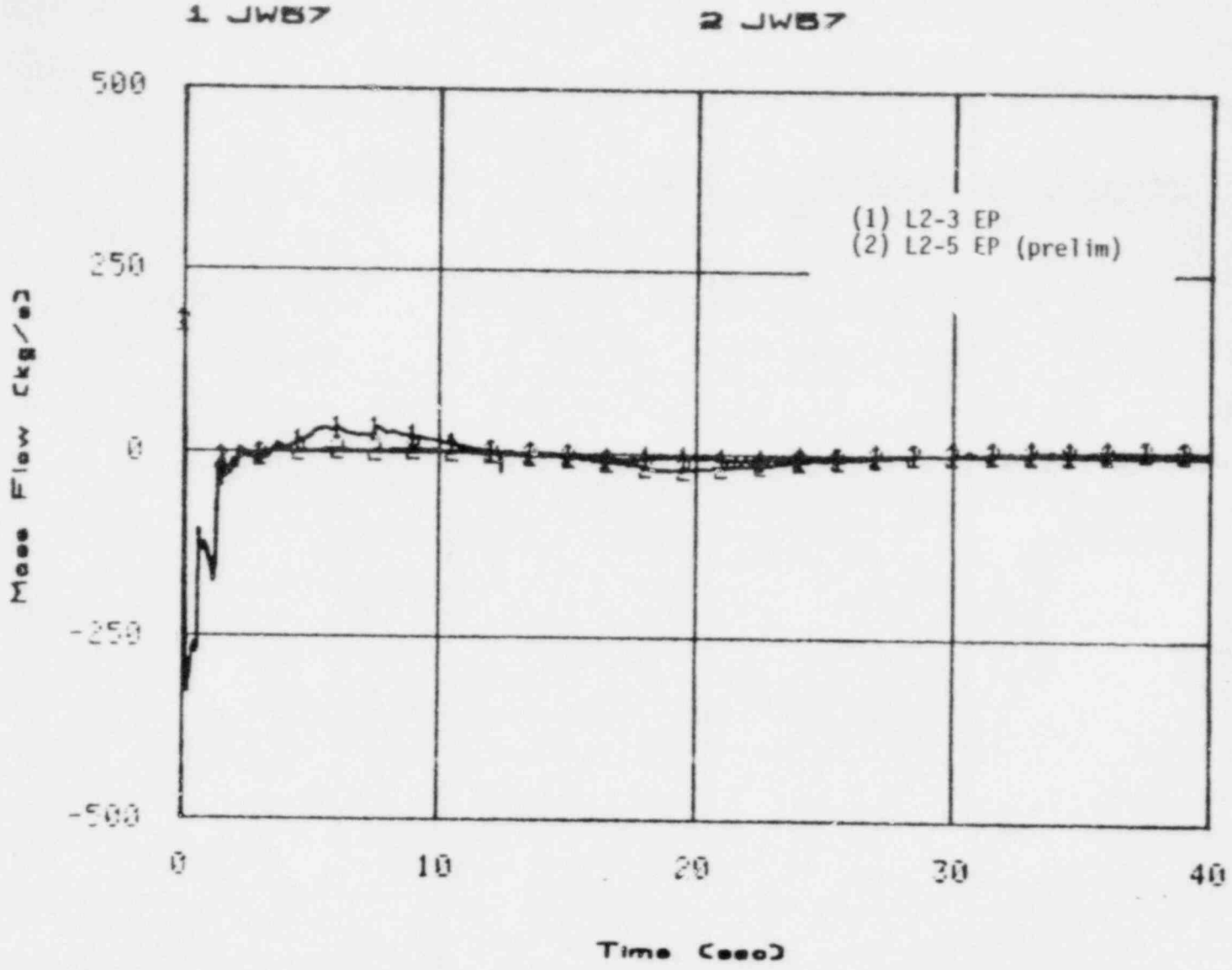

Fig. 5 Core Inlet Flow Rate; Comparison of L2-3 EP and preliminary L2-5 EP

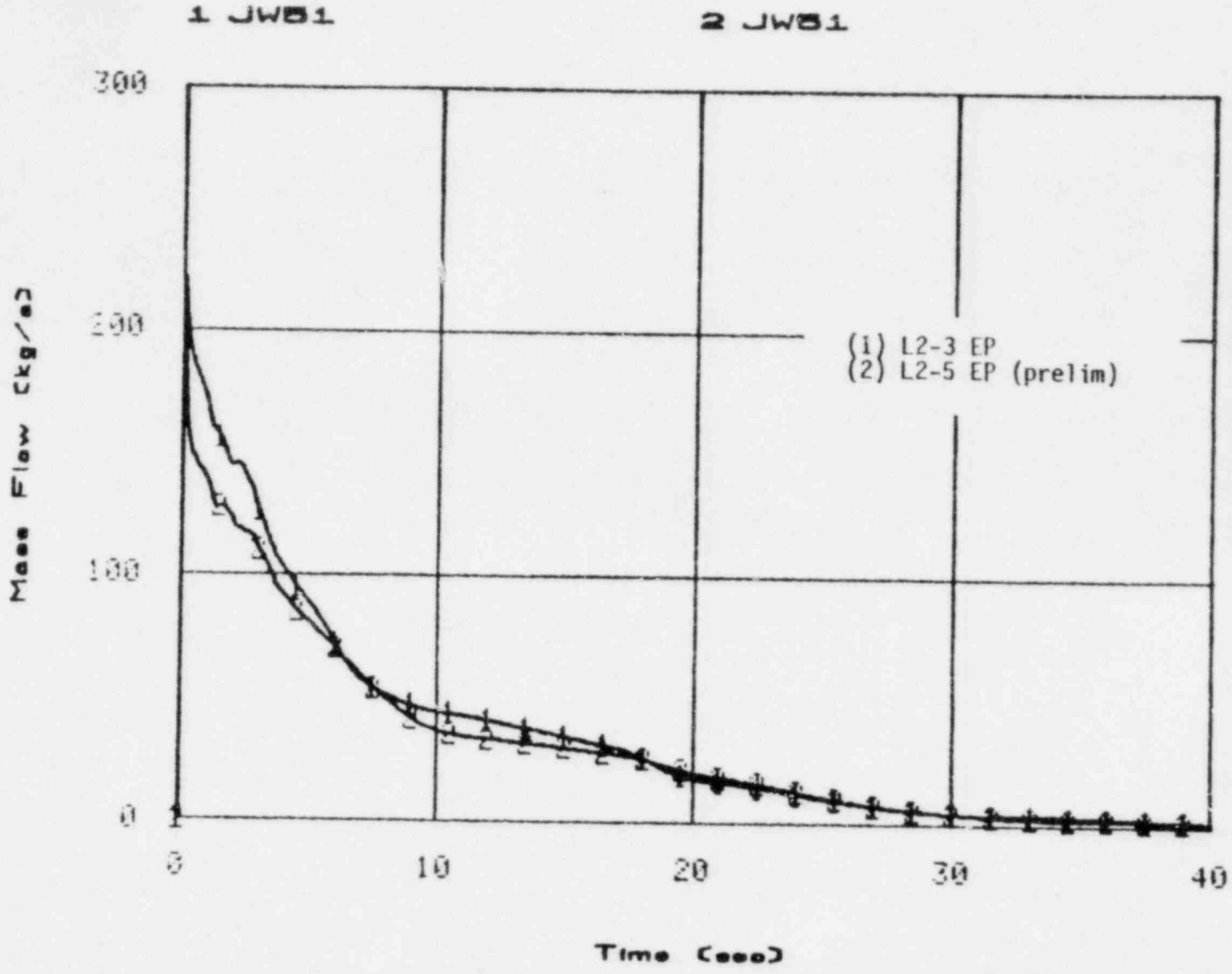

Fig. 6 Broken Loop Hot Leg Flow Rate; Comparison of L2-3 EP and preliminary L2-5 EP

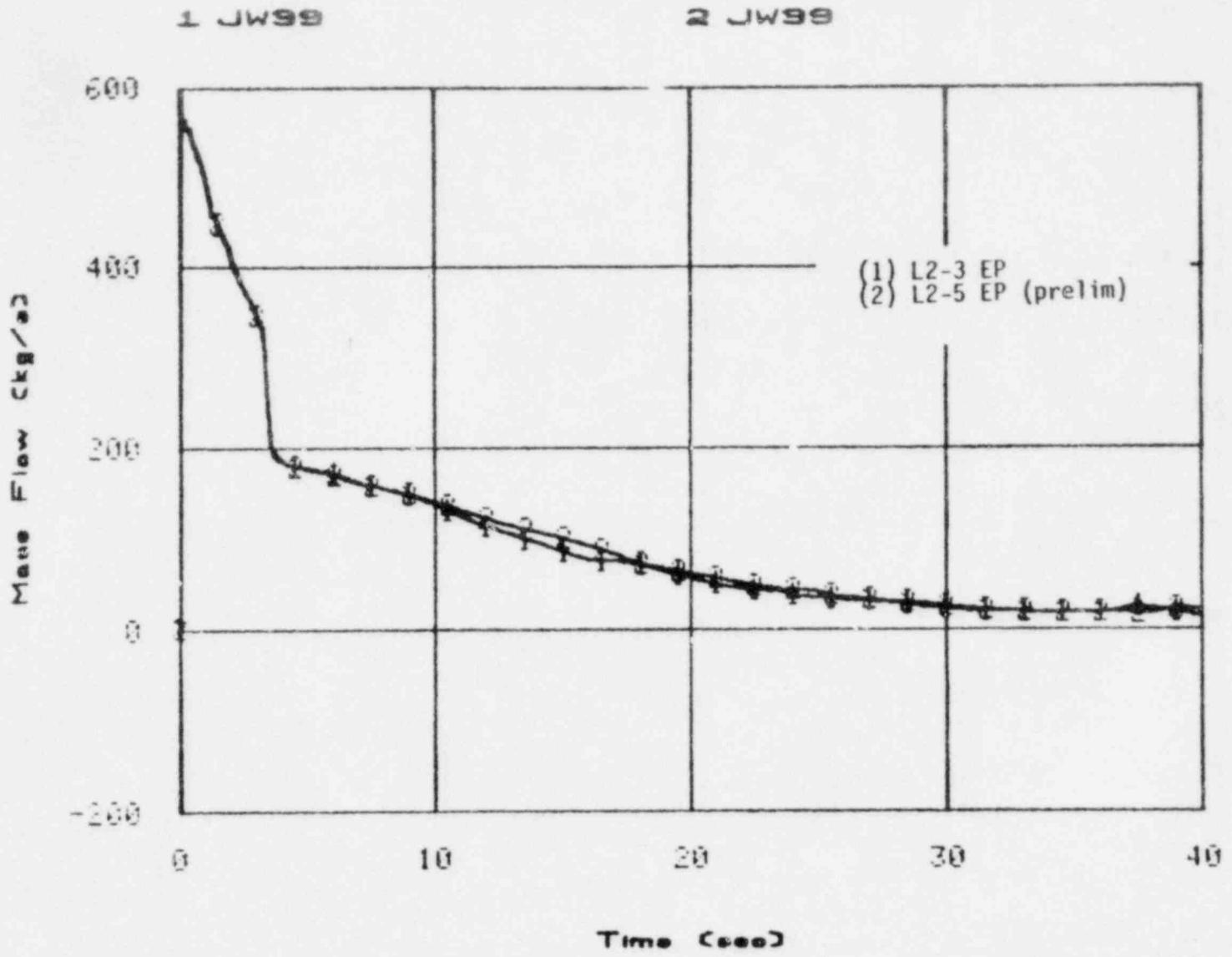

Fig. 7 Broken Loop Cold Leg Flow Rate; Comparison of L2-3 EP an preliminary L2-5 EP

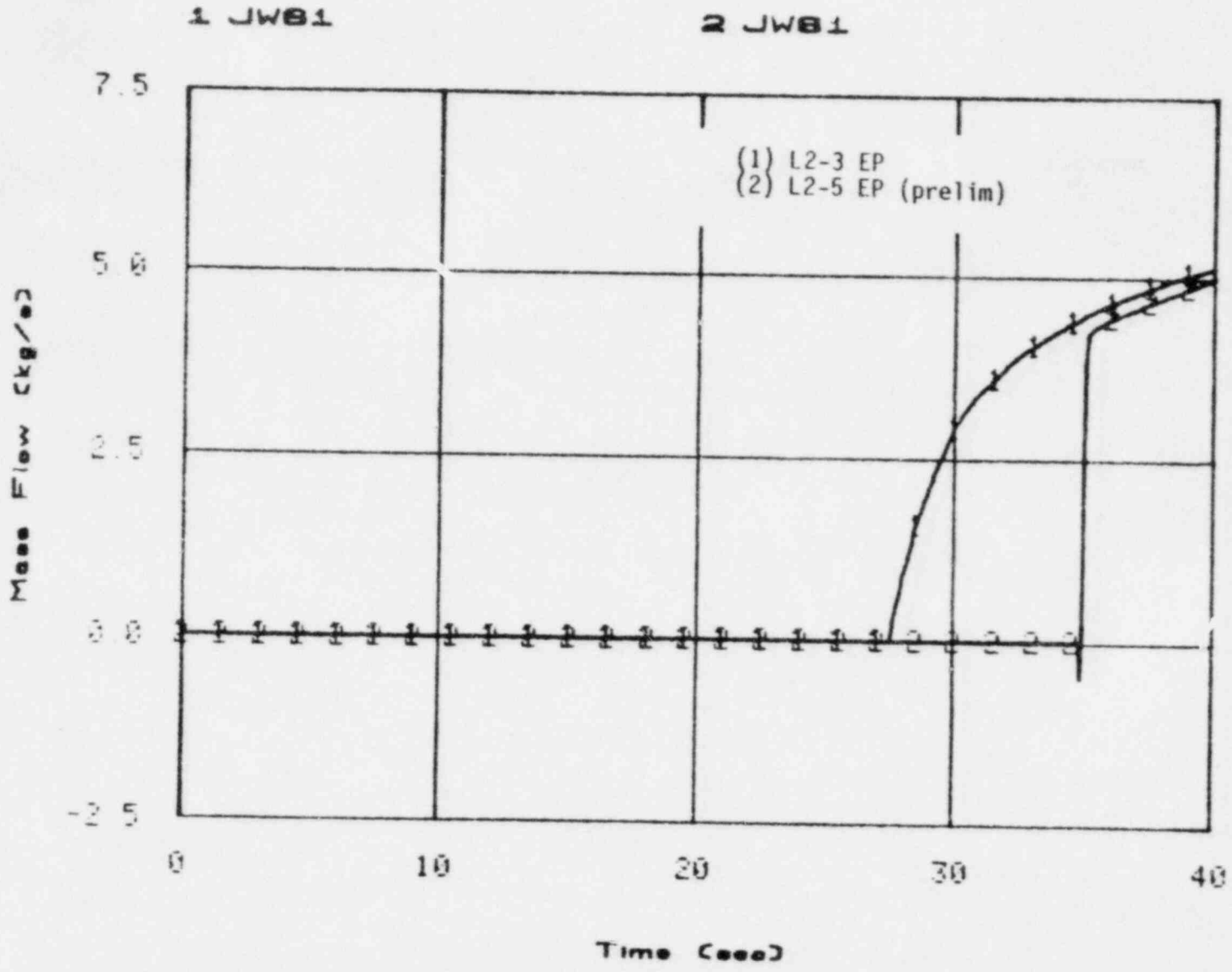

Fig. 8 LPIS Flow Rate; Comparison of L2-3 EP and preliminary L2-5 EP

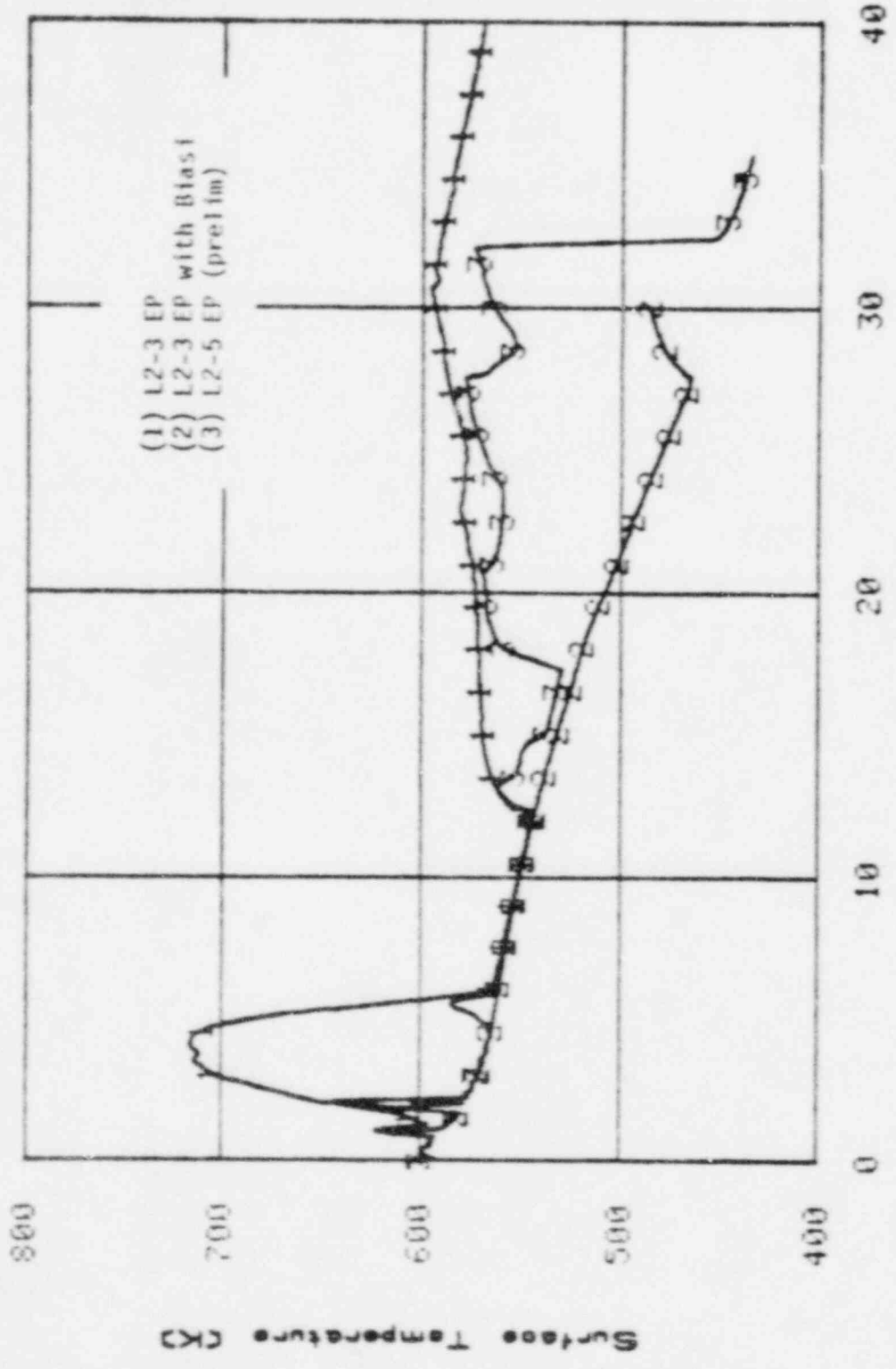

Fig. 9 Heat Slab 1 Cladding Temperature Comparison of L2-3 and L2-5 Predictions

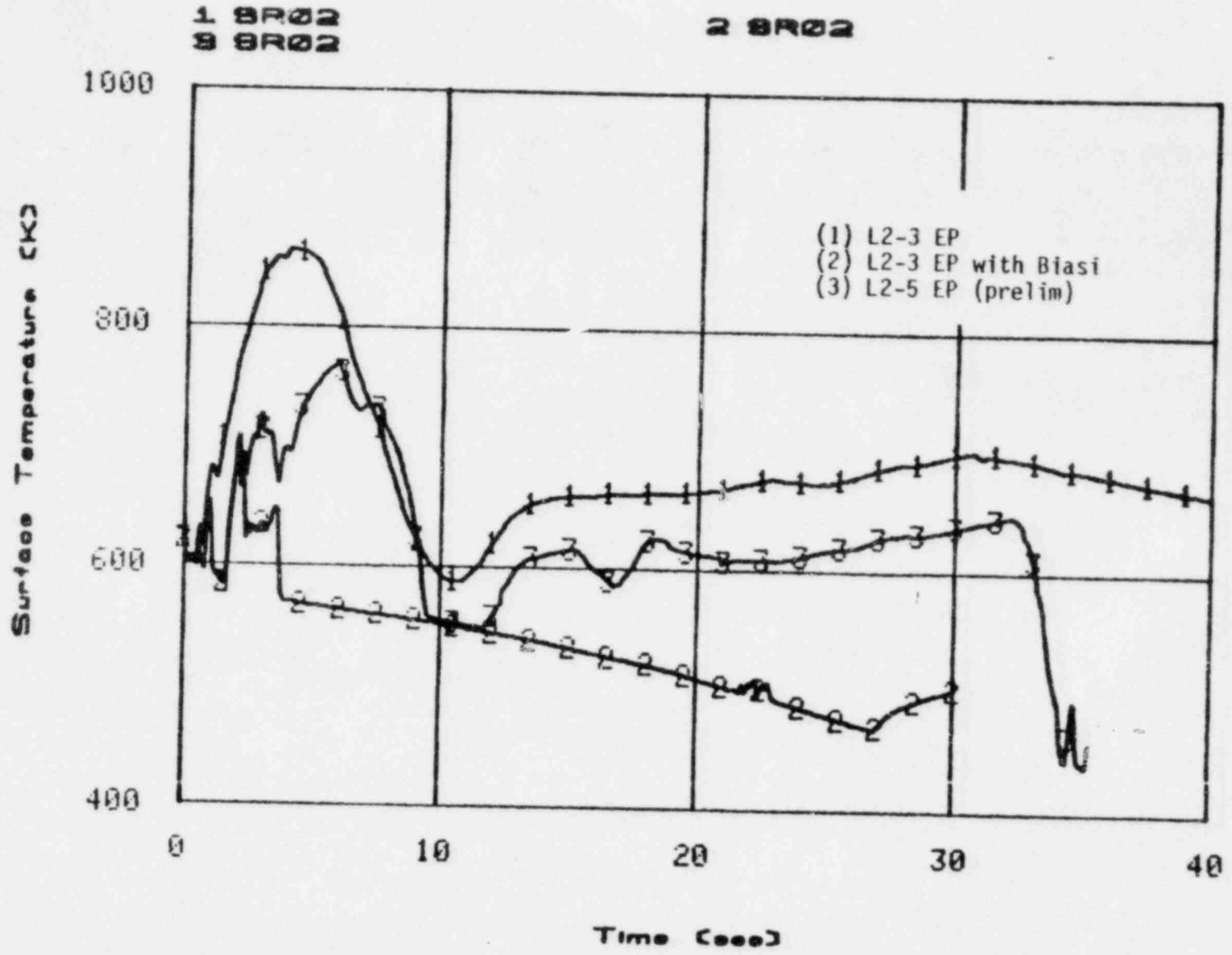

Fig. 10 Heat Slab 2 Cladding Temperature: Comparison of L2-3 and L2-5 Predictions

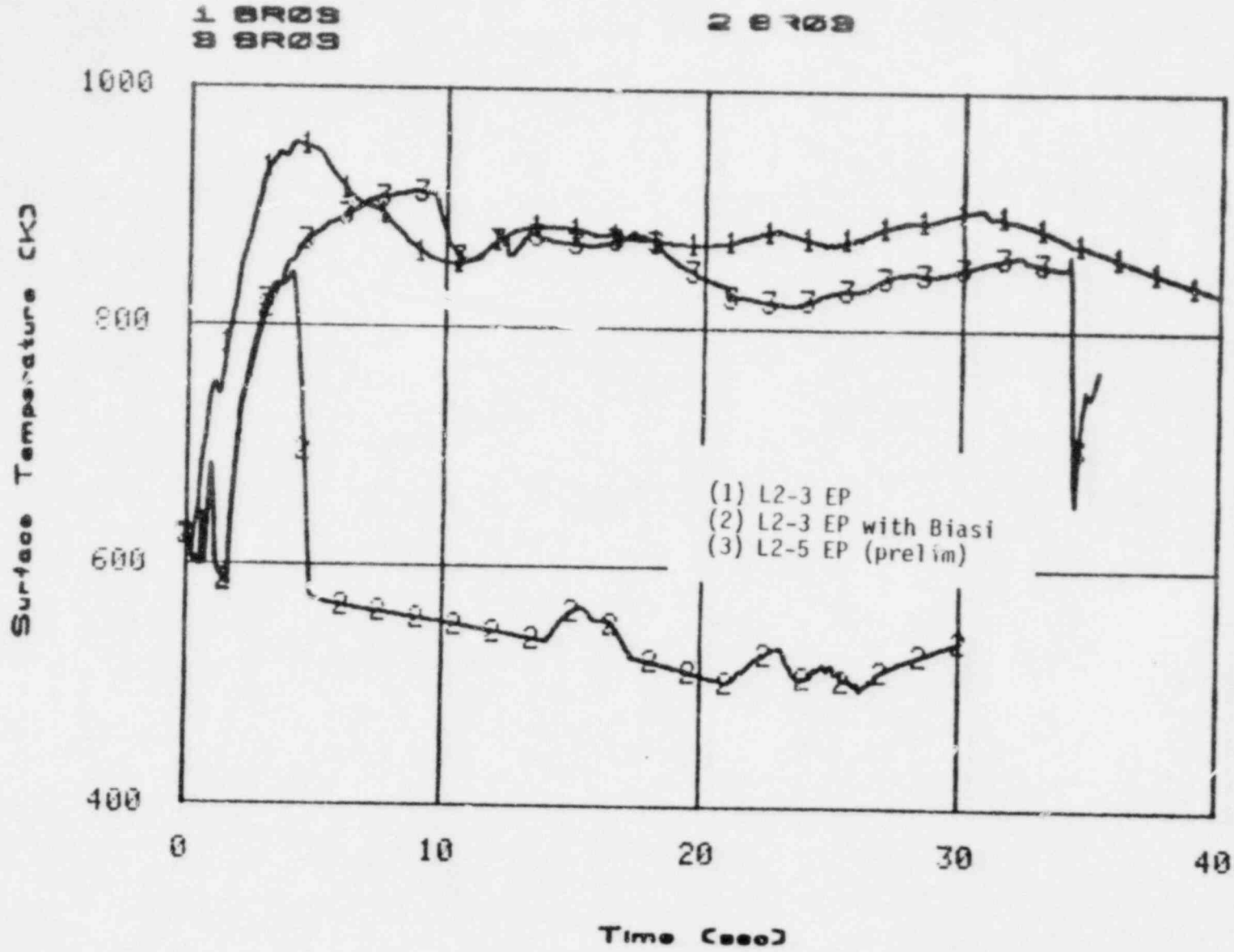

Fig. 11 Heat Slab 3 Cladding Temperature: Comparison of L2-3 and L2-5 Predictions

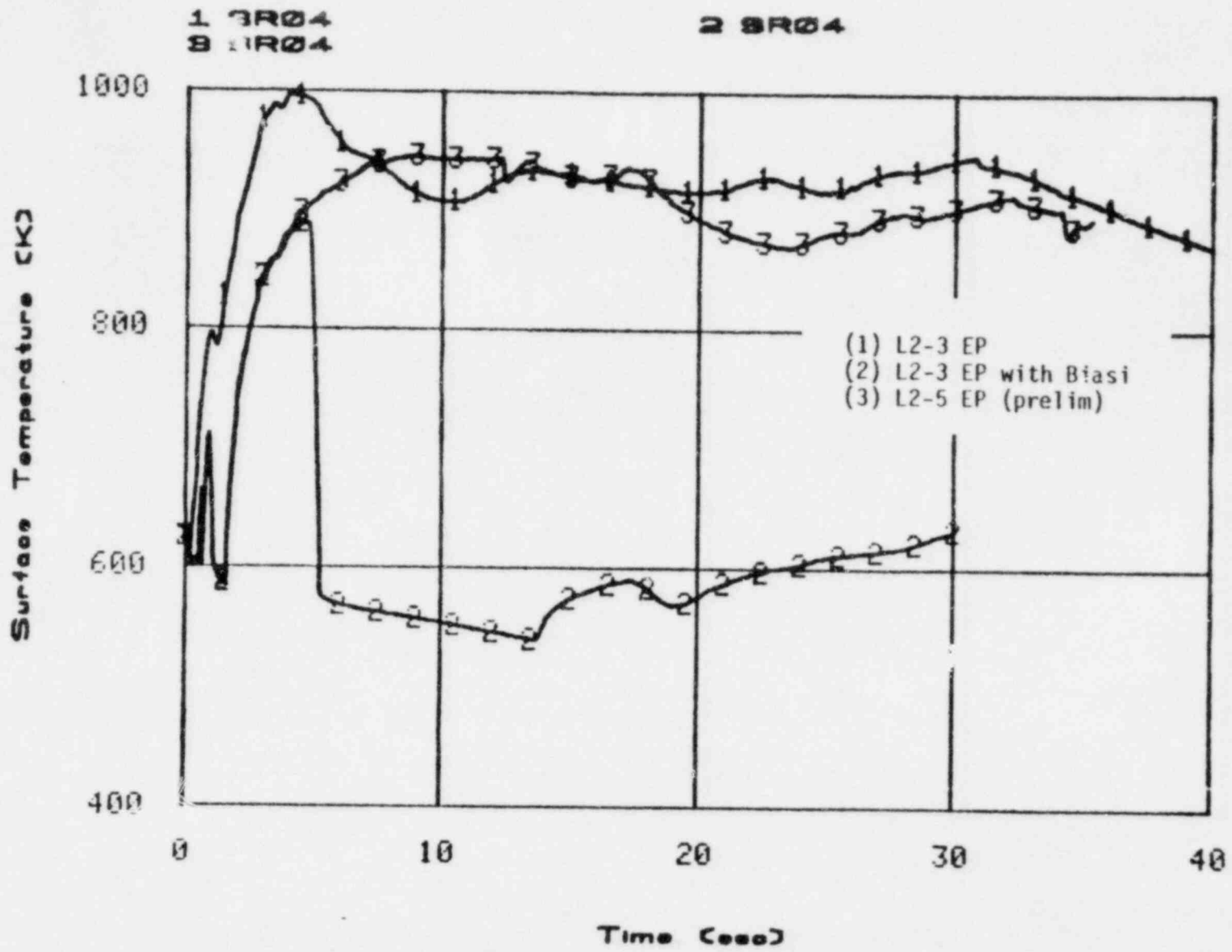

Fig. 12 Heat Slab 4 Cladding Temperature: Comparison of L2-3 and L2-5 Predictions

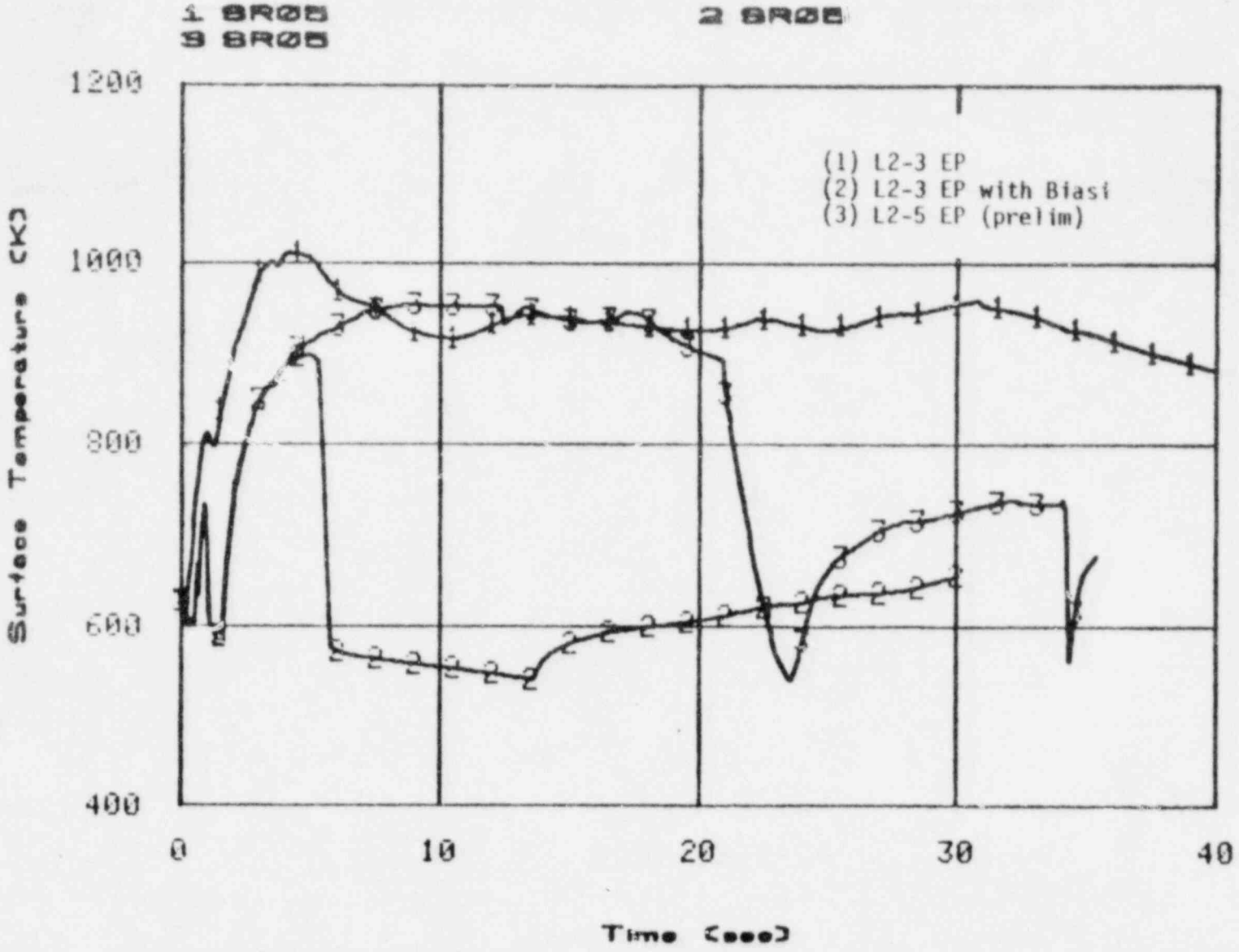

Fig. 13 Heat Slab 5 Cladding Temperature; Comparison of L2-3 and L2-5 Predictions

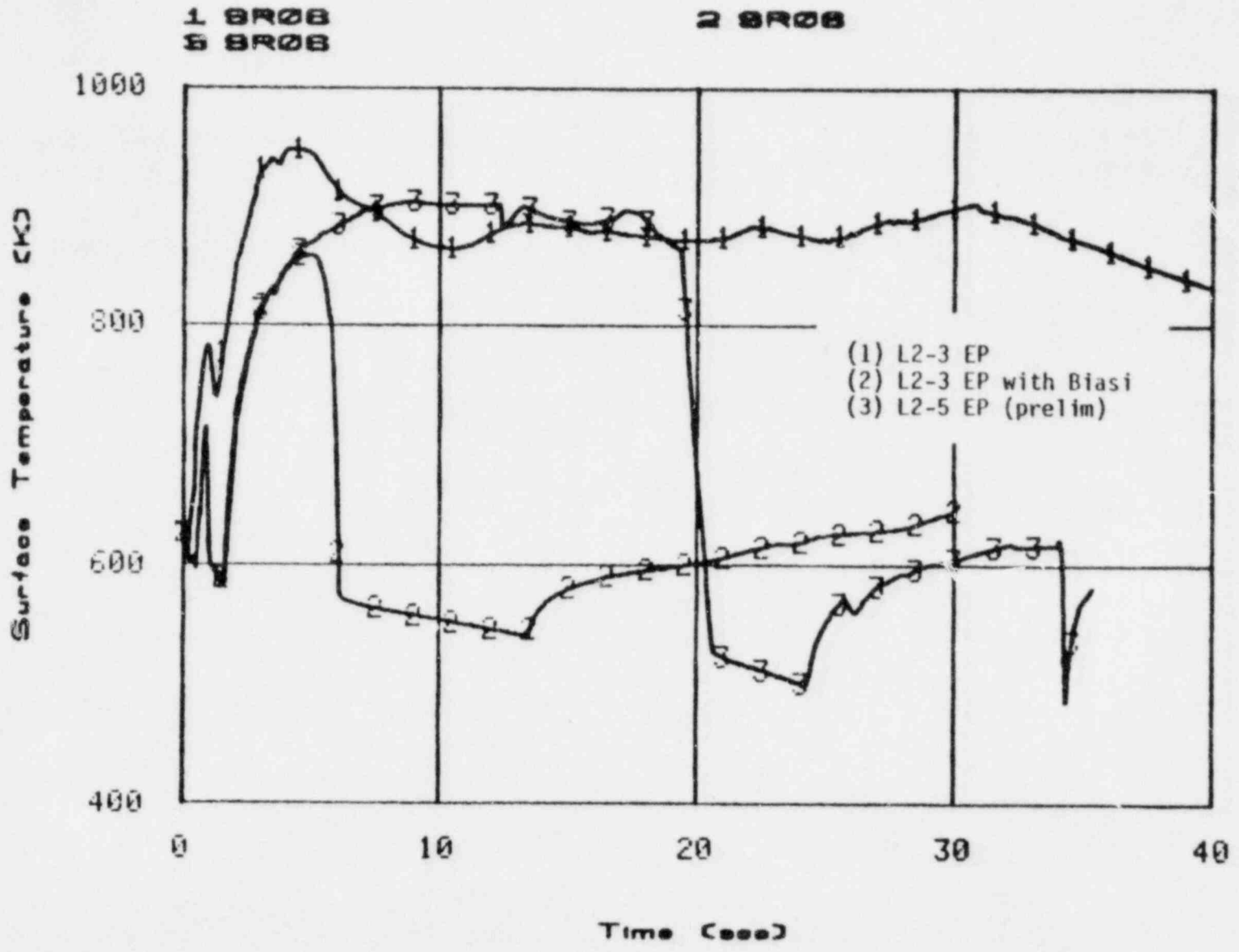

Fig. 14 Heat Slab 6 Cladding Temperature Comparison of L2-3 and L2-5 Predictions

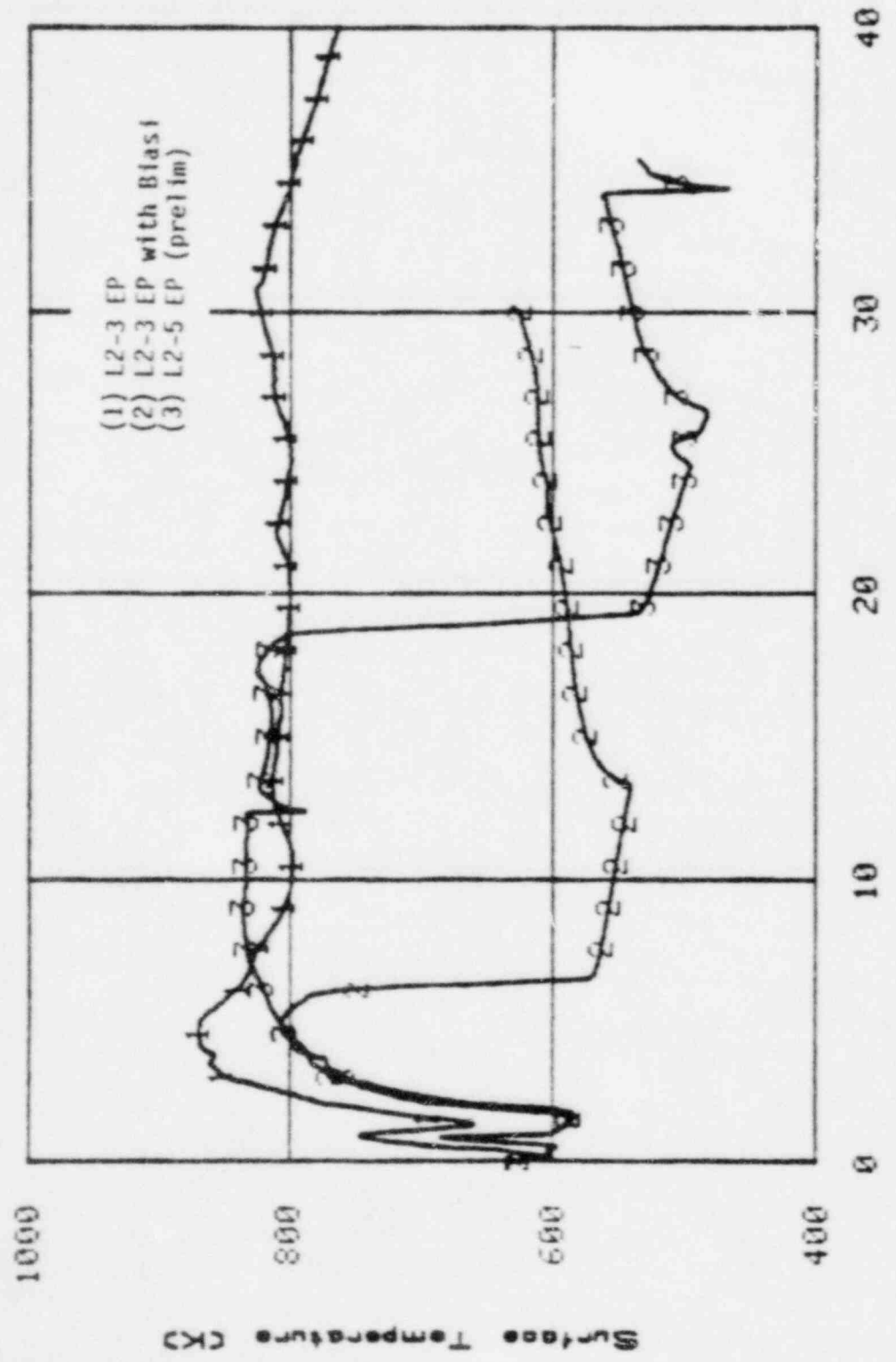

Fig. 15 Heat Slab 7 Cladding Temperature: Comparison of L2-3 and L2-5 Predictions

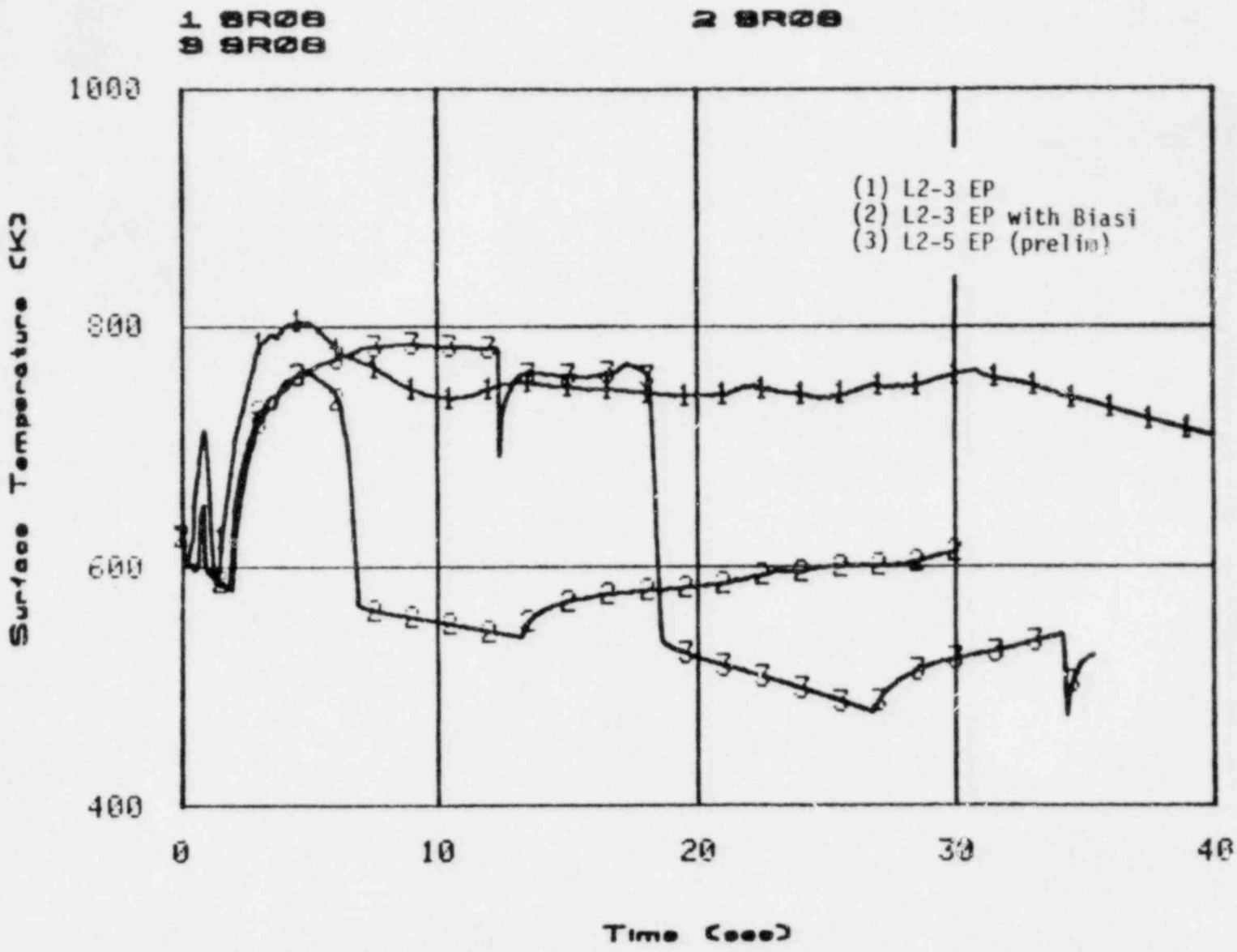

Fig. 16 Heat Slab 8 Cladding Temperature; Comparison of L2-3 and L2-5 Predictions

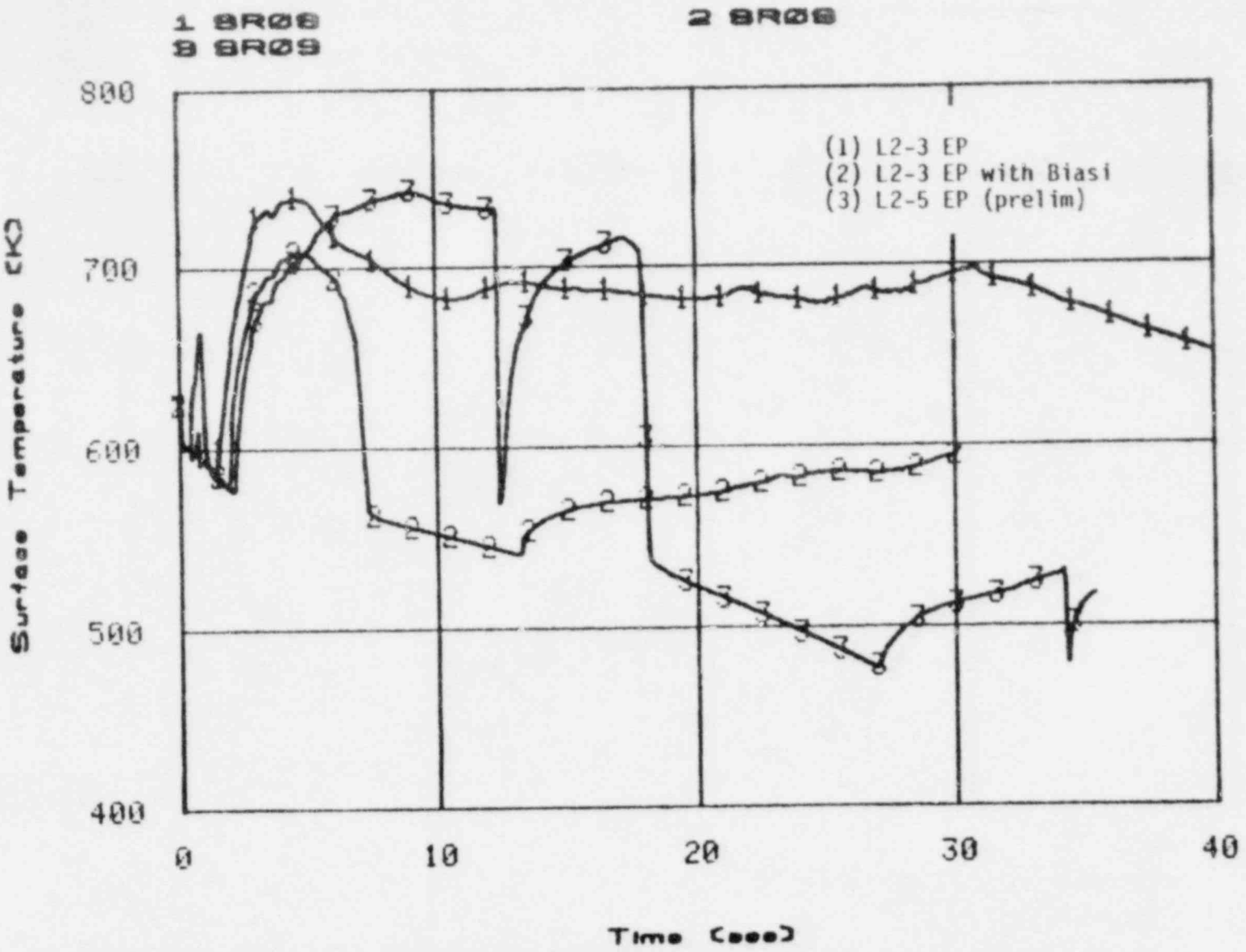

Fig. 17 Heat Slab 9 Cladding Temperature; Comparison of L2-3 and L2-5 Predictions

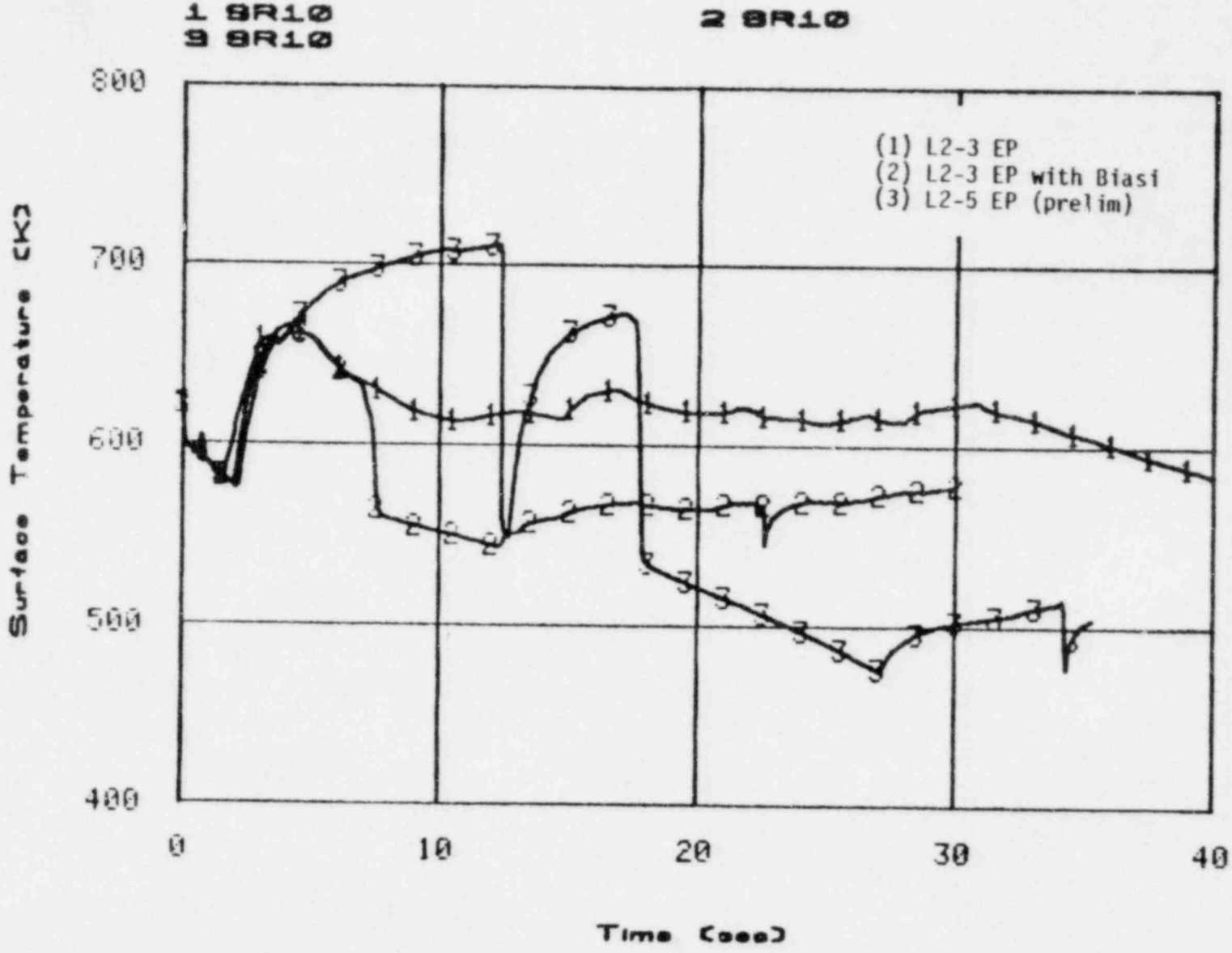

Fig. 18 Heat Slab 10 Cladding Temperature; Comparison of L2-3 and L2-5 Predictions

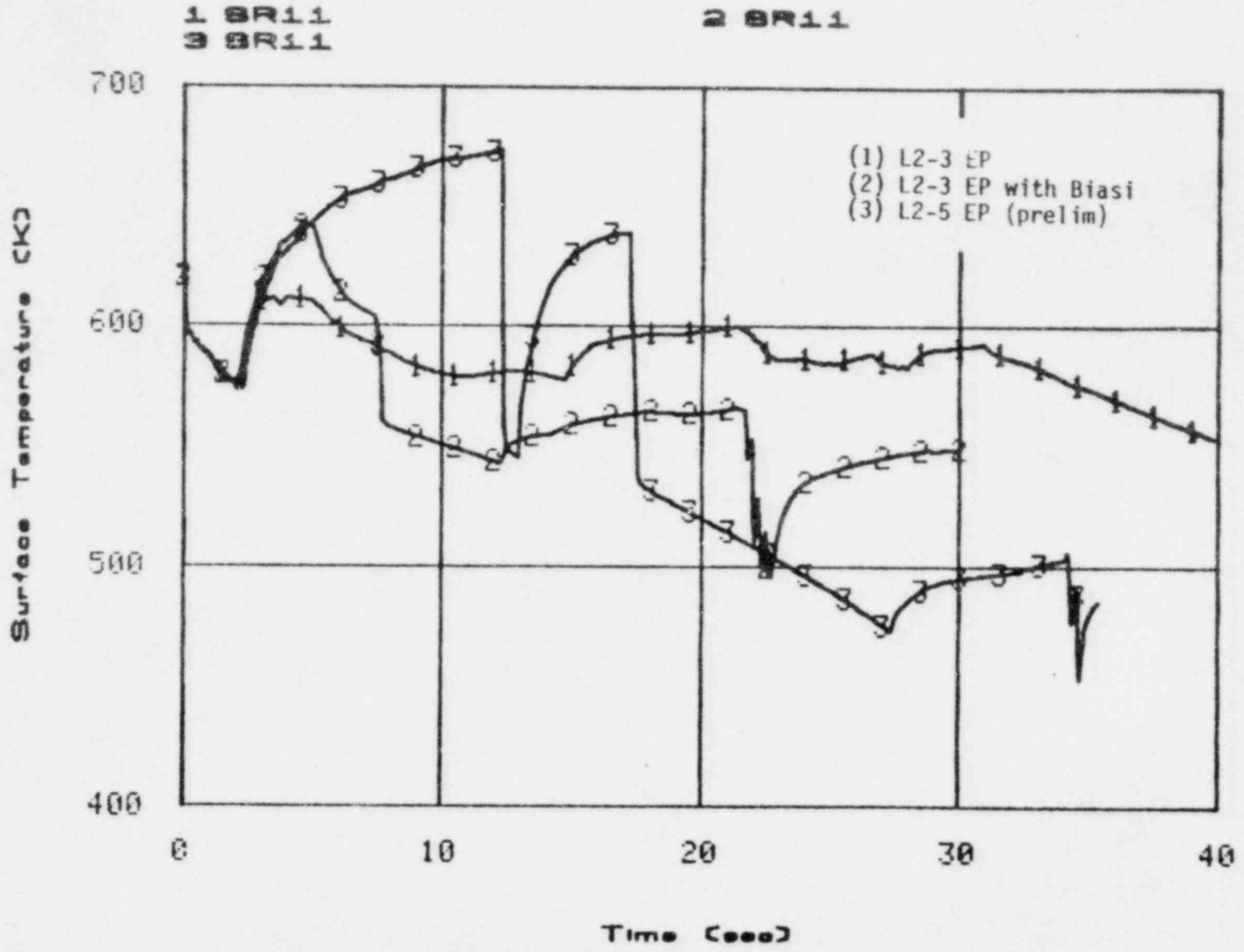

Fig. 19 Heat Slab 11 Cladding Temperature; Comparison of L2-3 and L2-5 Predictions

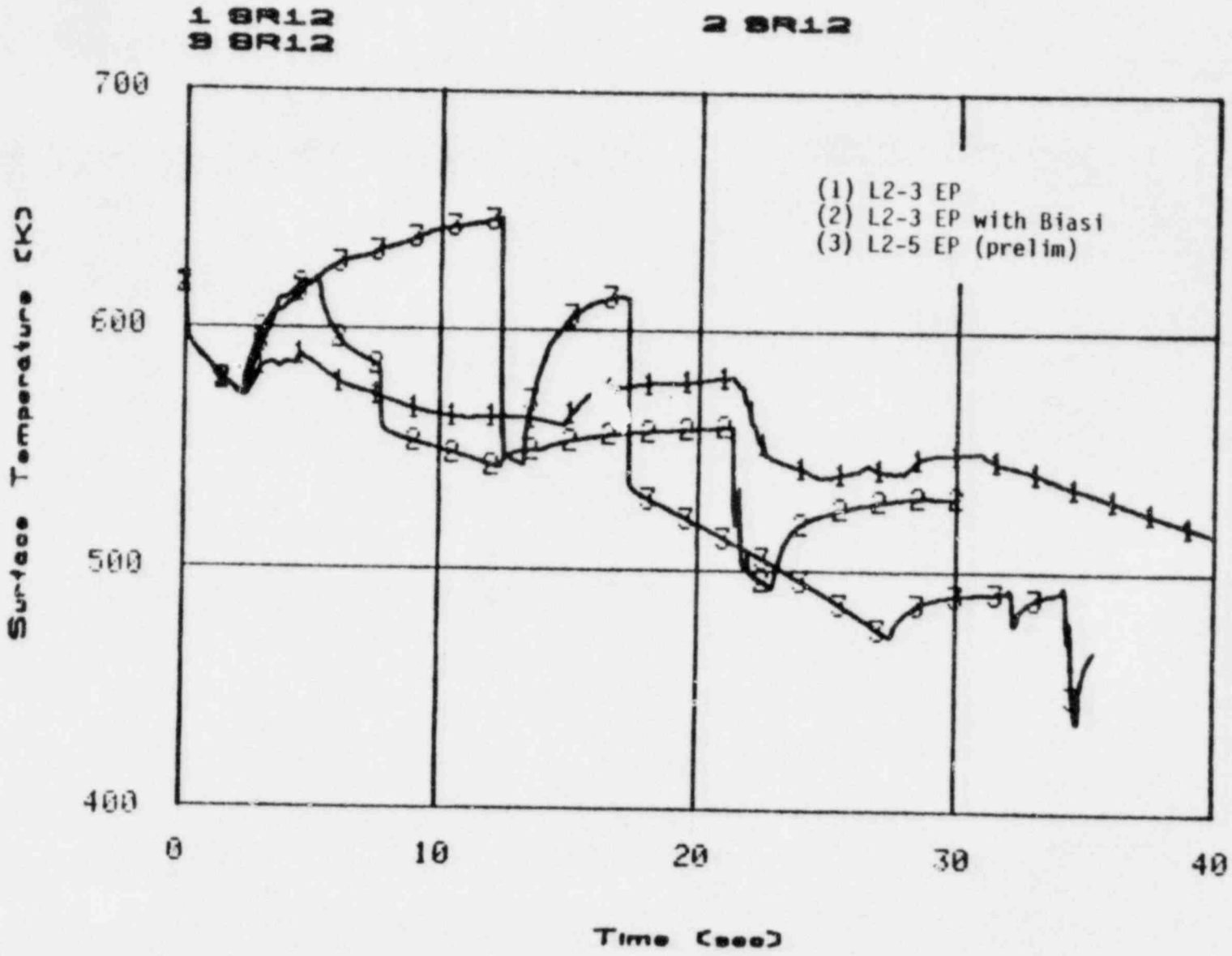

Fig. 20 Heat Slab 12 Cladding Temperature; Comparison of L2-3 and L2-5 Predictions

APPENDIX C

FRAP-T5 ANALYSIS FOR FUEL BEHAVIOR IN LOFT L2-5/L2-6

EG&G Idaho

INTEROFFICE CORRESPONDENCE

date January 8, 1980

to E. L. Tolman

from S. T. Kelppe

subject FRAP-T5 ANALYSIS FOR FUEL BEHAVIOR IN LOFT L2-5/L2-3 BLOWDOWN - STK-1-80

Ref: J. R. White ltr to S. A. Naff, JWR-17-79, Preliminary Prediction for LOFT LOCE L2-5, July 11, 1979

In this letter results of FRAP-T5 calculations for Loss-of-Fluid Test (LOFT) L2-6 test with some parameter analysis are described. L2-6 test is planned to be run with a number of prepressurized fuel rods in the core, with one of the goals being to produce ballooned fuel. In light of recent LOFT test data, this goal may not be achieved with conditions similar to those of the L2-3 test and typical beginning of the life rod initial gas pressurization. Therefore, applying L2-5 thermal hydraulic conditions, and variation of the fuel rod power, has been suggested.

These calculations have been made with L2-5 boundary conditions from RELAP4 preliminary predictions (see reference). Two power levels, peak powers of 39.4 kW/m (12 kW/ft) and 52.5 kW/m (16 kW/ft), as well as two pressurization levels 2.4 MPa and 4.0 MPa, are considered. Power levels represent those of the planned L2-5 and L2-4, respectively. Lower pressurization is typical of a pressurized water reactor (PWR) rod while the higher of the pressures is in the range of typical end-of-life pressures.

Results include the unpressurized case on both power levels which thus represent the L2-5 (39.4 kW/m) and (modified) L2-4 (52.5 kW/m) experiments.

The rod with 4.0 MPa helium prepressure and 52.5 kW/m initial power is predicted to burst to failure near the end of the blowdown. The 2.4 MPa pressure rod sees a maximum permanent hoop strain of 1.6% and does not burst. Neither does the lower power rod even at 4.0 MPa initial pressure.

Some of the input data are given in Table 1. FRAP-T5 input deck is shown in Table 2 (L2-5 unpressurized, 39.4 kW/m).

Axial power profile and radial distribution of heat generation rate in the fuel are seen in Figures 1 and 2, respectively. Rod maximum power versus time for both power levels with decay heat included is shown in Figure 3. Decay heat is assumed to be proportional to the steady state power. RELAP4/MOD6 surface heat transfer coefficient history is given in Figure 4. The prediction suggests quenching to take place from top down to segment number 5. Thus, axial segment number 4 provides the cladding with more severe thermal conditions than the peak power segment number 5 does.

Calculations include six cases; i.e., prepressures 0.1, 2.4. and 4.0 MPa, all with 39.4 kW/m and 52.5 kW/m. Cladding surface temperatures, cladding average hoop strains, fuel surface temperatures, fuel centerline temperatures, gas gap thicknesses, rod inside pressures and gap heat transfer coefficients are given for segments 4 and 5 of each case. Results for 39.4 kW/m unpressurized case are seen in Figures 5 - 11. Cladding collapse is predicted (Figure 6). Different clad temperature behavior of segments 4 and 5 due to quenching in segment 4 is obvious from Figure 5.

Figures 12 - 18 give results for 39.4 kW/m power with fuel pin pressurized to 2.4 MPa helium pressure. Clad temperatures decrease slightly with increasing prepressure (Figure 12). Cladding strain essentially consists of thermal strain only (Figure 13). No collapse is predicted. The effect of opening fuel-to-clad gas gap is reflected in the heat transfer coefficient in the manner seen in Figure 18.

In Figures 19 - 25 results for the case with 39.4 kW/m power and 4.0 MPa pressurization are given. Creep/plastic strain contributes markedly to cladding total strain after 10 s (Figure 20). No burst is predicted.

In unpressurized higher power (52.5 kW/m) case (Figures 26 - 32), maximum cladding surface temperature of about 115 K higher than with 39.4 kW/m power is achieved (Figure 26). Cladding collapse is accordingly predicted to occur somewhat earlier (Figure 27). Fuel maximum temperature is 390 K higher than with the lower power.

Introducing 2.4 MPa helium pressure in the 52.5 kW/m case leads to results depicted in Figures. 33 - 39. Cladding sees a permanent hoop strain of 1.6% by the end of the calculation.

Results for 52.5 kW/m, 4.0 MPa pressurization case are given in Figures 40 - 46. Cladding burst to failure is seen (Figure 41). Differential pressure of 5.6 MPa over cladding is seen before failure (Figure 45). In FRAP-T5 a probablistic approach for rod failure is assumed. The probabilities of rod failure versus time as returned by FRAIL subcode are given in Figure 47 for the analyzed cases.

Finally, calculated clad temperatures in pressurized cases versus the differential pressure between the coolant and the rod inside are depicted in Figure 48. Clad burst failure limit has been included for reference. The figure suggests that 52 kW/m case with 2.4 MPa pressurization is not far away from bursting, which actually might have happened if the analysis had been carried on a bit further.

The calculations with higher power have been performed with the same L2-5 thermal hydraulic conditions because these are the only available so far. Elevated power should have some influence on the thermal hydraulic behavior. More appropriate boundary conditions would obviously increase the propensity of the rods to balloon.

tc

cc: L. P. Leach
S. A. Naff
J. R. White
Central File
S. T. Kelppe File (2)

TABLE 1

LOFT FUEL ROD DIMENSIONAL DATA

Fuel pellet outer diameter	9.294 mm
Fuel to clad gap (diameter)	0.190 mm
Clad inside diameter	9.484 mm
Clad thickness	0.62 mm
Rod outer diameter	10.718 mm
Fuel pellet stack length	1.680 m
Fuel density	10126 kg/m^3
	(92.4% of T.D.)
Pellet end dish volume	1.9% of fuel volume
Plenum volume	$5.38.10^{-6}$ m^3
Fuel surface roughness	0.64 µm
Clad inner surface roughness	0.41 µm

TABLE 2

```
         1         2         3         4         5         6         7         8
12345678901234567890123456789012345678901234567890123456789012345678901234567890
     1    1   12    0    5    1    C    0    3    C    0    0    C    C
     0    0    0    0    0    0    6    C    1         0    0    0    0
   0.0      35.
 10126.    .0035     .00056    .015      1.68     .01072    294.     .2
   2.0     1873.                         1.92E-06   0.0        0.0
   1.1
   .02     0.0       .02                                   1.
   0.1     10.0      .1        3.99      .05      4.00     .05      9.96
     1               -45.
             1    1.
      0      0
  .1       .0
   1.      10.       .1        2.99      .5       3.0      .5       9.9
   100  100   50  50  1.       45.
   300.     4500.    300.      2000.
=  L2-5  PRELIMINARY PREDICTION   39.4 KW/M (12 KW/FT)    .1 MPA
01010001  14         2         0.0       1.       260      1.       260
01010200  0          1
01010201  10         .004647   1         .004742  2        .005359
01010301  1          10        3         11       2        13
01010401  .965       1         .967      2        .969     3
01010402  .972       4         .977      5        .983     6
01010403  .992       7         1.003     8        1.015    9
01010404  1.036      10        0.        13
01010601     600.       14
.
    1    28    23
  24.47     0.       24.47     .1        15.30    .2       3.392    .4
  2.271     .6       1.927     .8        1.700    1.       1.553    1.5
  1.482     2.       1.440     2.5       1.408    3.       1.382    3.5
 1.356      4.       1.336     4.5       1.317    5.       1.279    6.
  1.221        8.     1.176    10.       1.093    15.      1.033    20.
  .991      25.      .95       30.       .92      35.      .890     40.
  .871      45.      .837      50.       .793     60.      .757     70.
  .582      0.0      .714      .076      1.026    .152     1.260    .229
 1.440      .305     1.525     .381      1.489    .457     1.605    .533
  1.621     .610     1.572     .686      1.483    .762     1.357    .638
  1.204     .914     1.131     .991      1.016    1.067    .880     1.143
  .744      1.219    .556      1.295     .414     1.372    .305     1.448
 .205       1.524    .125      1.600     .073     1.676
    4
  .41       .64                12    1    50
    1   25           5.38E-06     .1E06   .0762    .0091    .0014    294.
  1.0
    1
    5
  0.          40.    5.        TIME (SEC)        L2-5 HOT PIN 12 KW/M .1 MPA
  500.      1200.    5.                 SURFACE TEMPERATURE (K)
  500.      2200.    6.        FUEL CENTERLINE TEMPERATURE (K)
  0.          2.E07  10.                INTERNAL PRESSURE (PA)
  -0.01     0.01     10.                CLADDING HOOP STRAIN
         1         2         3         4         5         6         7         8
12345678901234567890123456789012345678901234567890123456789012345678901234567890
```

45

LTR LO-14-80-069

TABLE 2 (CONT'D)

```
1234567890123456789012345678901234567890123456789012345678901234567890123456789012345678901234567890
   0.          .02         5.        FUEL STACK LENGTH CHANGE (M)
   0.          0.01        8.         CLADDING AXIAL LENGTH CHANGE (M)
   4.          25.         5.            LOCAL LINEAR ROD POWER (KW/M)
 500.        1400.         5.            FUEL PELLET SURFACE TEMP (K)
   0.       50000.         8.            GAP H.T.C. (W/M**2-K)
  10.         1.E06        8.            SURFACE H.T.C. (W/M**2-K)
 500.        1200.         10.           AVERAGE CLADDING TEMP (K)
   0.          55.      5.              HEAT OUT (KW/M)
   0.           2.E07     10.           PLENUM PRESSURE (PA)
   0.         900.         10.           PLENUM TEMPERATURE (K)
   0.         .001         10.           GAS FLOW FROM PLENUM (MOL/SEC)
   0.      1000000.        10.           MASS FLUX
   0.          1.          10.       QUALITY
   0.        160.E+05      8.        COOLANT PRESSURE (PA)
   0.        .0001         5.        GAP THICKNESS (M)
 200.        700.       5.           BULK COOLANT TEMPERATURE (K)

1234567890123456789012345678901234567890123456789012345678901234567890123456789012345678901234567890
66 INPUT CARDS
```

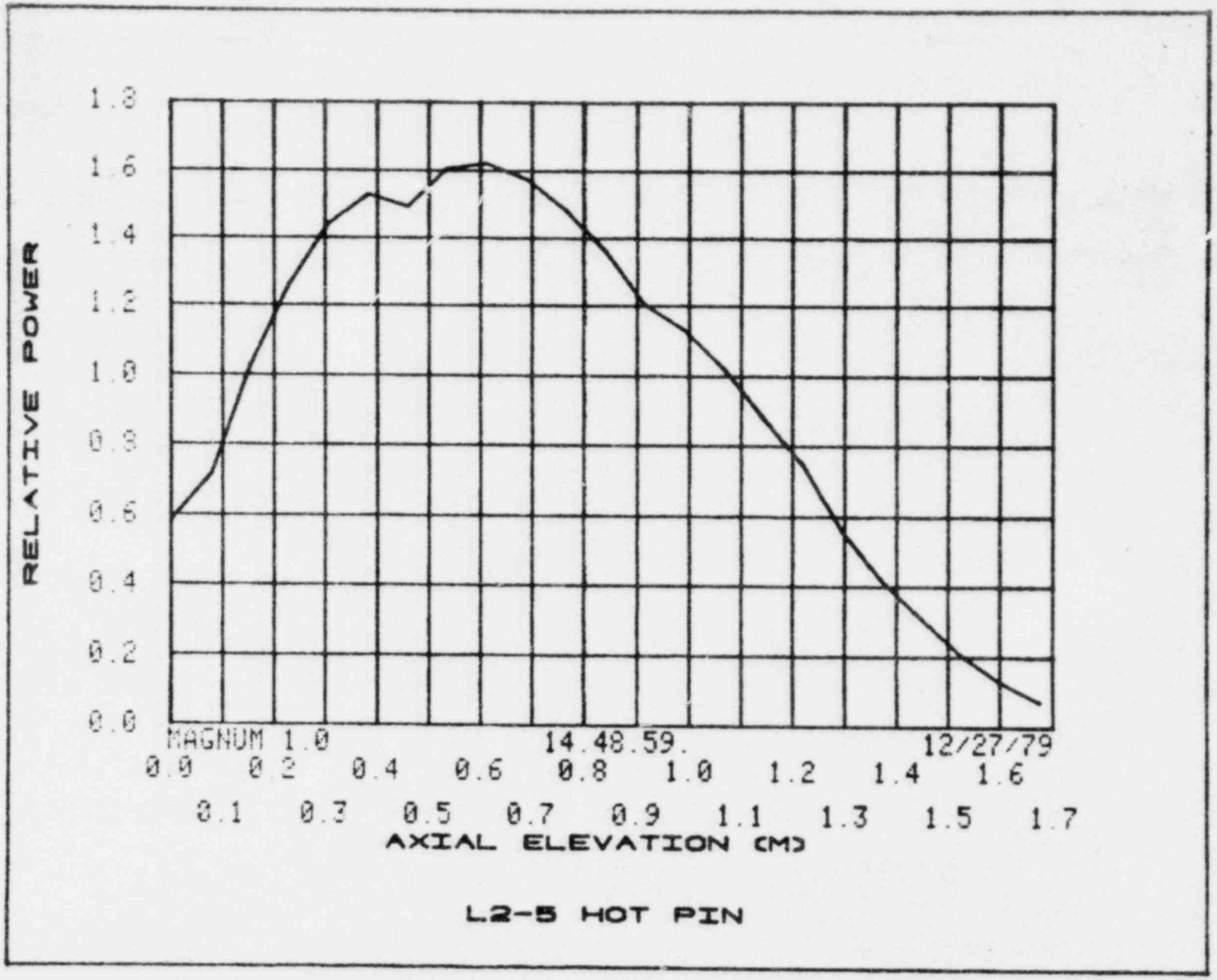

FIG. 1 Axial power profile

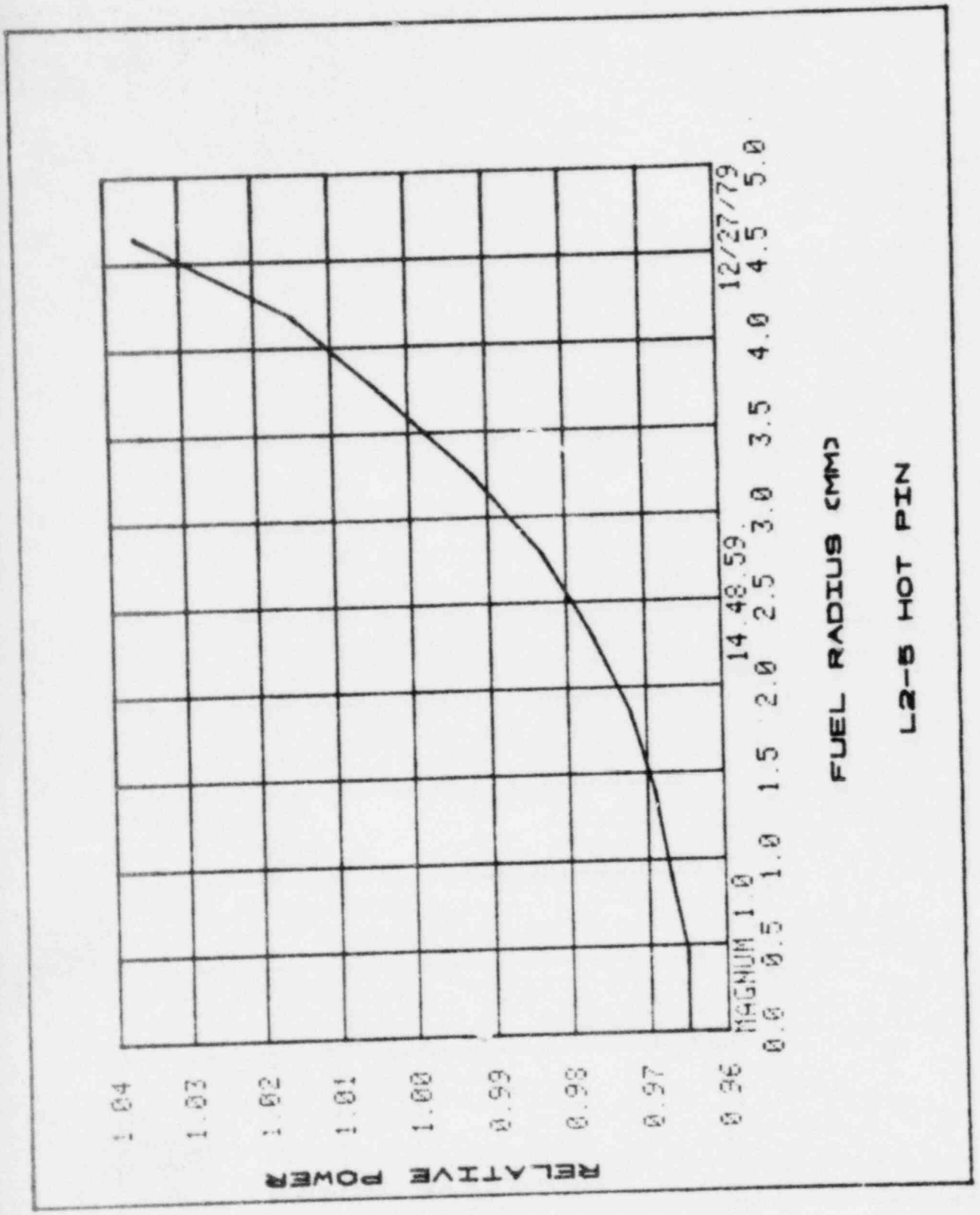

FIG. 2 Radial distribution of the power density in the fuel.

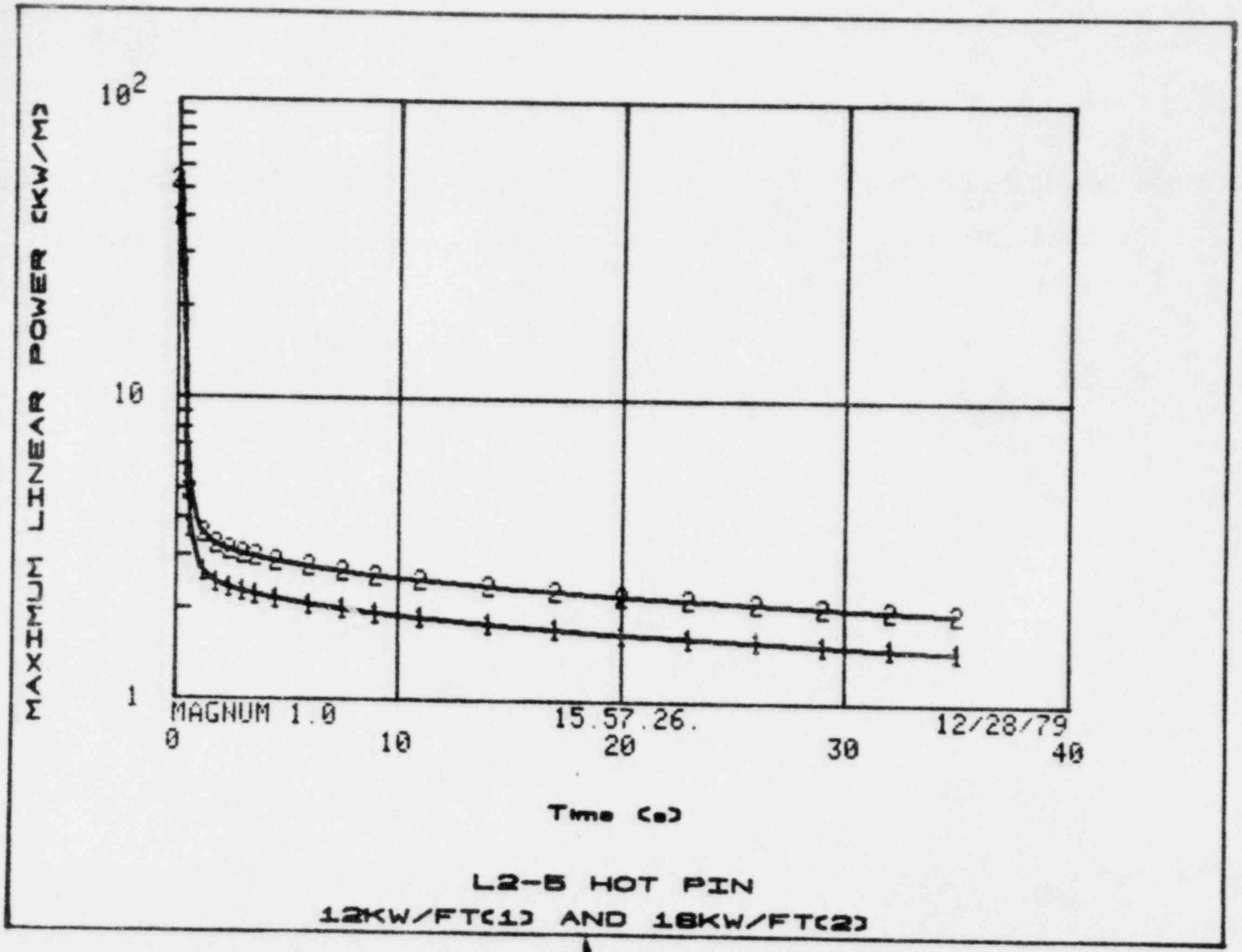

FIG. 3 Rod maximum linear power vs. time.

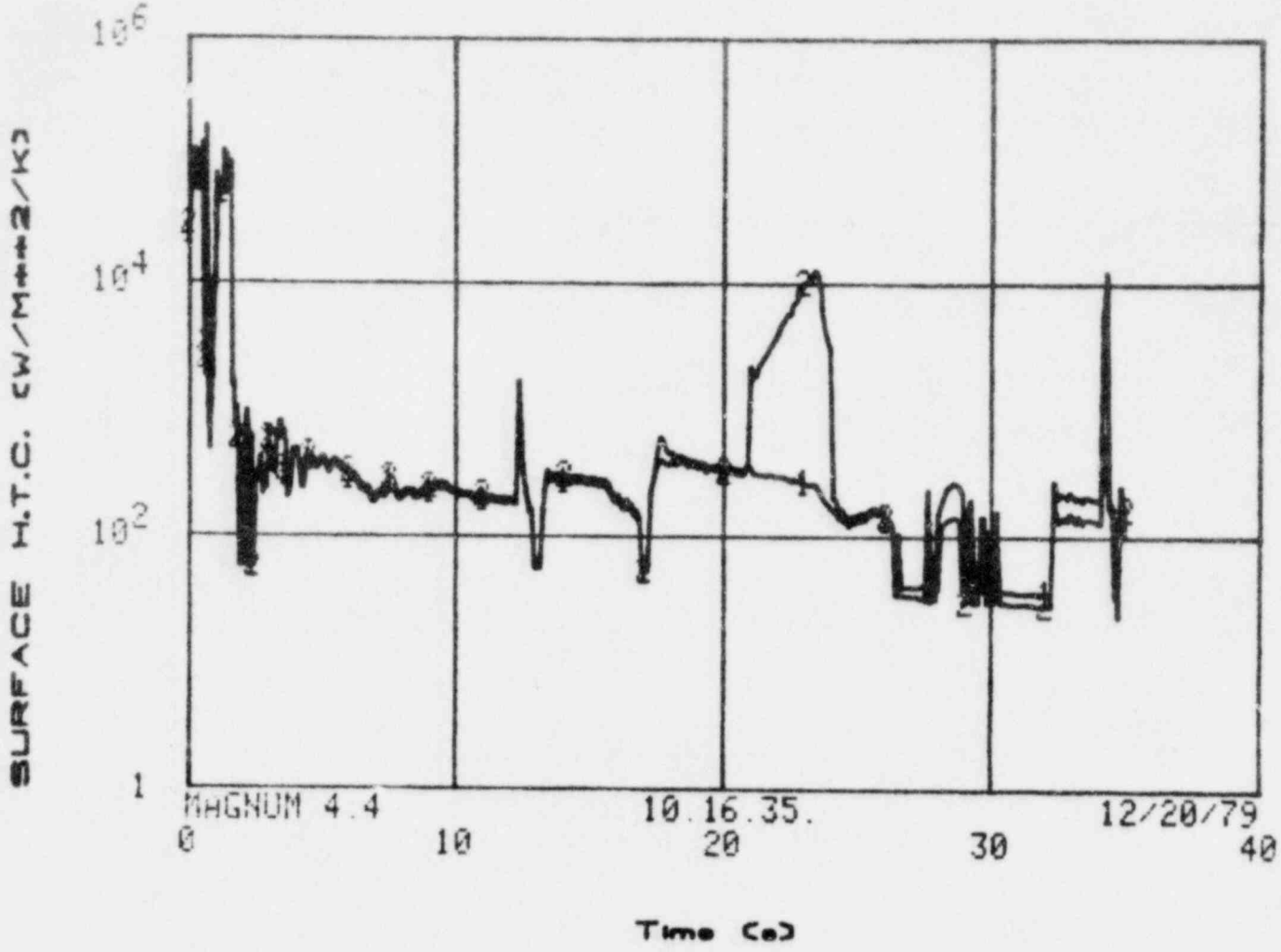

FIG. 4. Rod surface heat transfer coefficient from RELAP4 preliminary prediction for L2-5 hot pin.

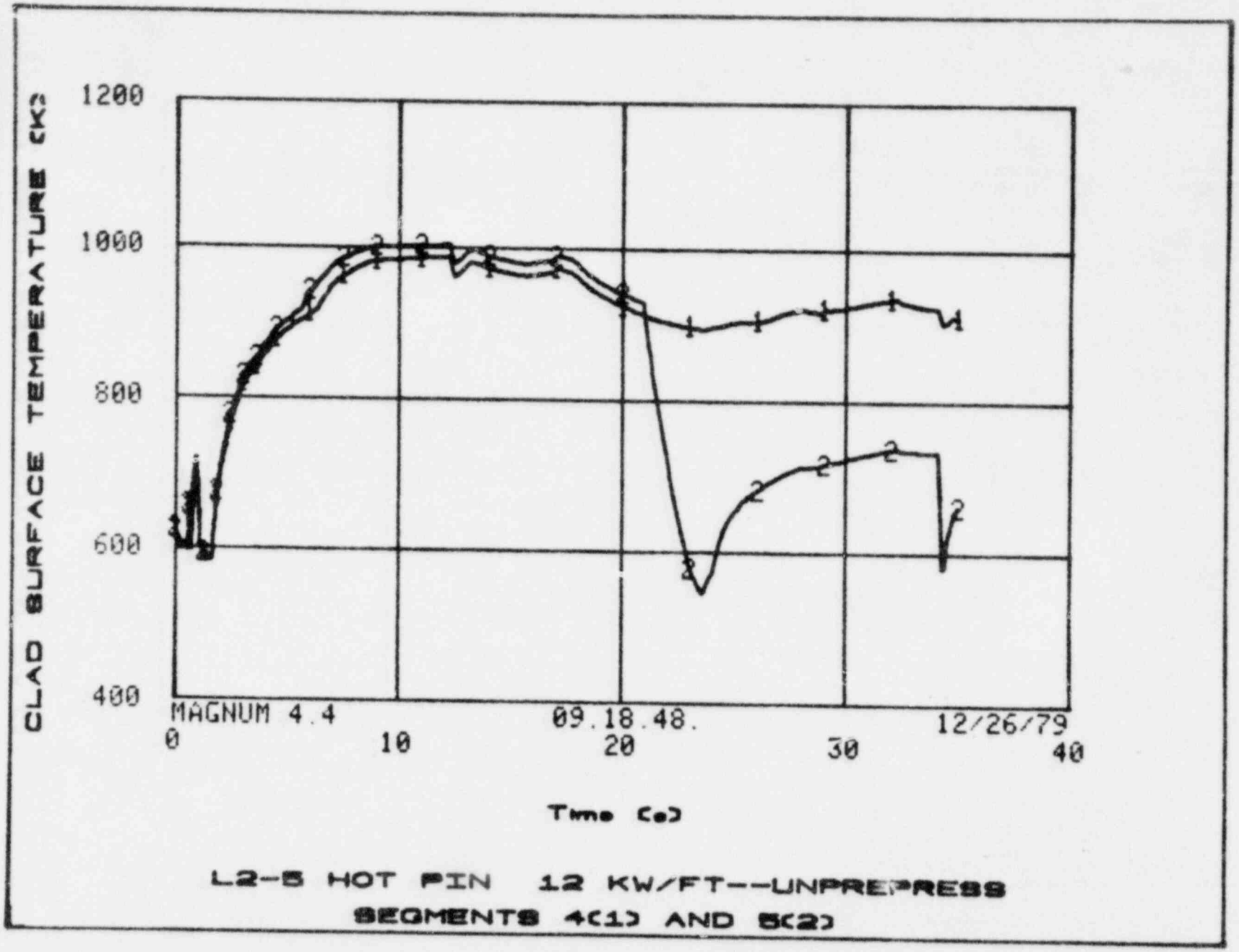

FIG. 5 Clad surface temperatures with 39.4 kW/m initial power and unpressurized rod.

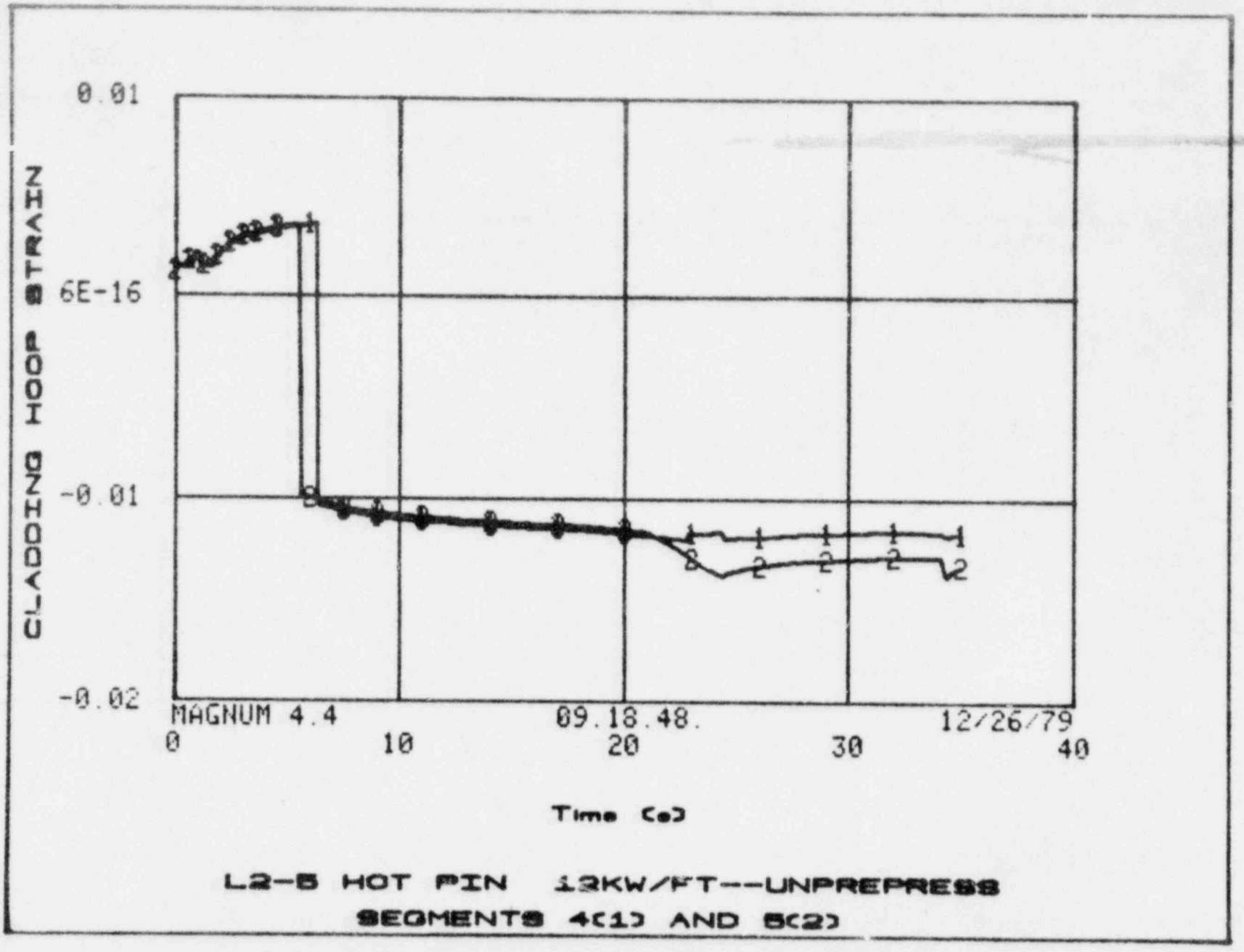

FIG. 6 Cladding average hoop strain with 39.4 kW/m initial power and unpressurized rod

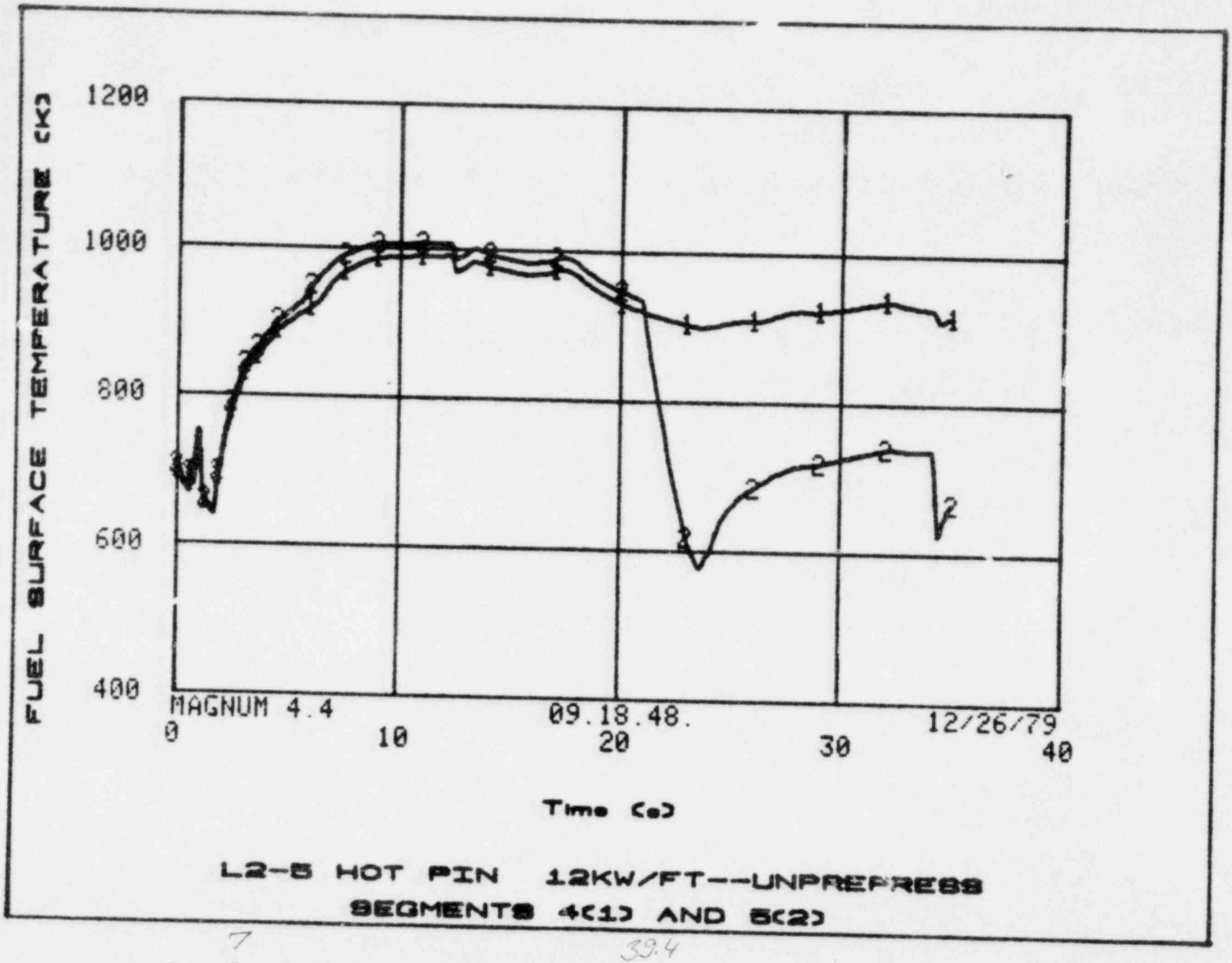

7 39.4

FIG. 7 Fuel surface temperature with 39.4 kW/m initial power and unpressurized rod

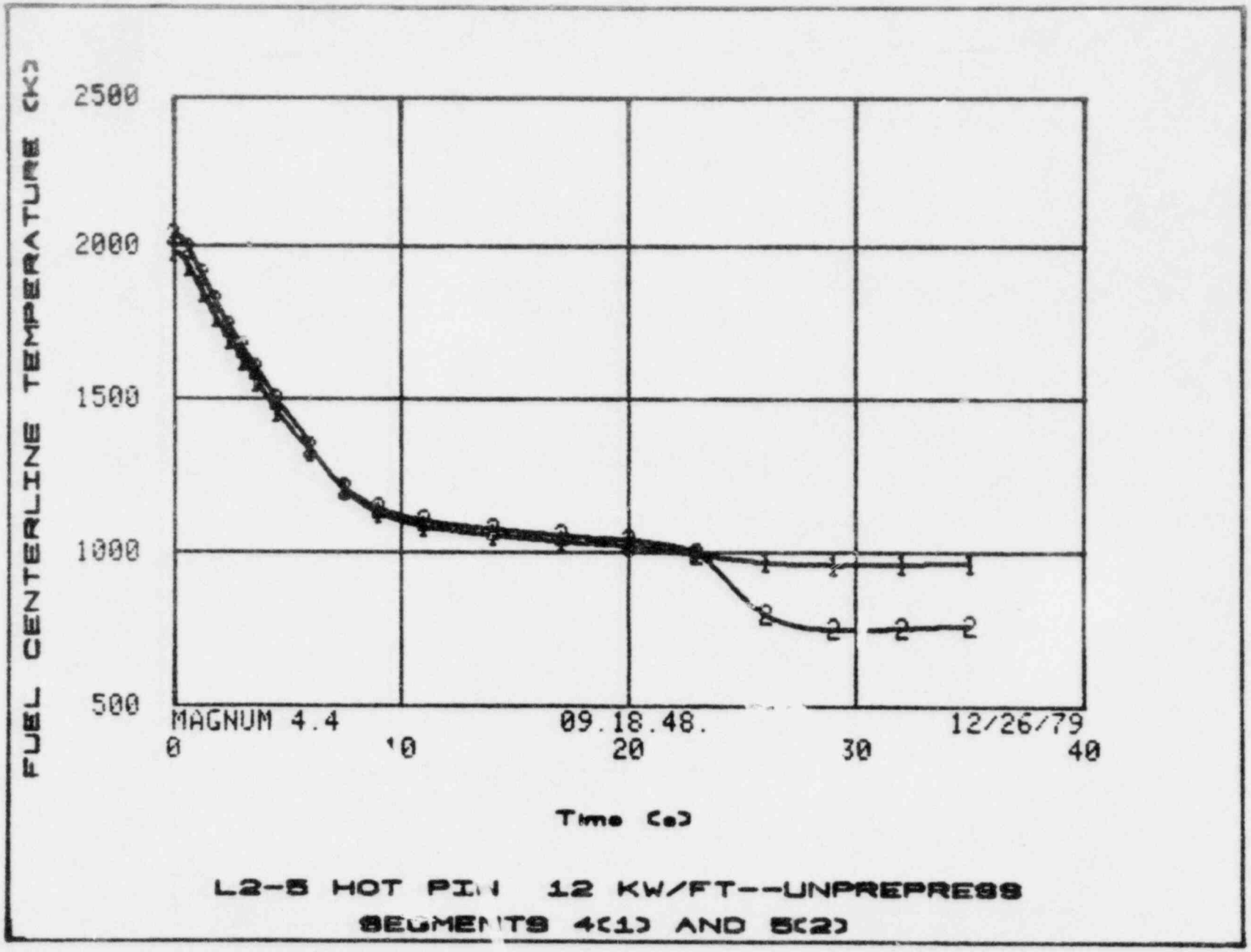

FIG. 8 Fuel centerline temperature with 39.4 kW/m initial power and unpressurized rod

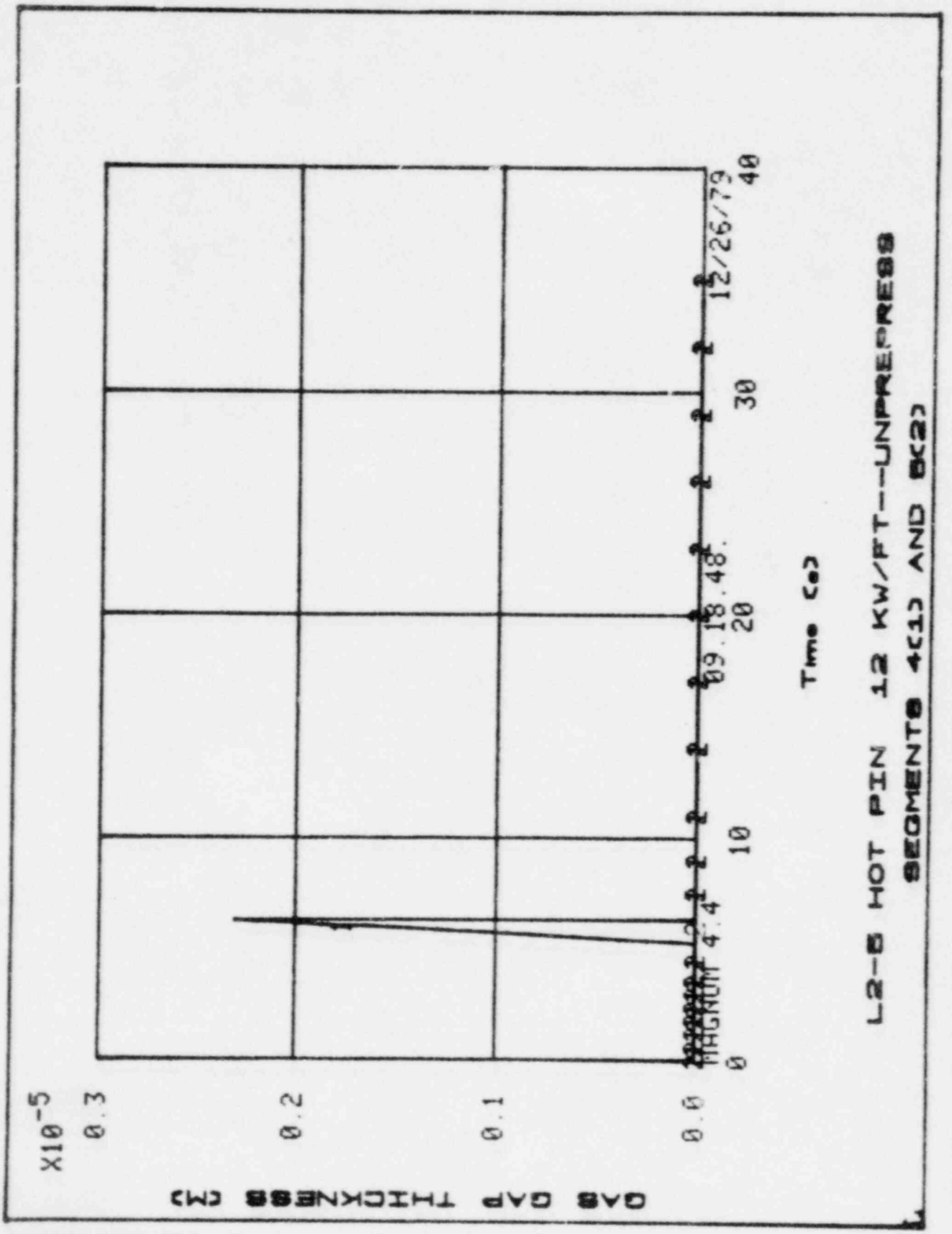

FIG. 9 Fuel-to-clad gap width (radial) with 39.4 kW/m initial power and unpressurized rod

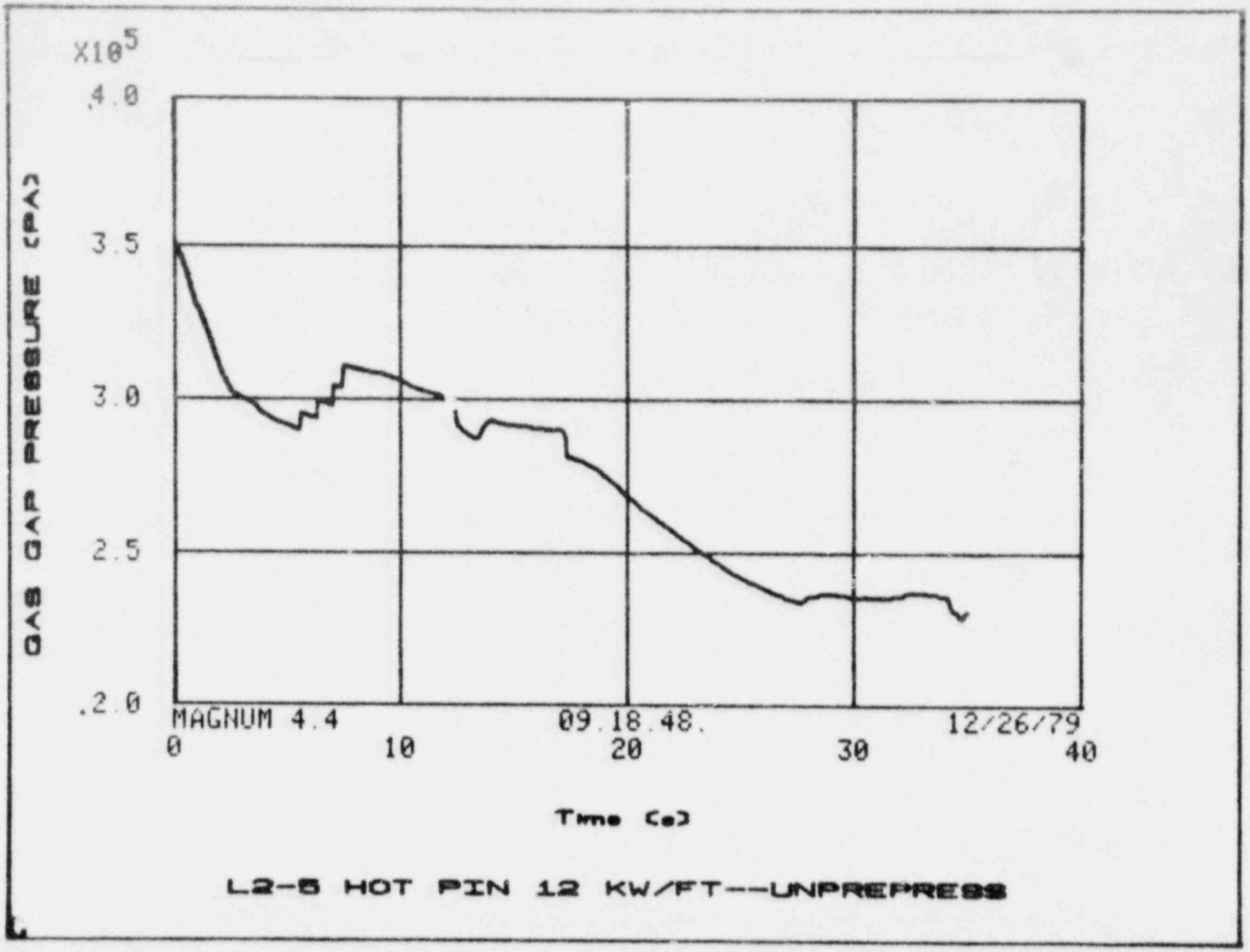

FIG. 10 Rod internal gas pressure with 39.9 kW/m initial power and unpressurized rod

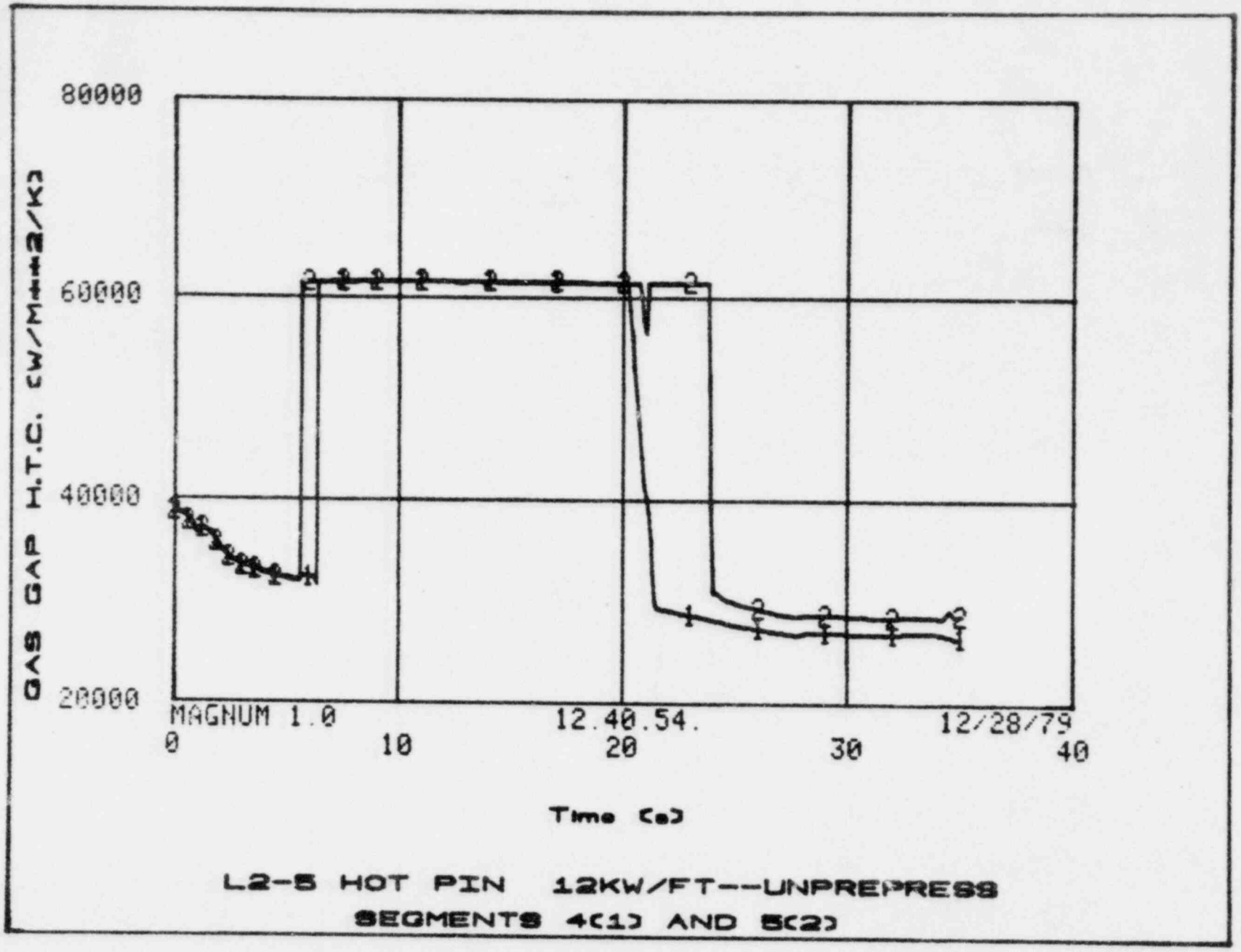

FIG. 11 Fuel-to-clad gap heat transfer coefficient with 39.4 kW/m initial power and unpressurized rod

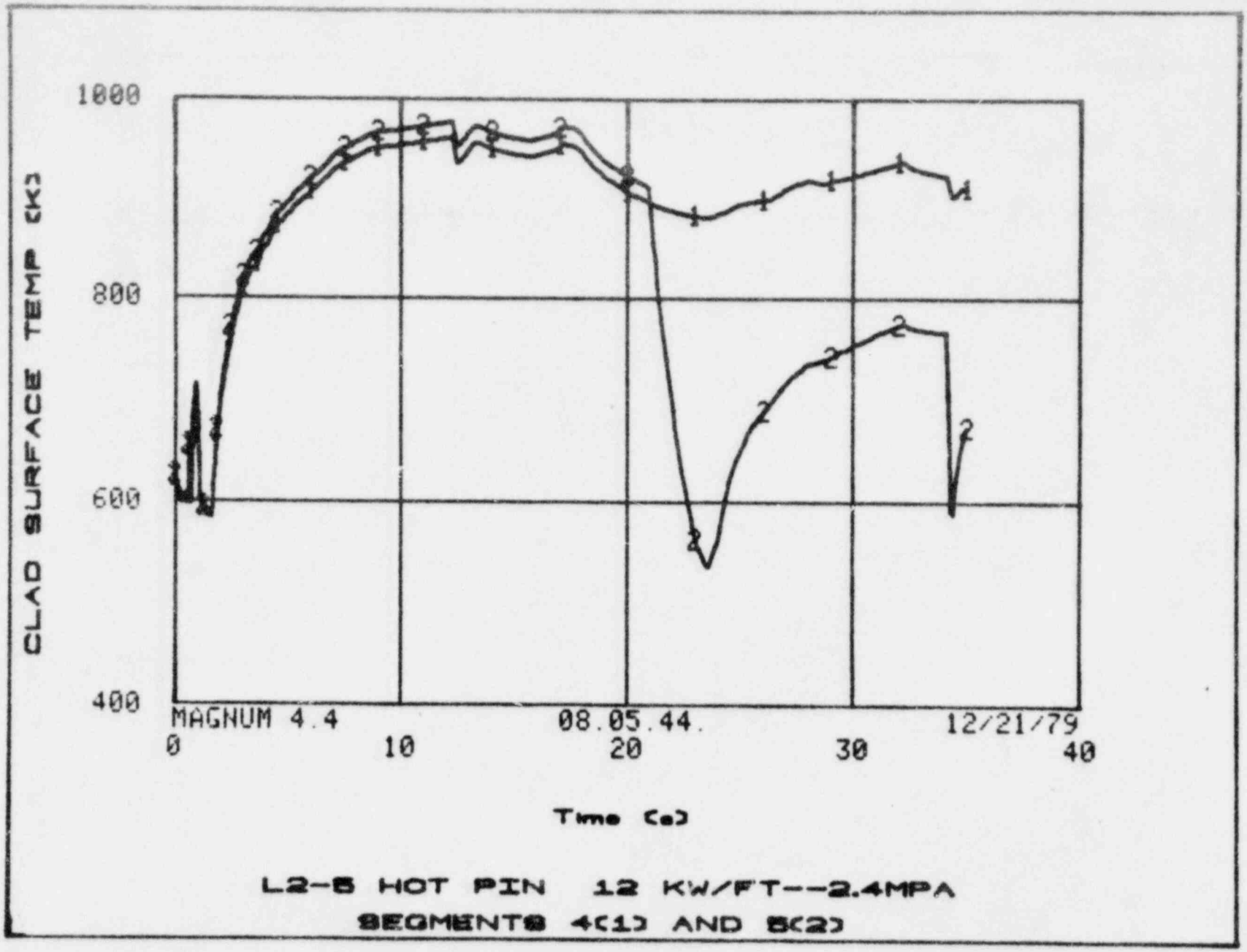

FIG. 12 Clad surface temperatures with 39.4 kW/m initial power and 2.4 MPa pressurization

LTR LO-14-80-069

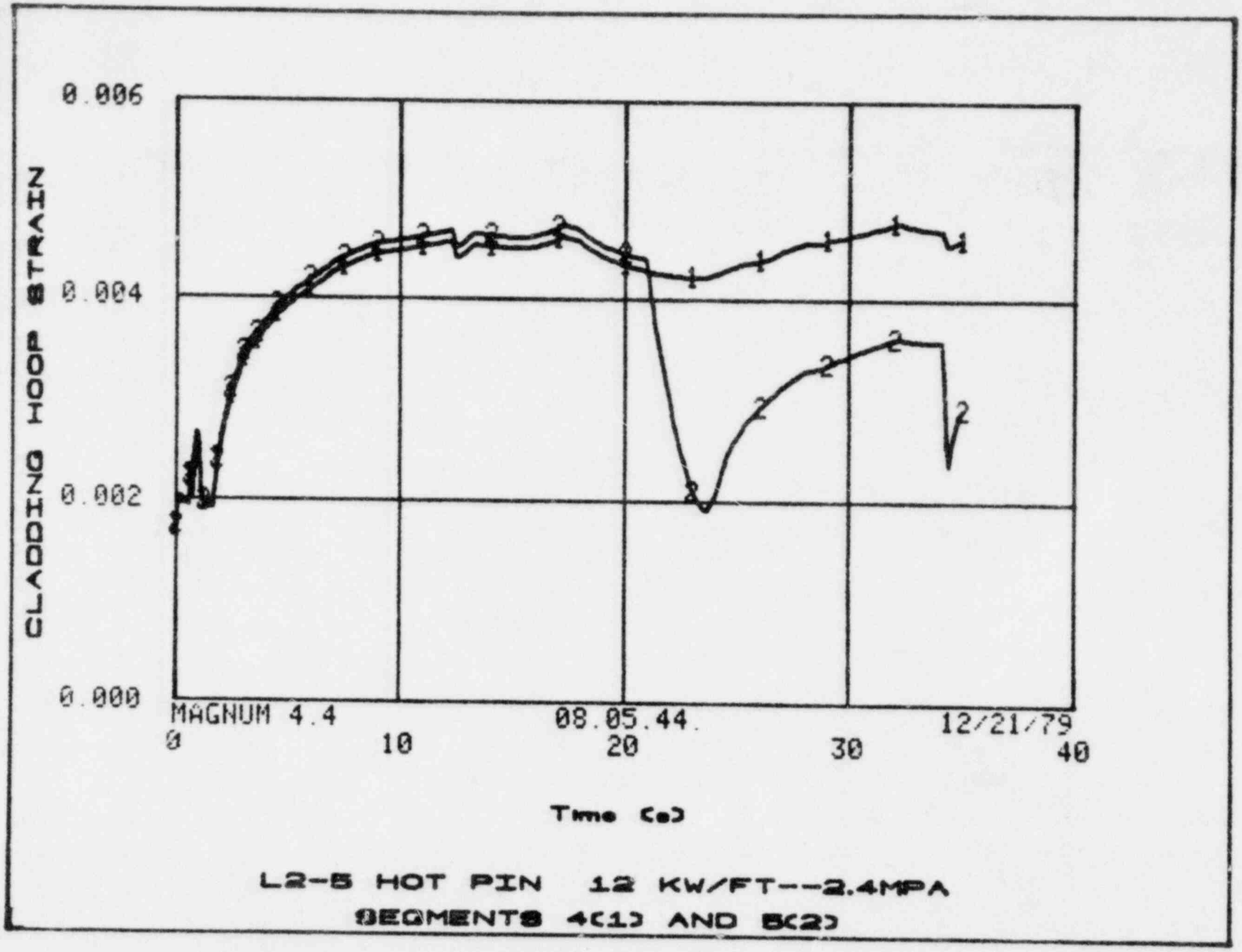

FIG. 13 Cladding average hoop strain with 39.4 kW/m initial power and 2.4 MPa pressurization

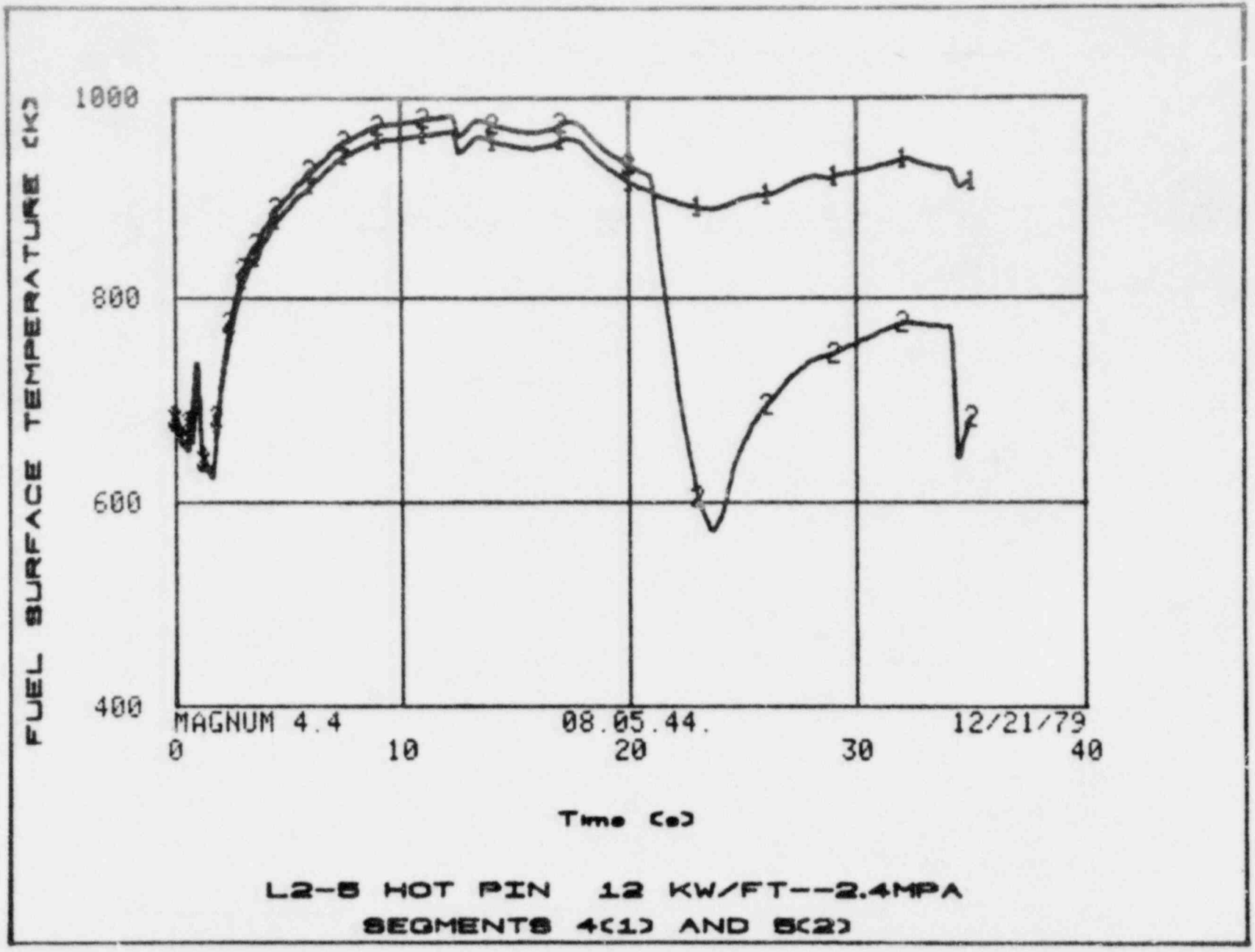

FIG. 14 Fuel surface temperature with 39.4 kW/m initial power and 2.4 MPa pressurization

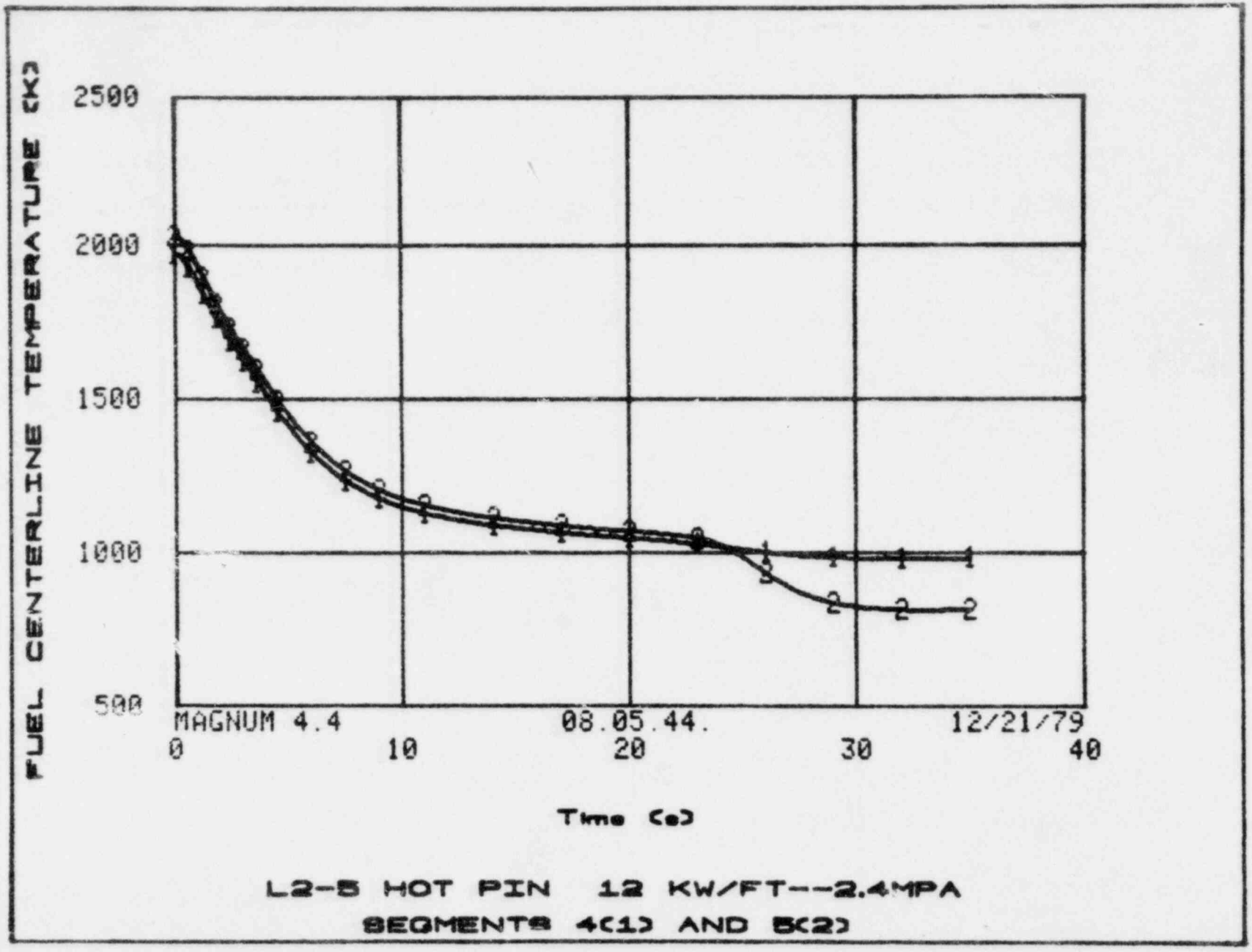

FIG. 15 Fuel centerline temperature with 39.4 kW/m initial power and 2.4 MPa pressurization

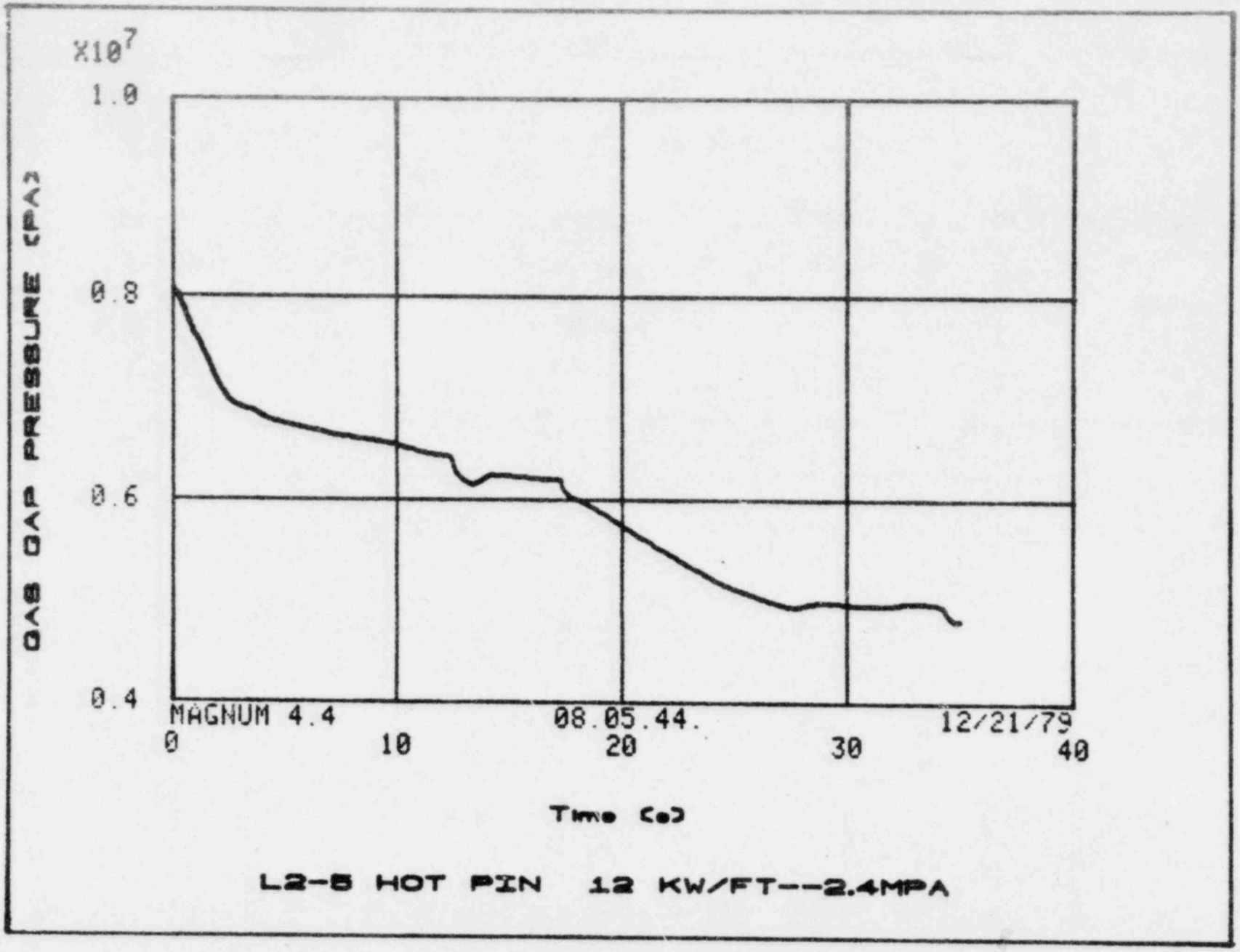

FIG. 16 Rod internal gas pressure with 39.4 kW/m initial power and 2.4 MPa pressurization

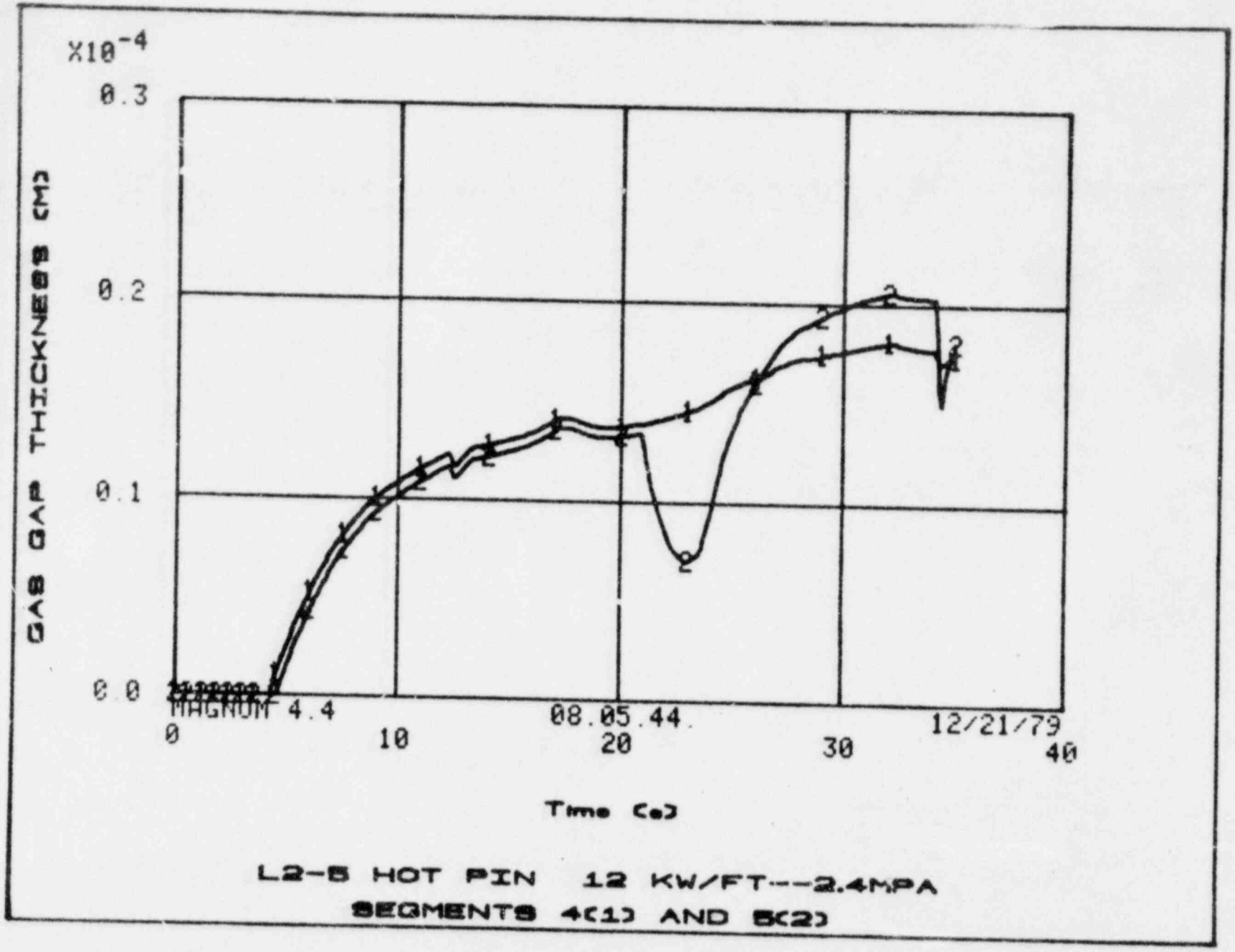

FIG. 17 Fuel-to-clad gap width (radial) with 39.4 kW/m initial power and 2.4 MPa pressurization

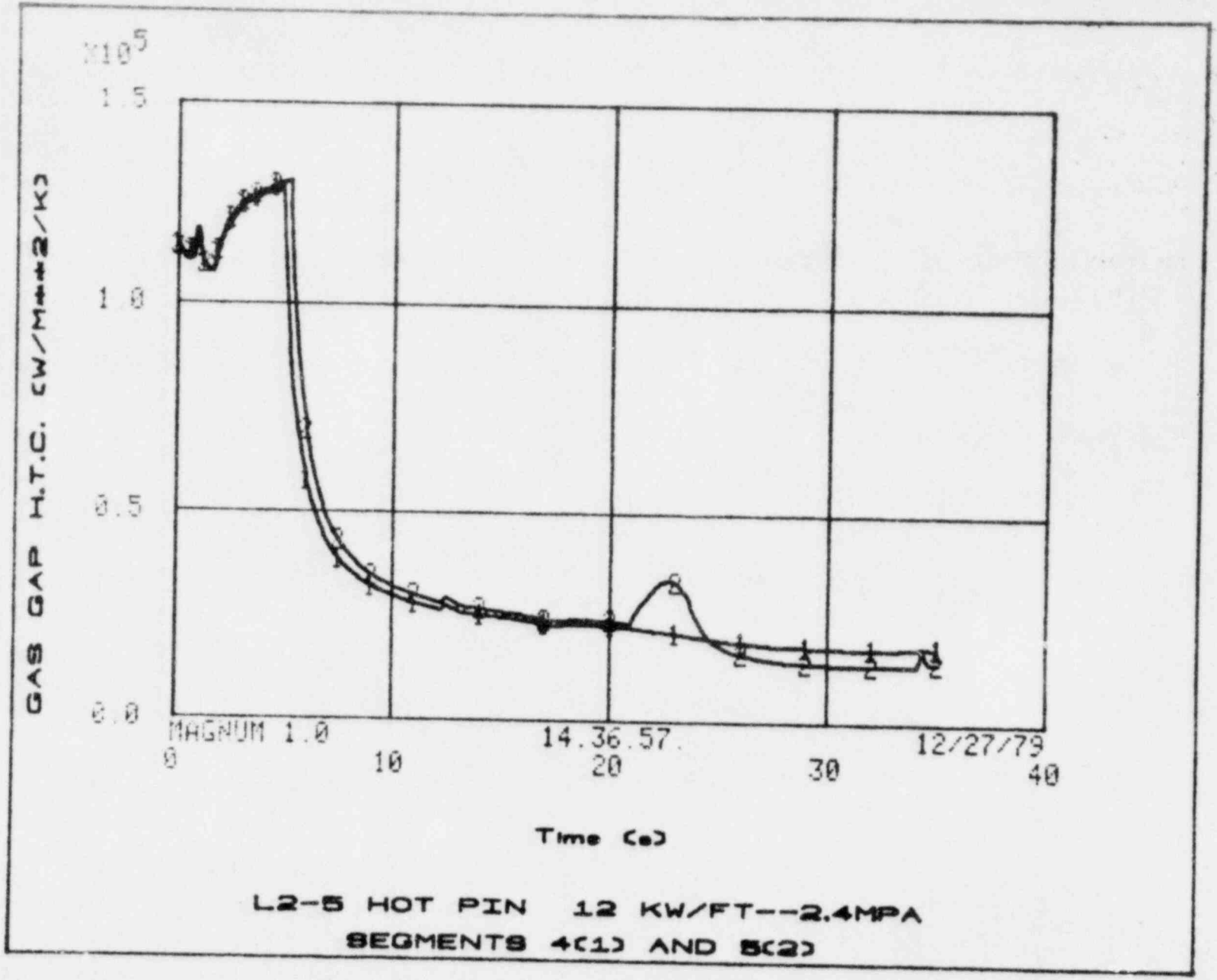

FIG. 18 Fuel-to-clad gap heat transfer coefficient with 39.4 kW/m initial power and 2.4 MPa pressurization

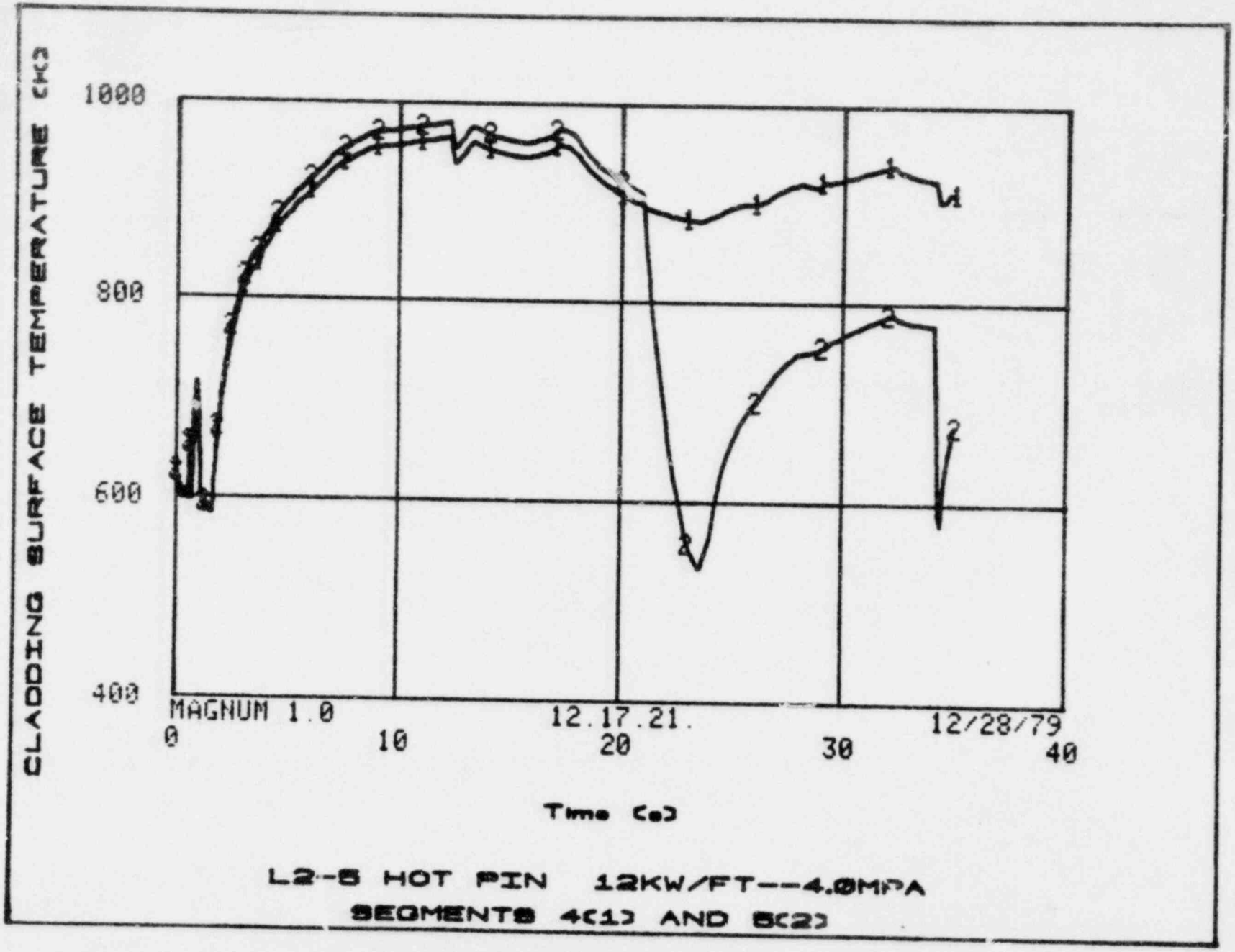

FIG. 19 Clad surface temperatures with 39.4 kW/m initial power and 4.0 MPa pressurization

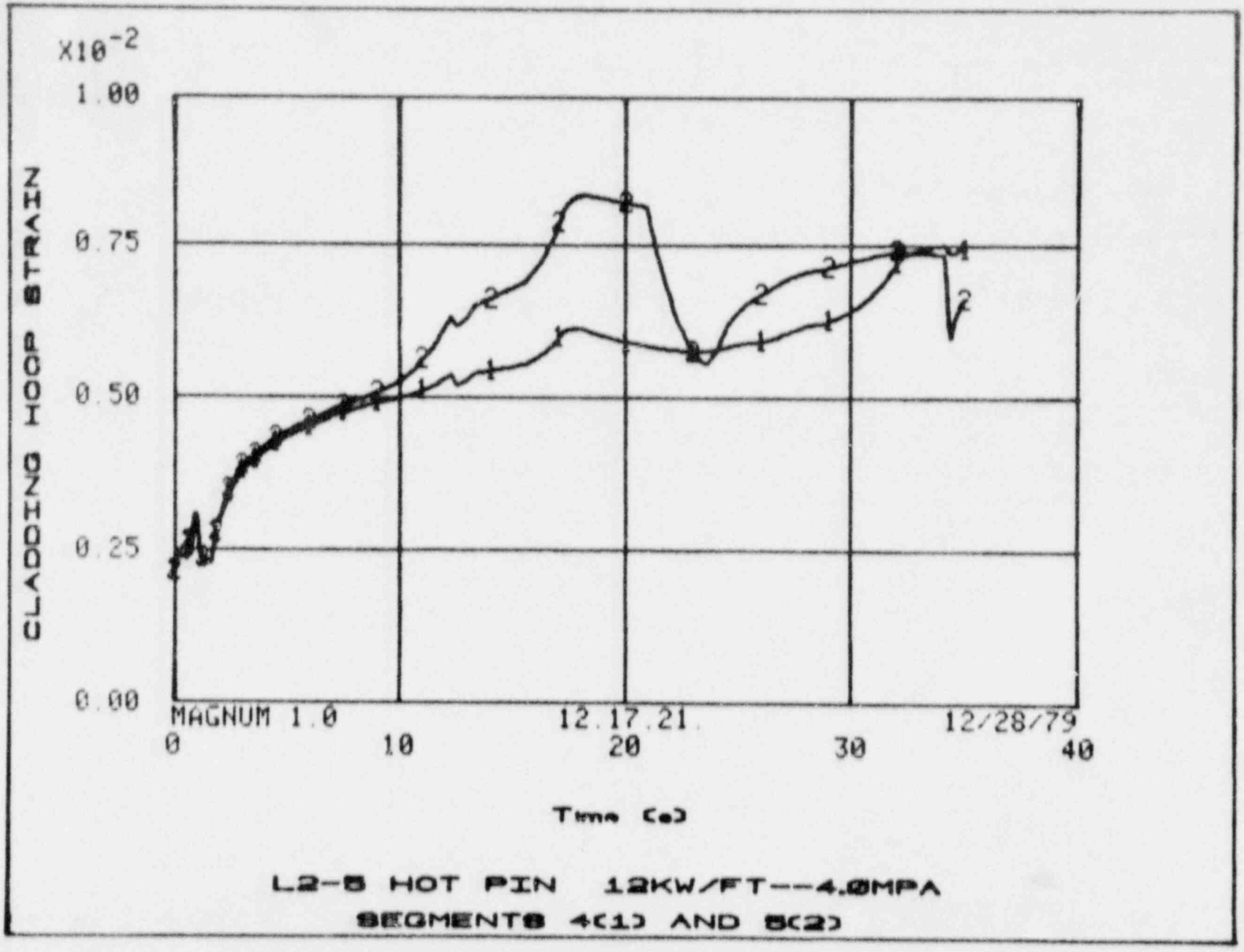

FIG. 20 Cladding average hoop strain with 39.4 kW/m initial power and 4.0 MPa pressurization

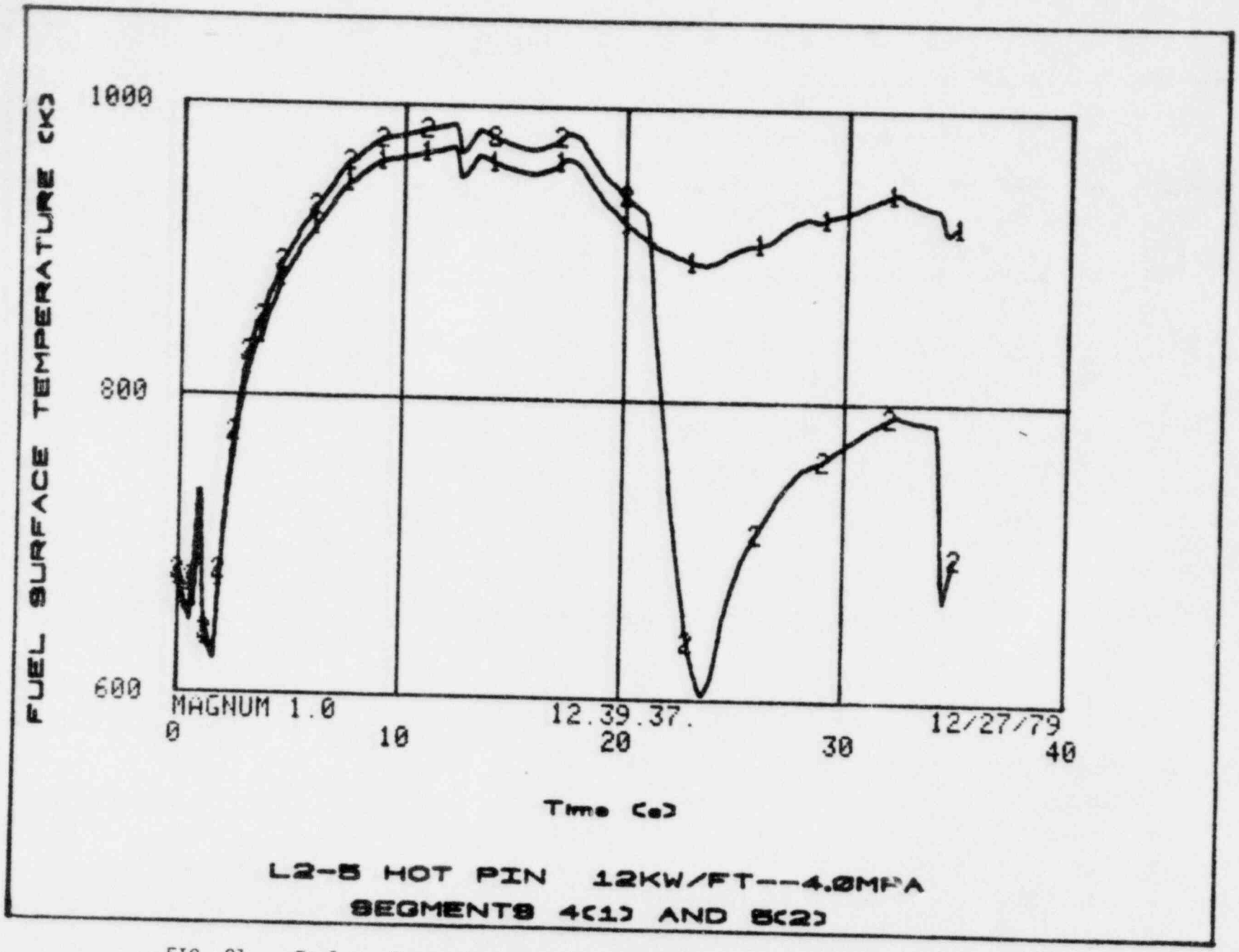

FIG. 21 Fuel surface temperature with 39.4 kW/m initial power and 4.0 MPO+pressurization

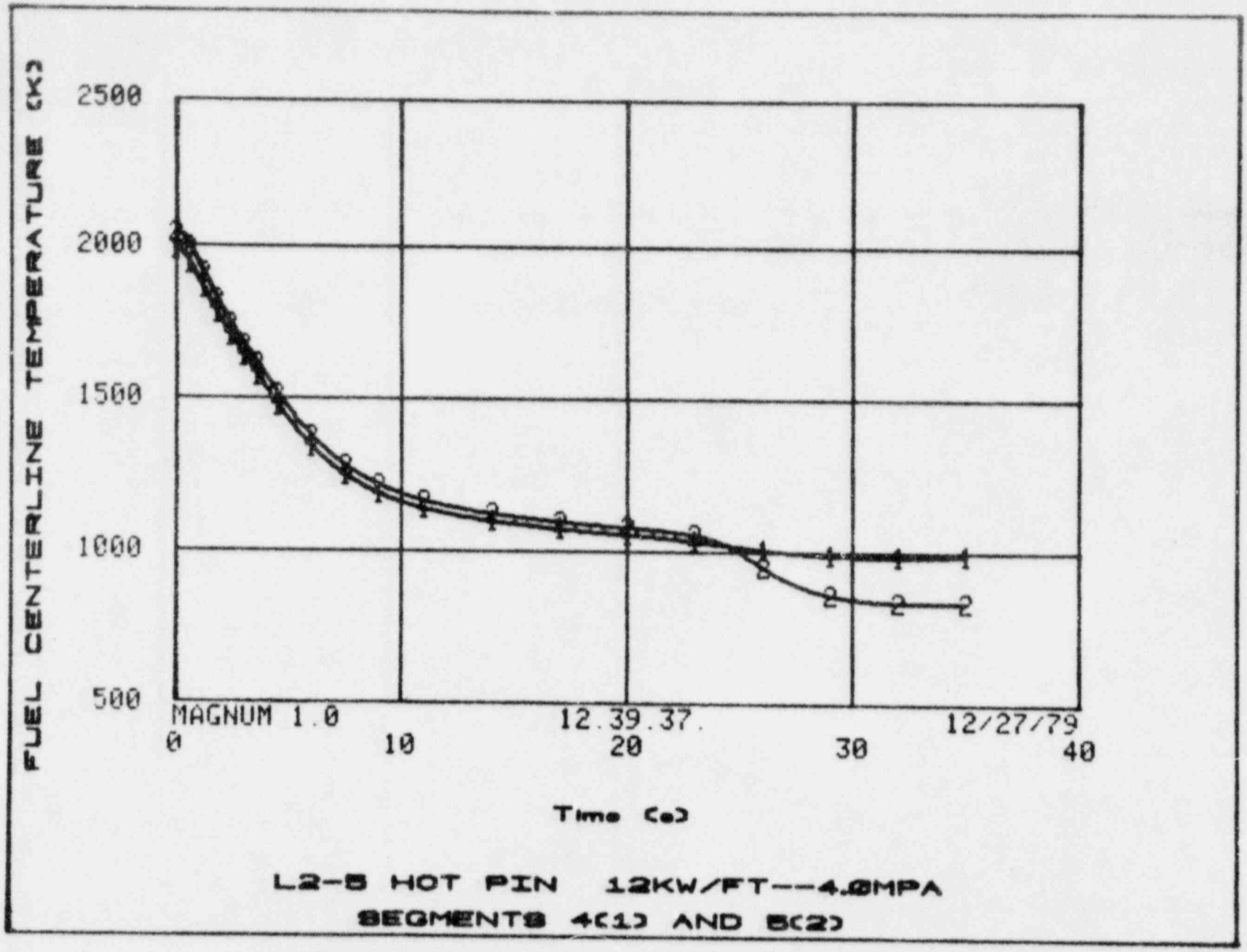

FIG. 22 Fuel centerline temperature with 39.4 kW/m initial power and 4.0 MPa pressurization

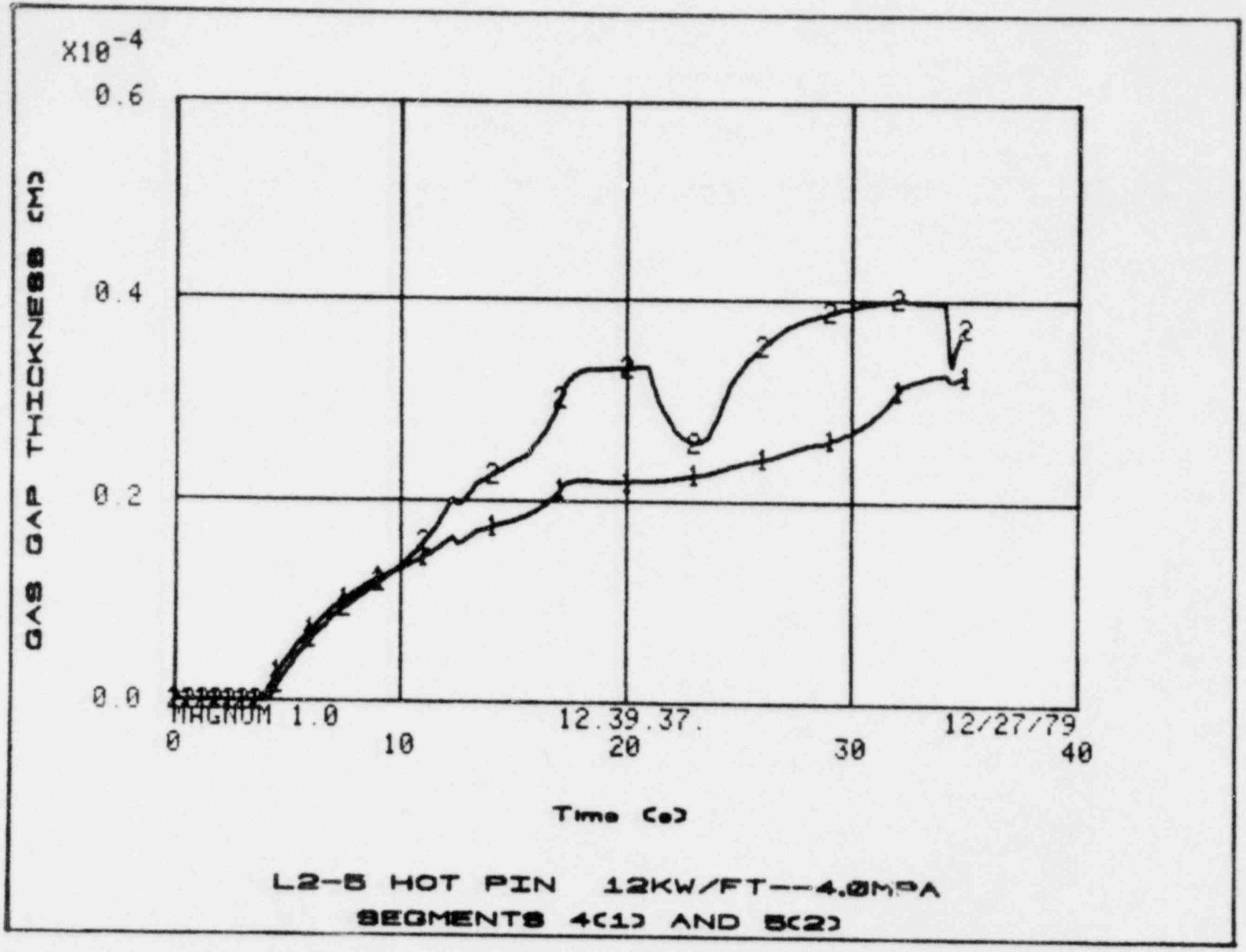

FIG. 23 Fuel-to-clad gap width (radial) with 39.4 kW/m initial power and 4.0 MPa pressurization

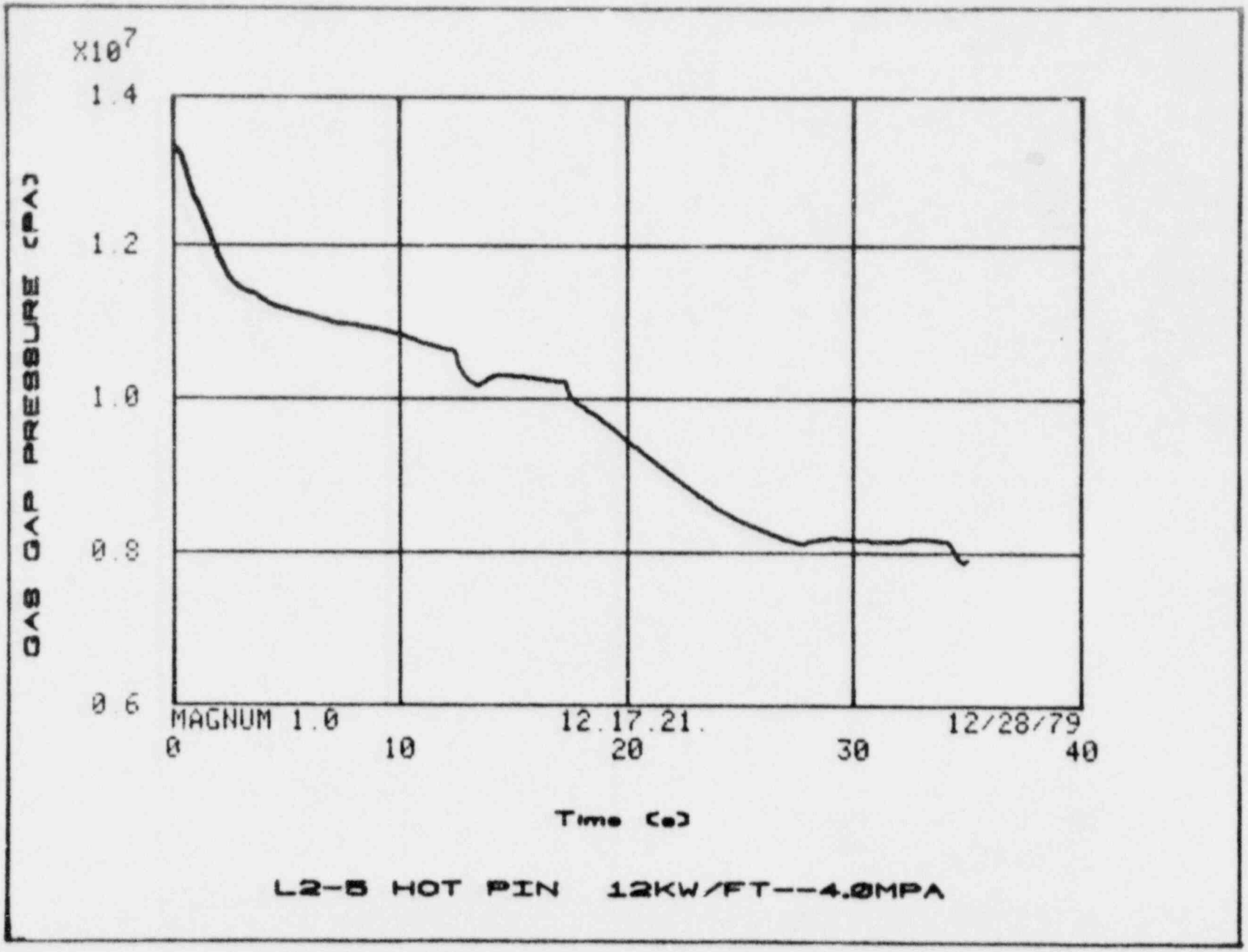

FIG. 24 Rod internal gas pressure with 39.4 kW/m initial power and 4.0 MPa pressurization

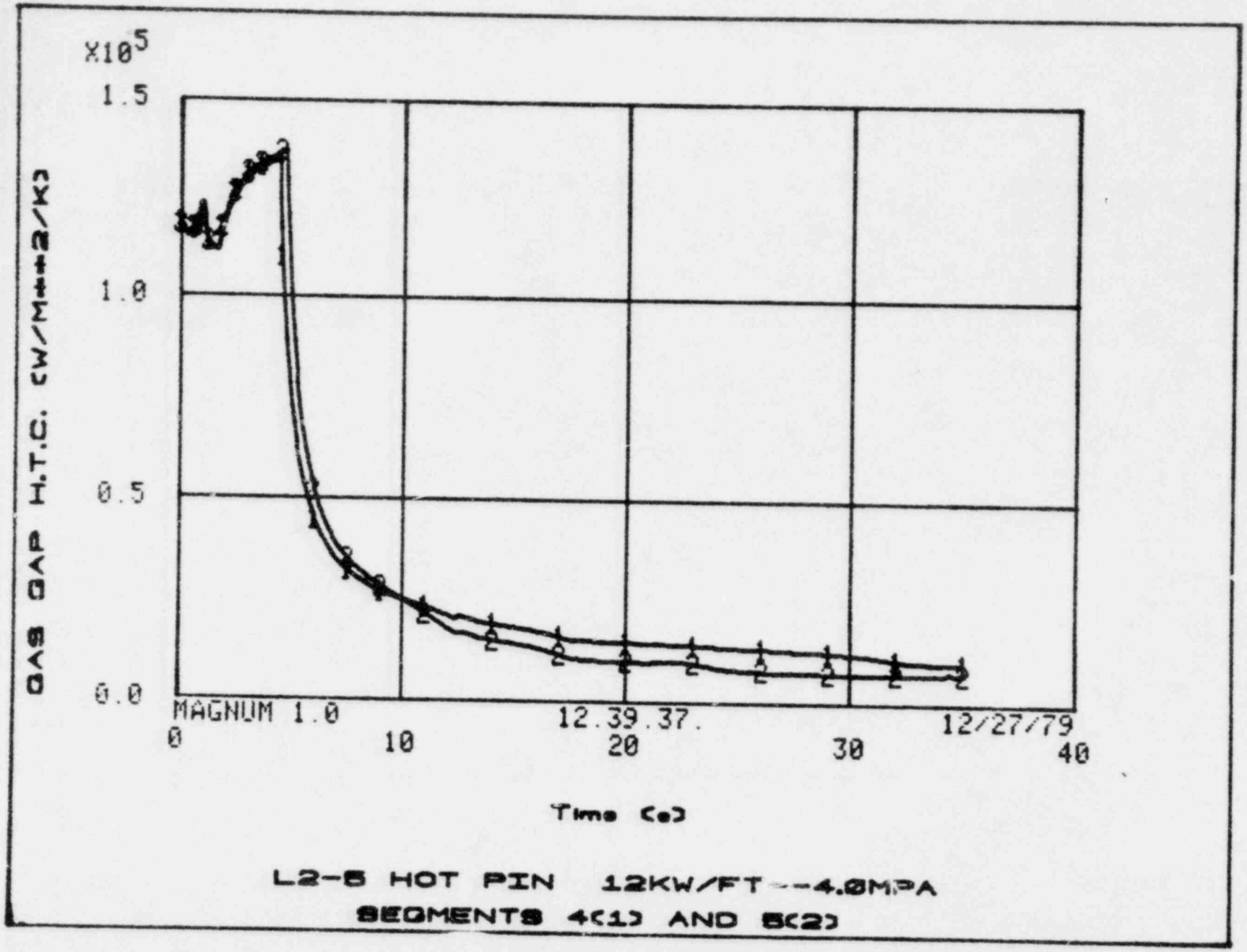

FIG. 25 Fuel-to-clad gap heat transfer coefficient with 39.4 kW/m initial power and 4.0 MPa pressurization

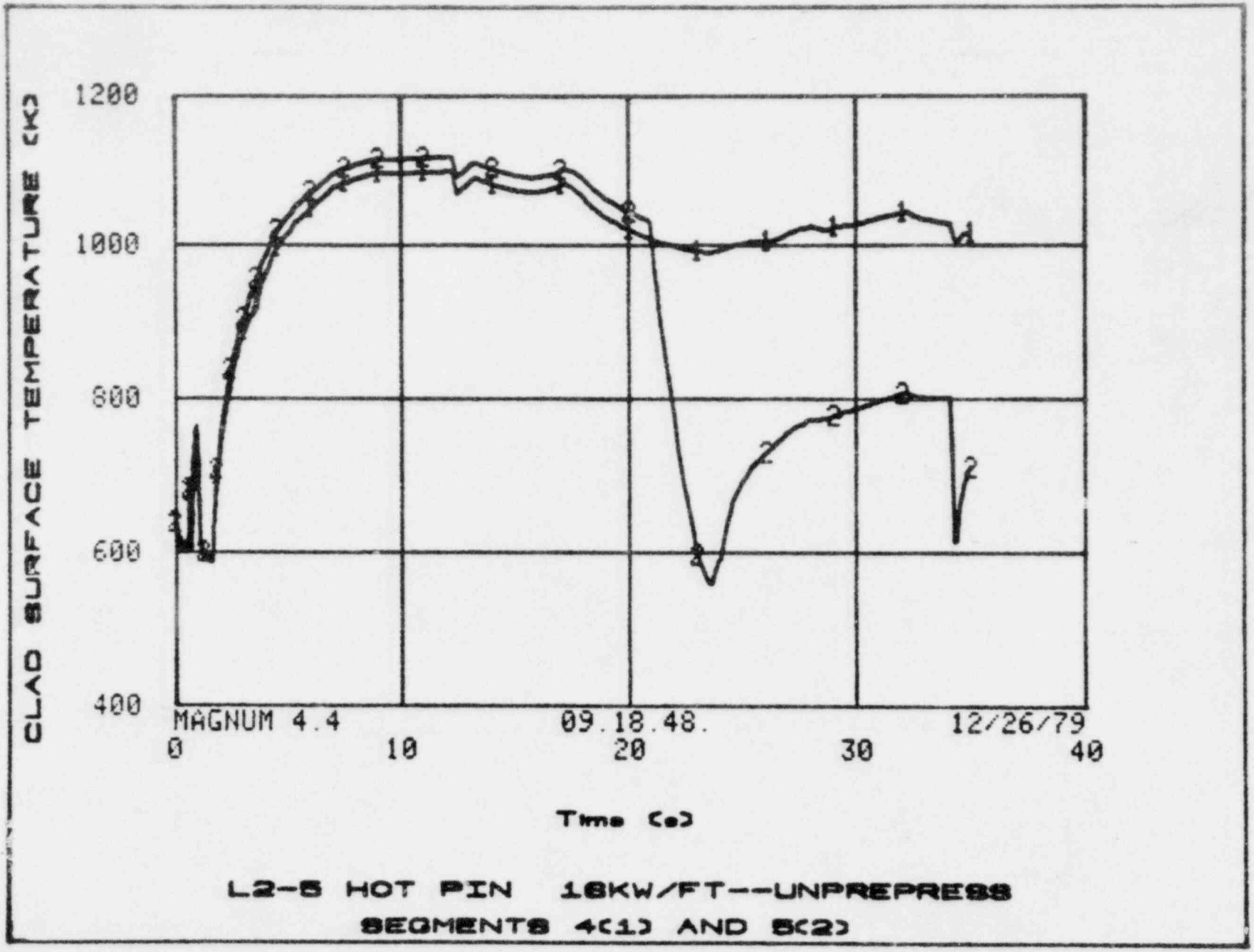

FIG. 20 Clad surface temperatures with 52.5 kW/m initial power and unpressurized rod

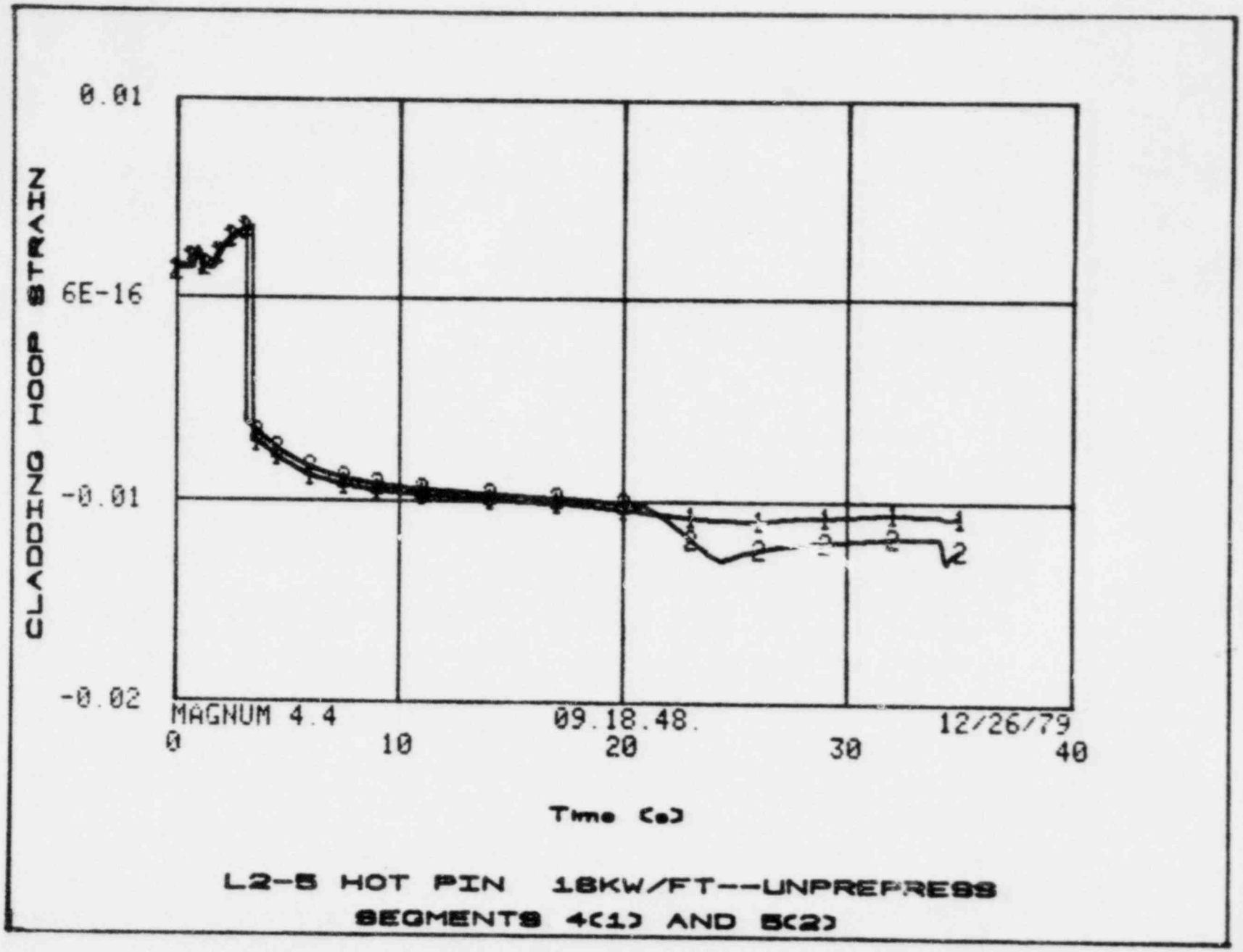

FIG. 27 Cladding average hoop strain with 52.5 kW/m initial power and unpressurized rod

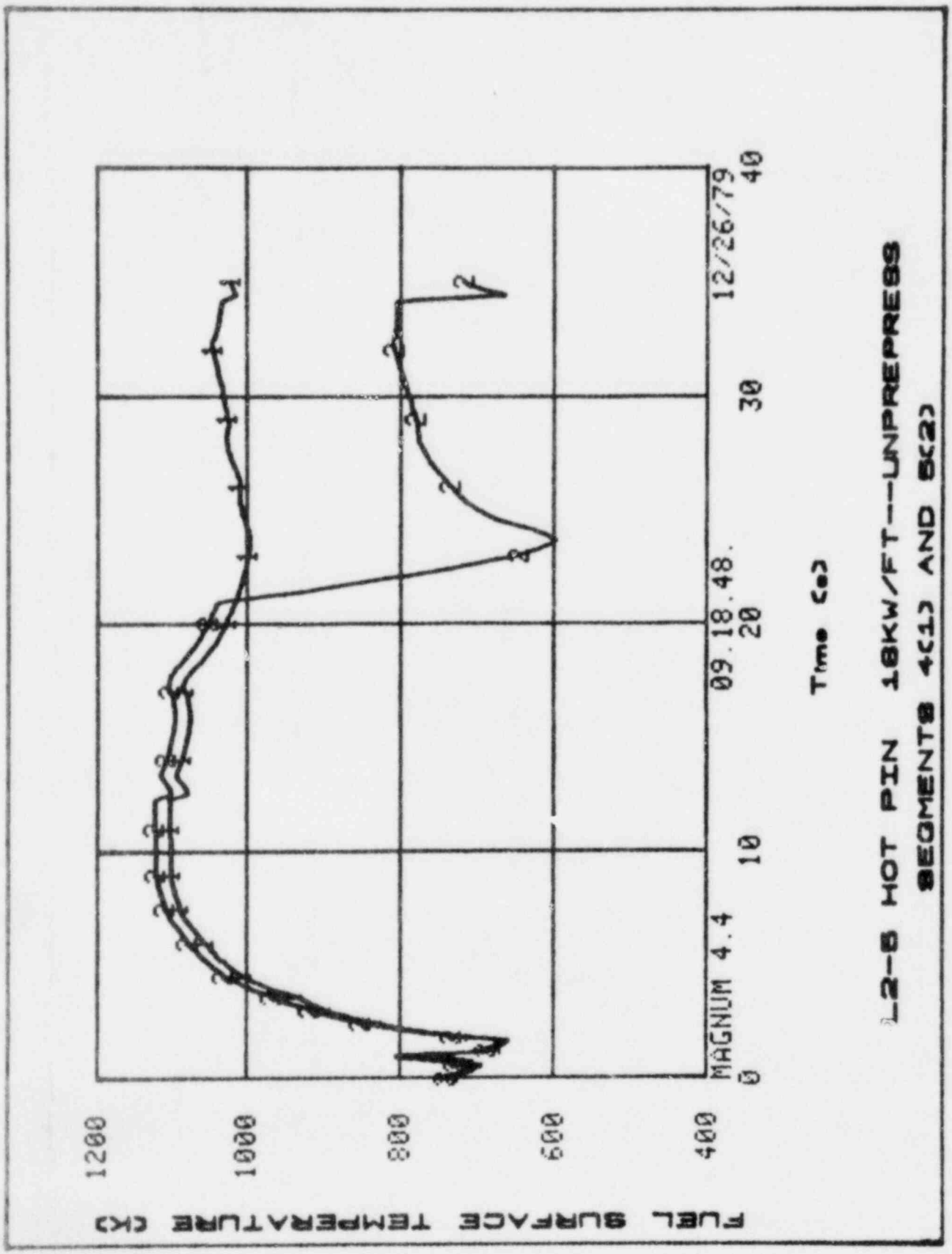

FIG. 28 Fuel surface temperature with 52.5 kW/m initial power and unpressurized rod

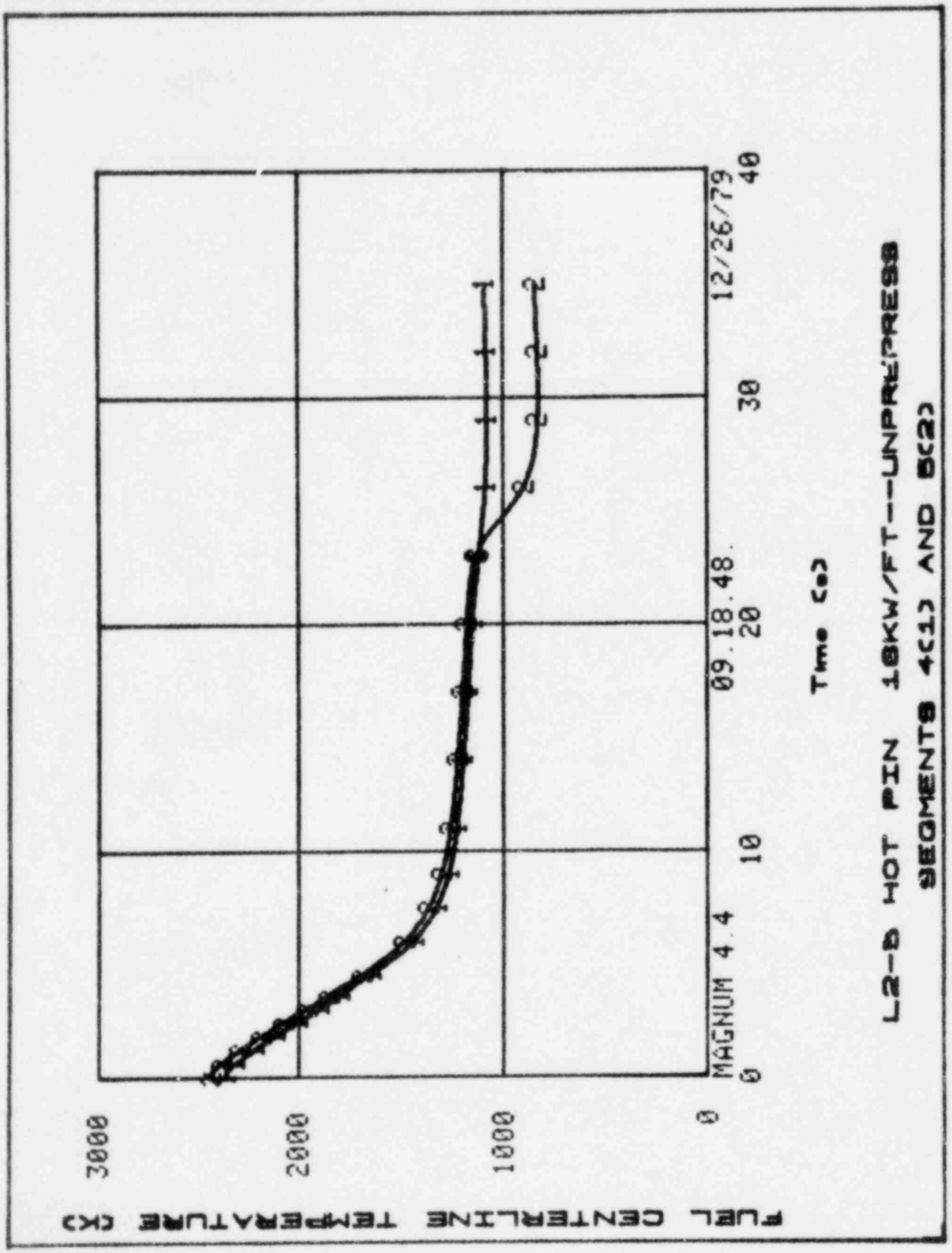

FIG. 29 Fuel centerline temperature with 52.5 kW/m initial power and unpressurized rod

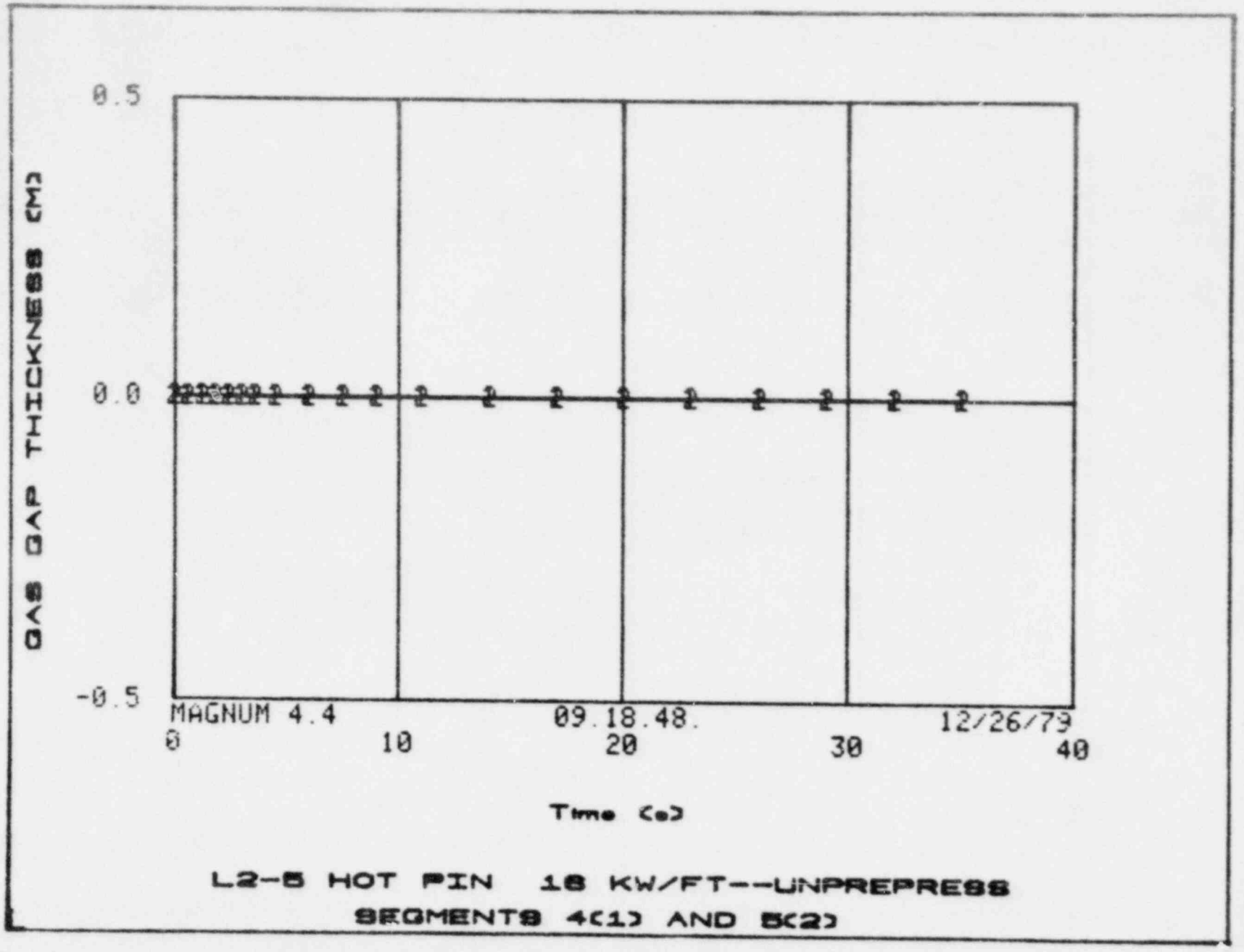

FIG. 30 Fuel-to-clad gap width (radial) with 52.5 kW/m initial power and unpressurized rod

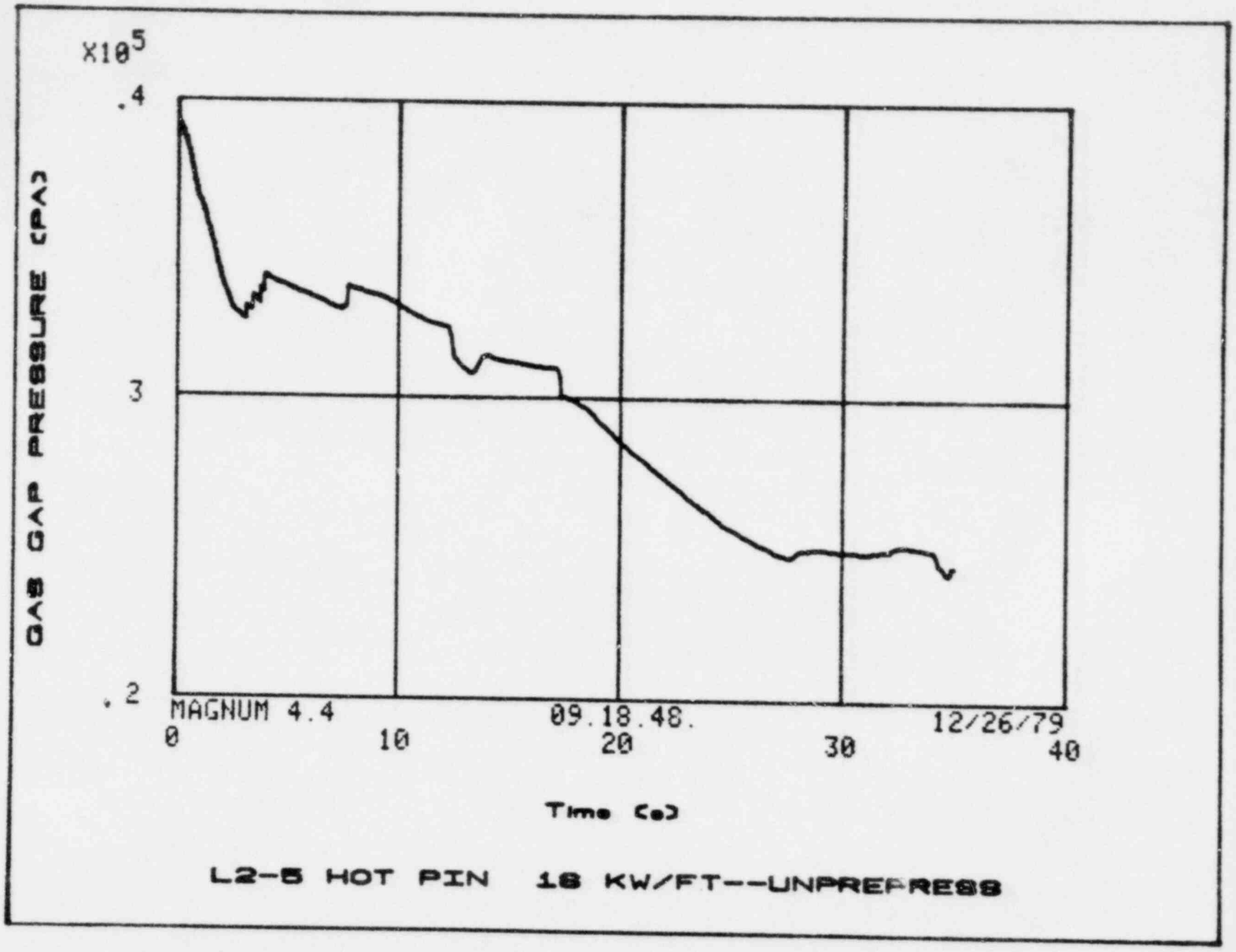

FIG. 31 Rod internal gas pressure with 52.5 kW/m initial power and unpressurized rod

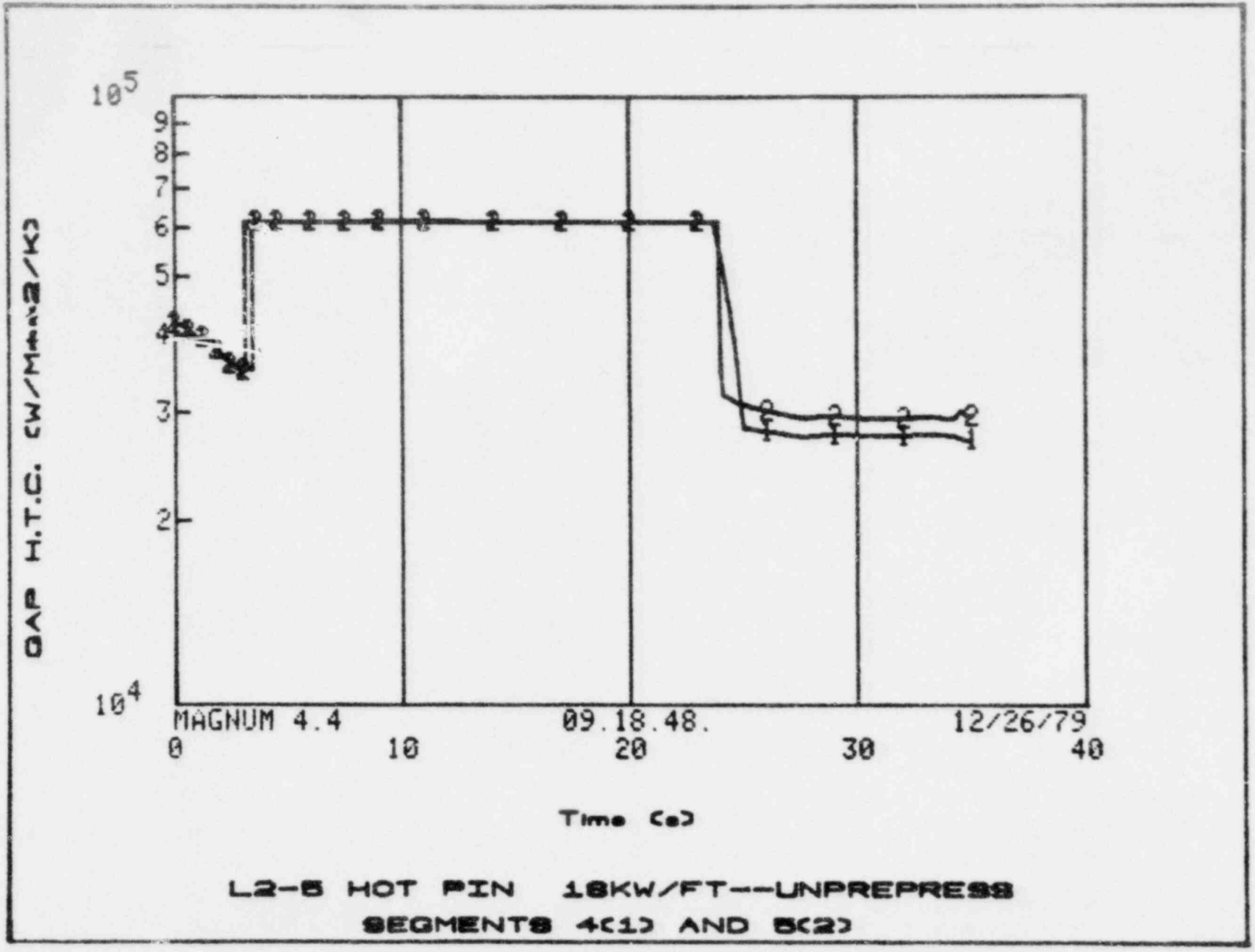

FIG. 32 Fuel-to-clad gap heat transfer coefficient with 52.5 kW/m initial power and unpressurized rod

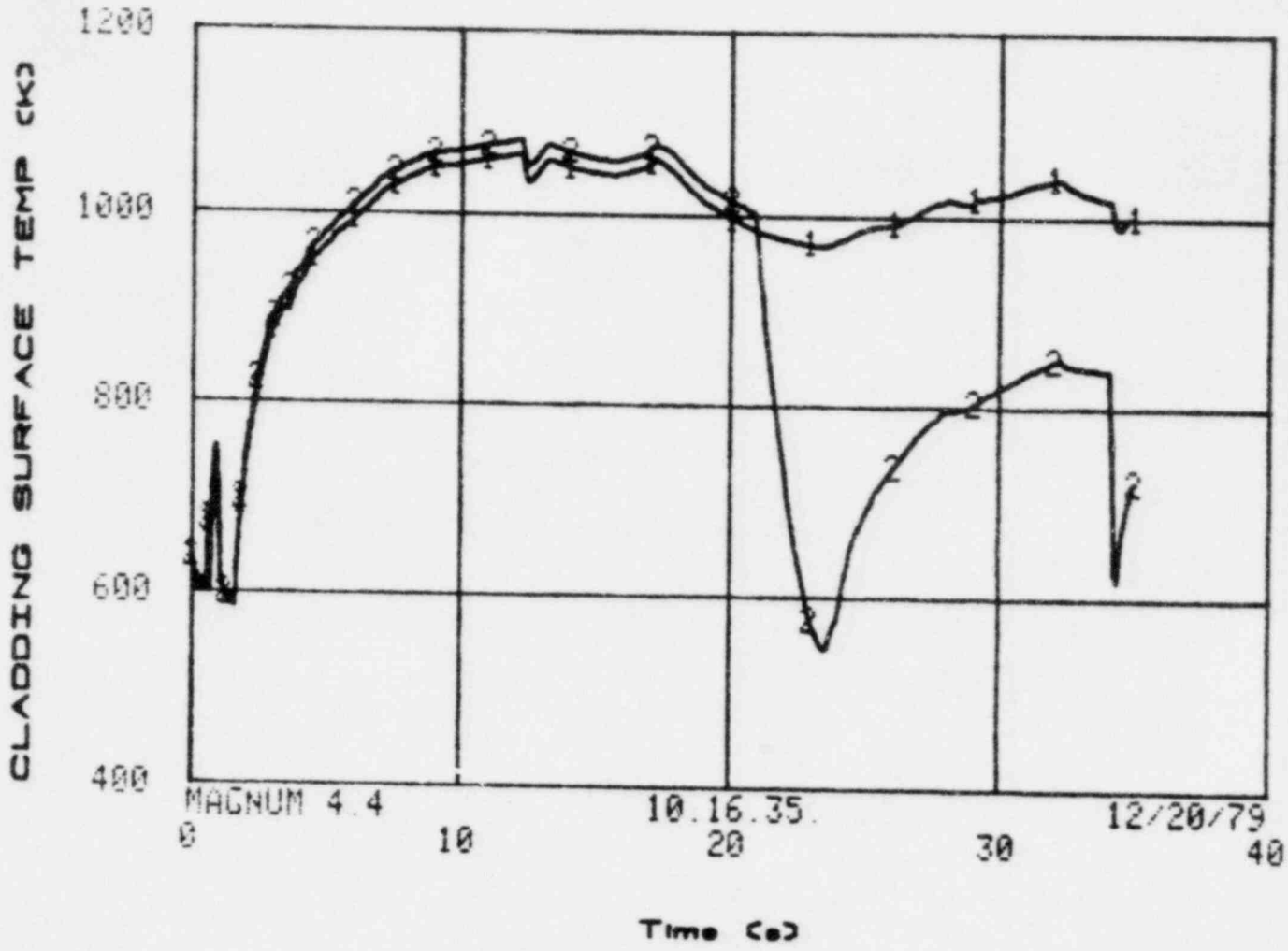

L2-5 HOT ROD 18KW/FT--2.4MPA
SEGMENTS 4(1) AND 3(2)

FIG. 33 Clad surface temperatures with 52.5 kW/m initial power and 2.4 MPa pressurization

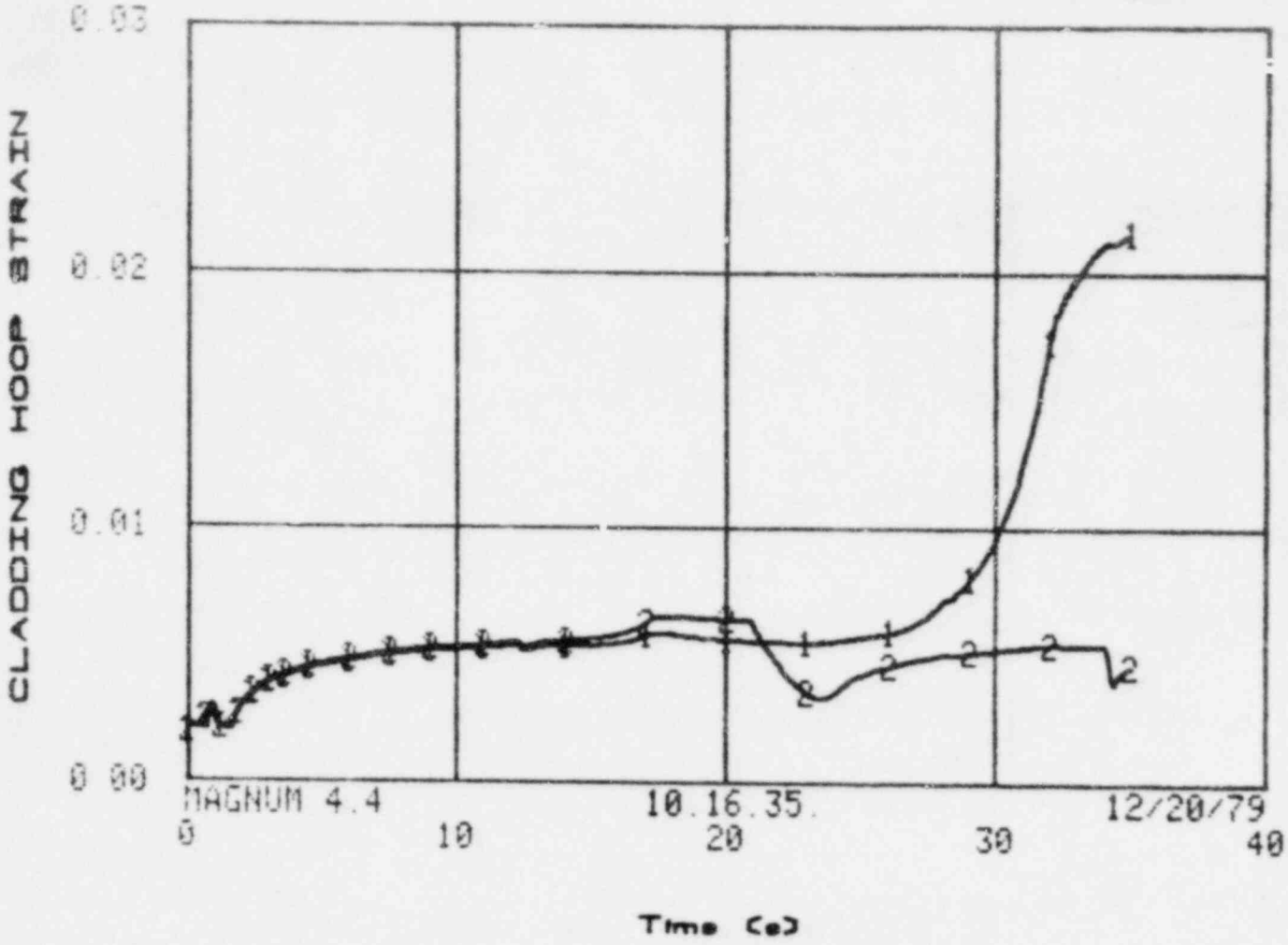

FIG. 34 Cladding average loop strain with 52.5 kW/m initial power and 2.4 MPa pressurization

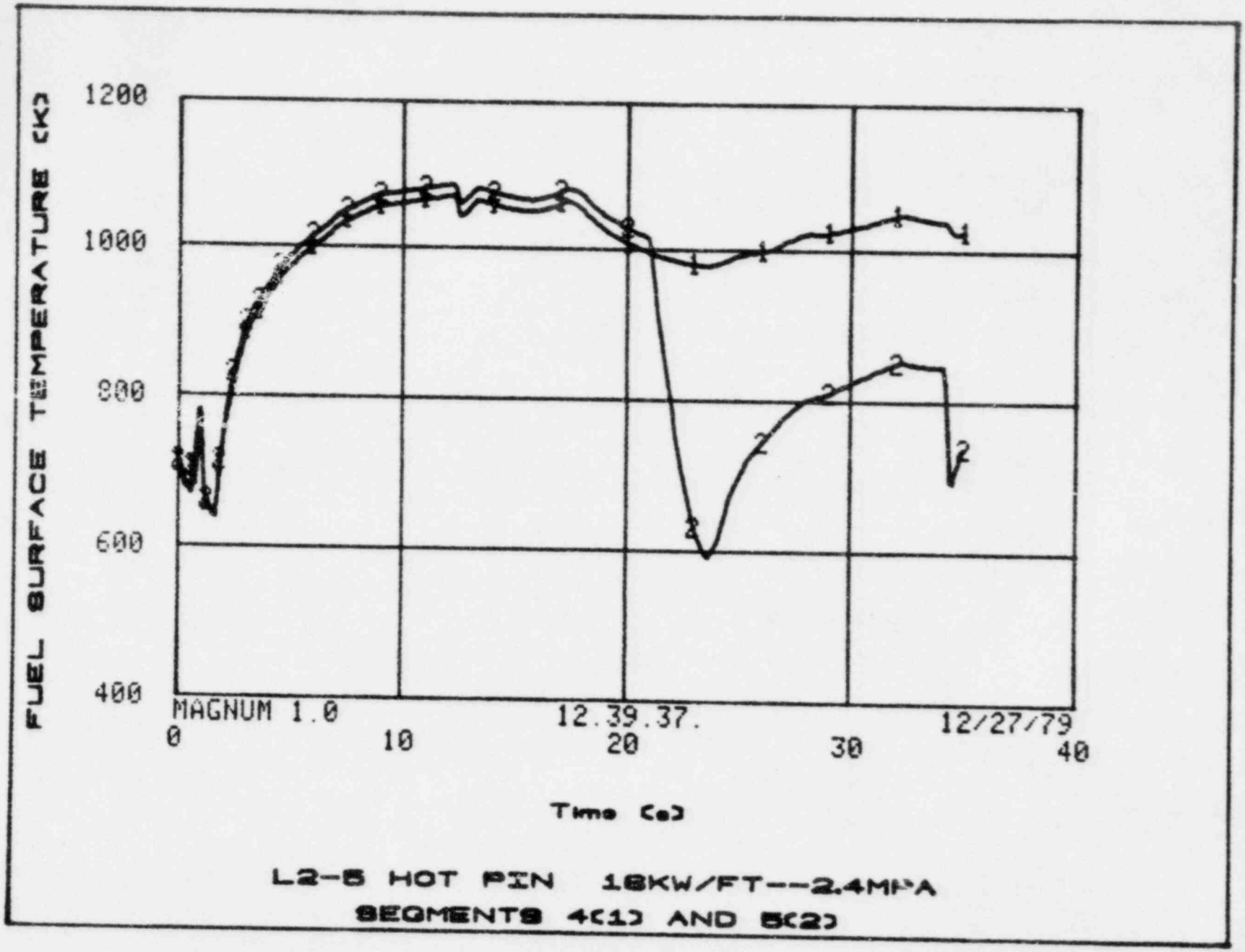

FIG. 35 Fuel surface temperature with 52.5 kW/m initial power and 2.4 MPa pressurization

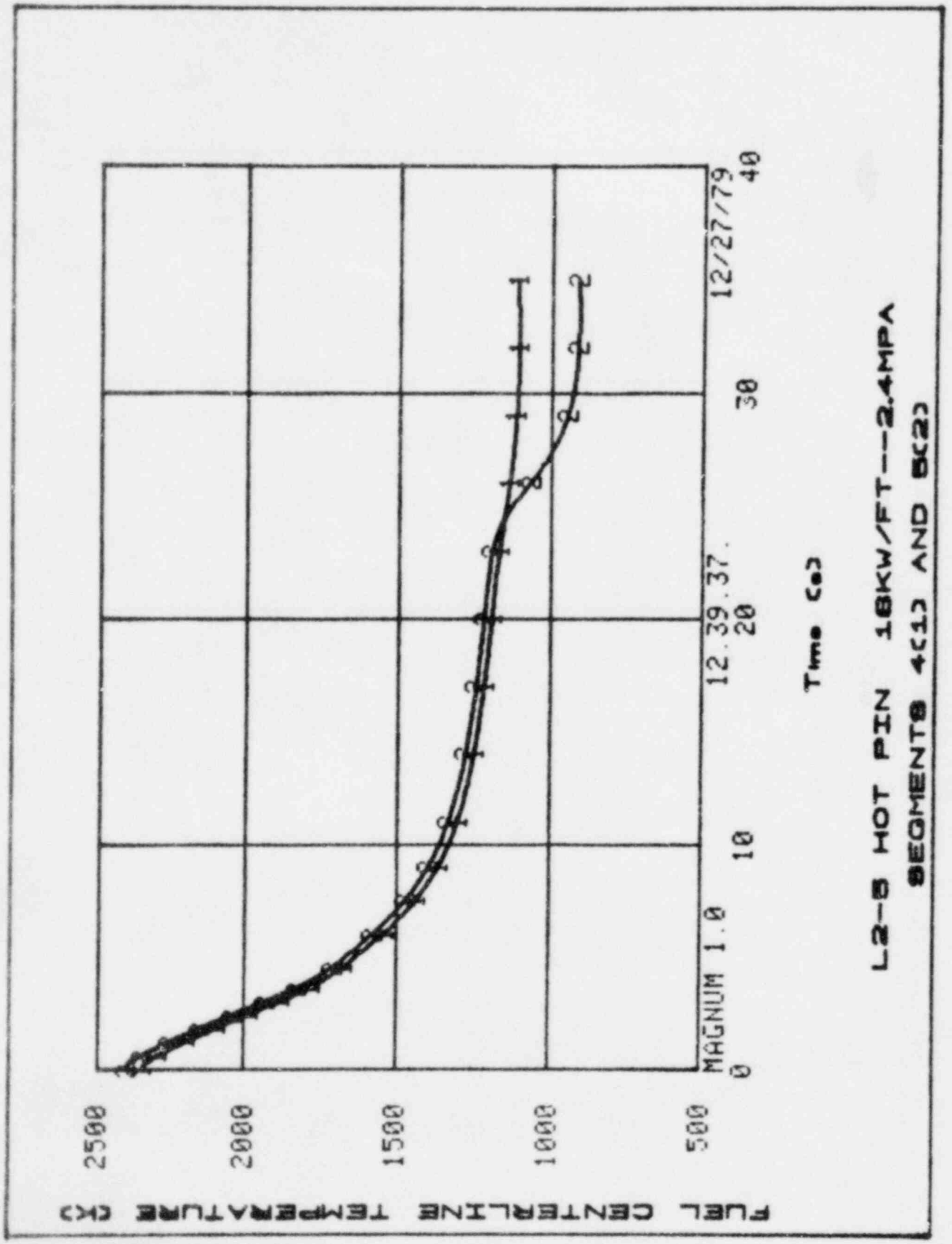

FIG. 36 Fuel centerline temperature with 52.5 kW/m initial power and 2.4 MPa pressurization

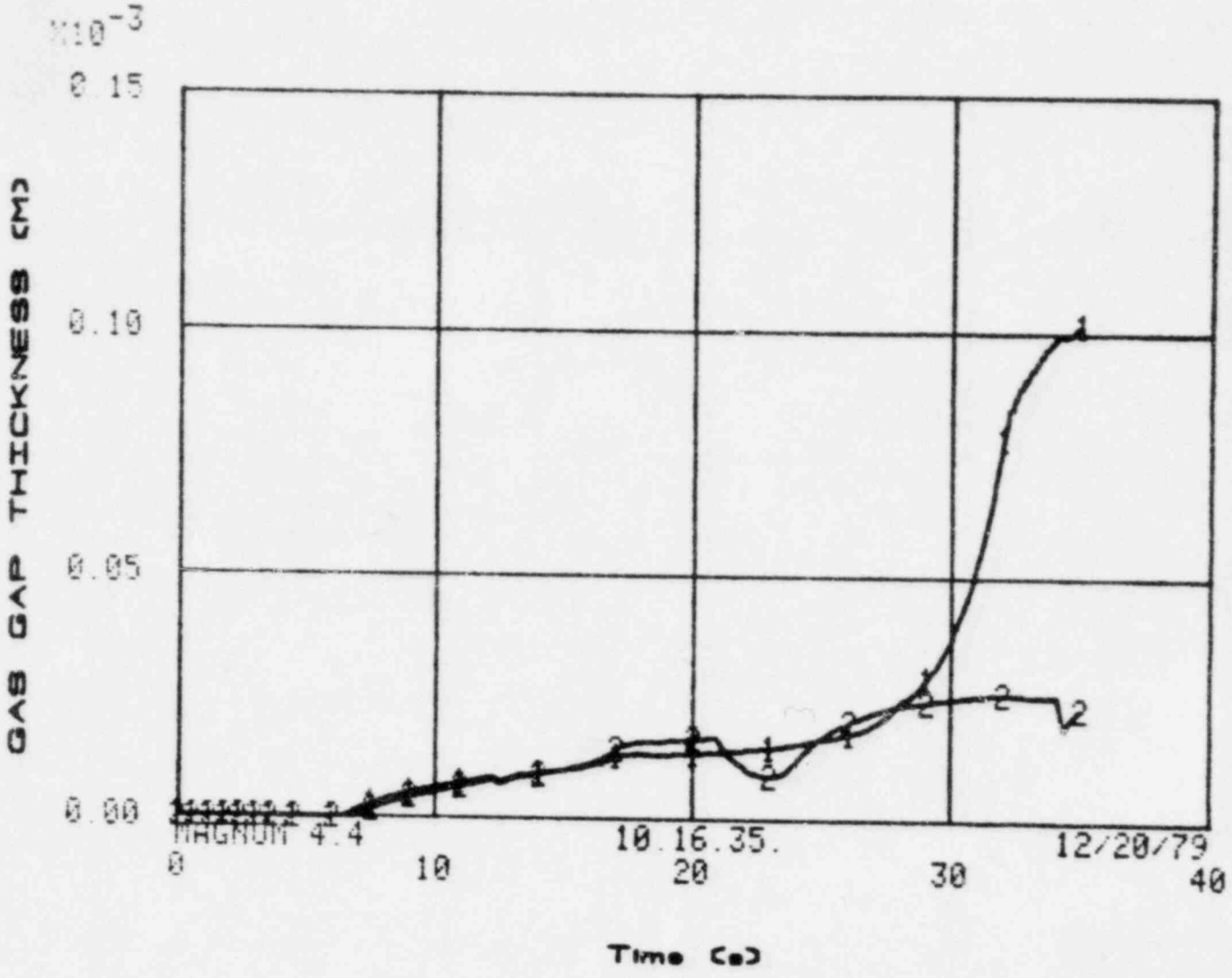

FIG. 37 Fuel-to-clad gap width (radial) with 52.5 kW/m initial power and 2.4 MPa pressurization

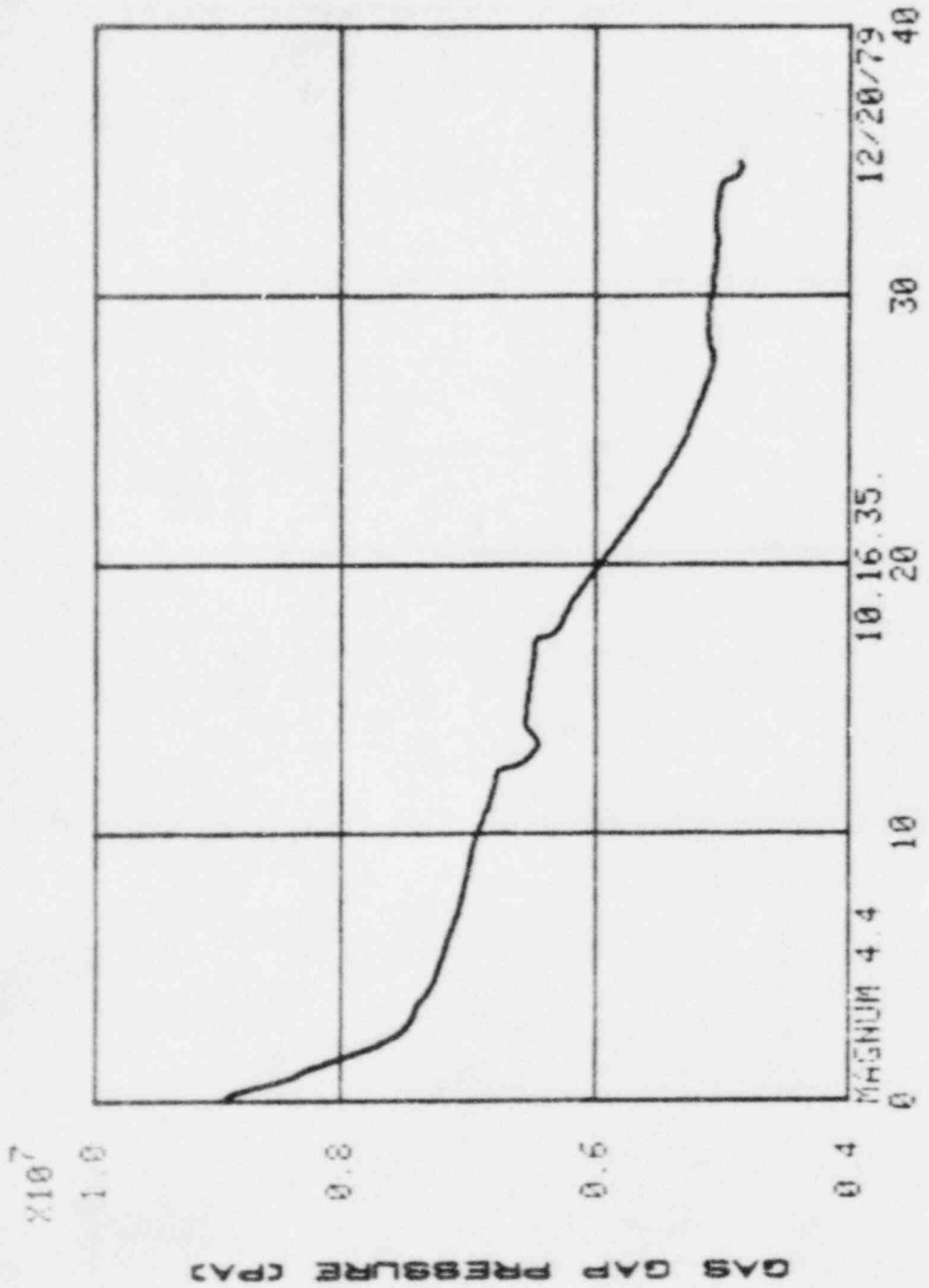

FIG. 38 Rod internal gas pressure with 52.5 kW/m initial power and 2.4 MPa pressurization

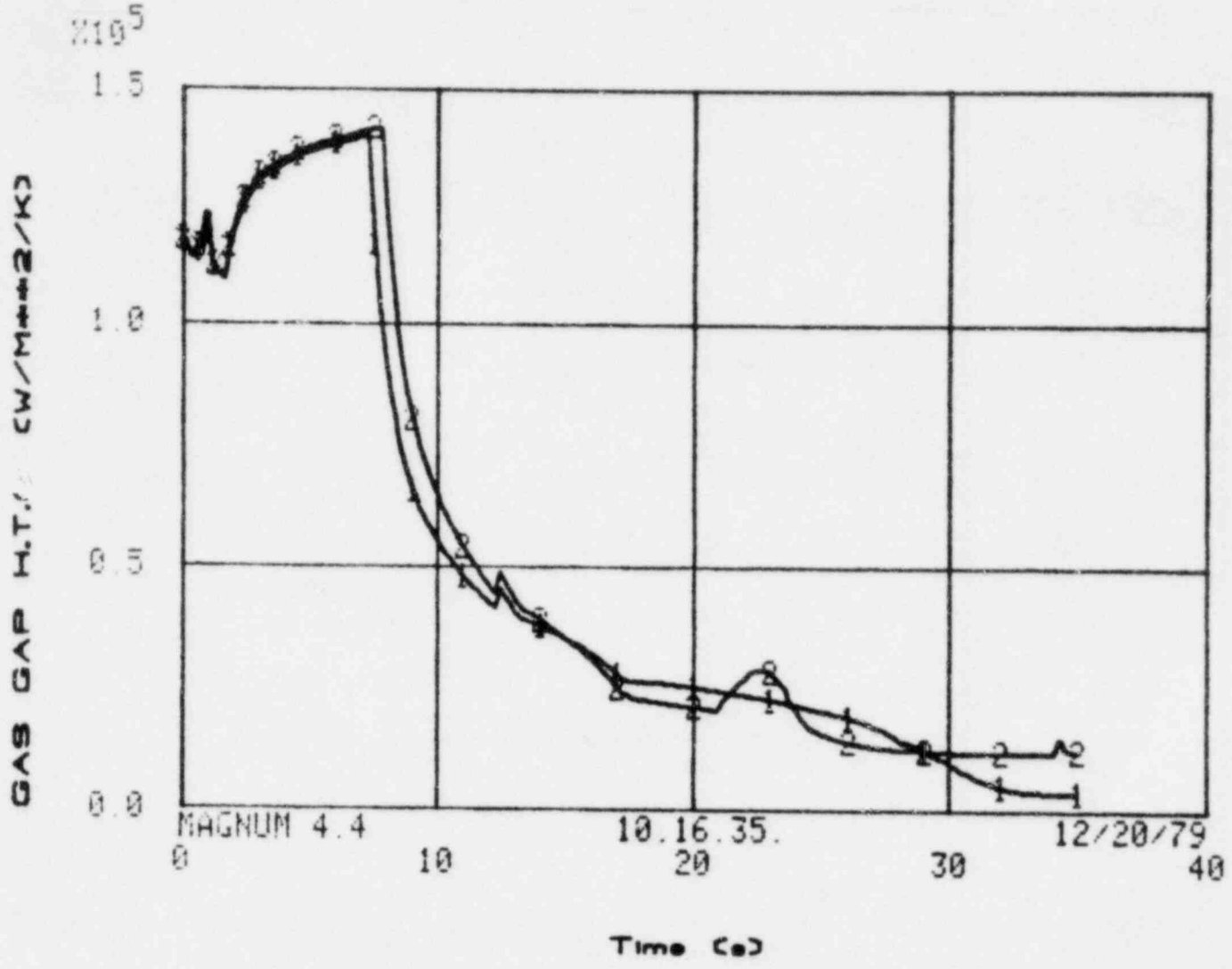

FIG. 39 Fuel-to-clad gap heat transfer coefficient with 52.5 kW/m initial power and 2.4 MPa pressurization

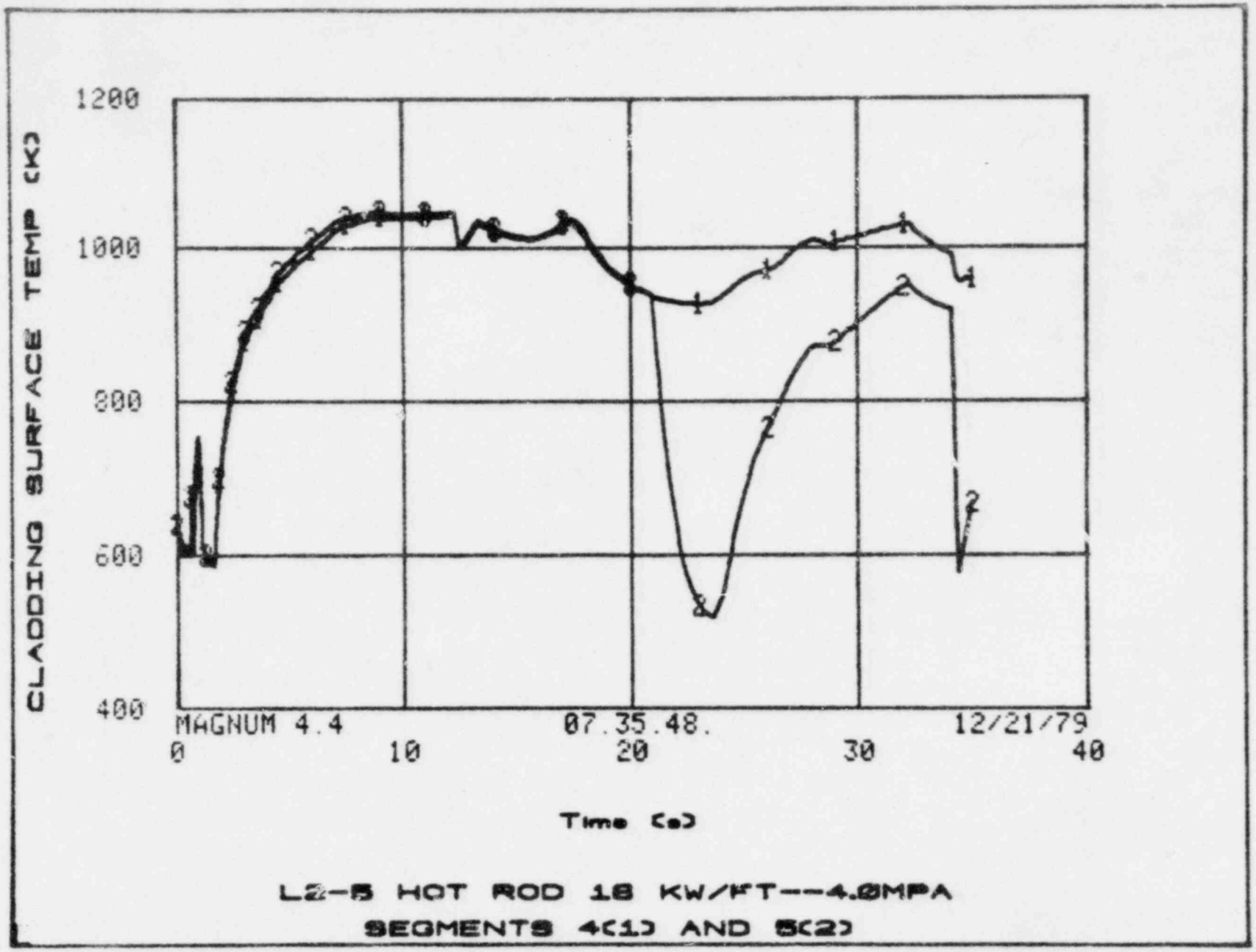

FIG. 40 Clad surface temperatures with 52.5 kW/m initial power and 4.0 MPa pressurization

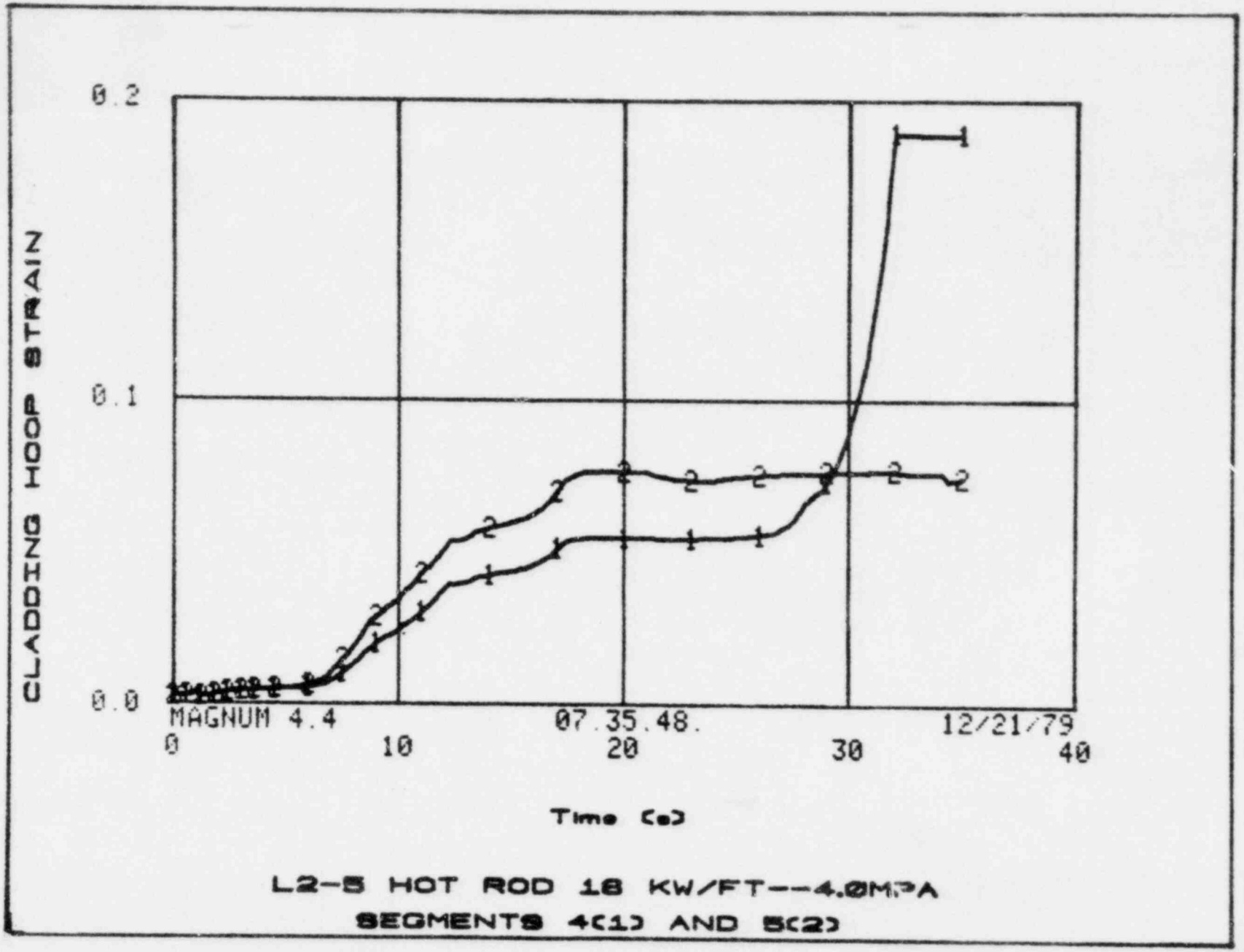

FIG. 41 Cladding avg. to loop strain with 52.5 kW/m initial power and 4.0 MPa pressurization

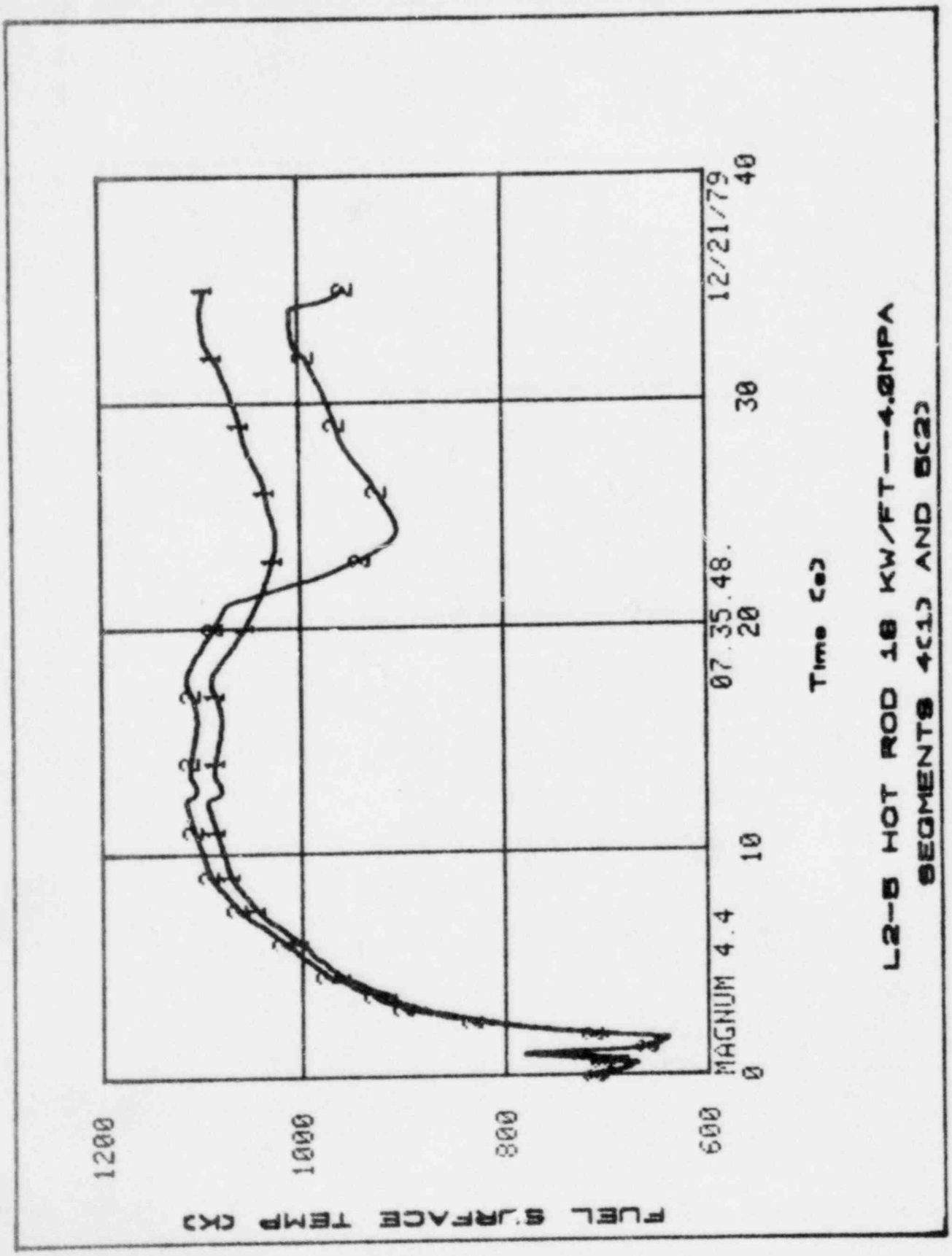

FIG. 42 Fuel surface temperature with 52.5 kW/m initial power and 4.0 MPa pressurization

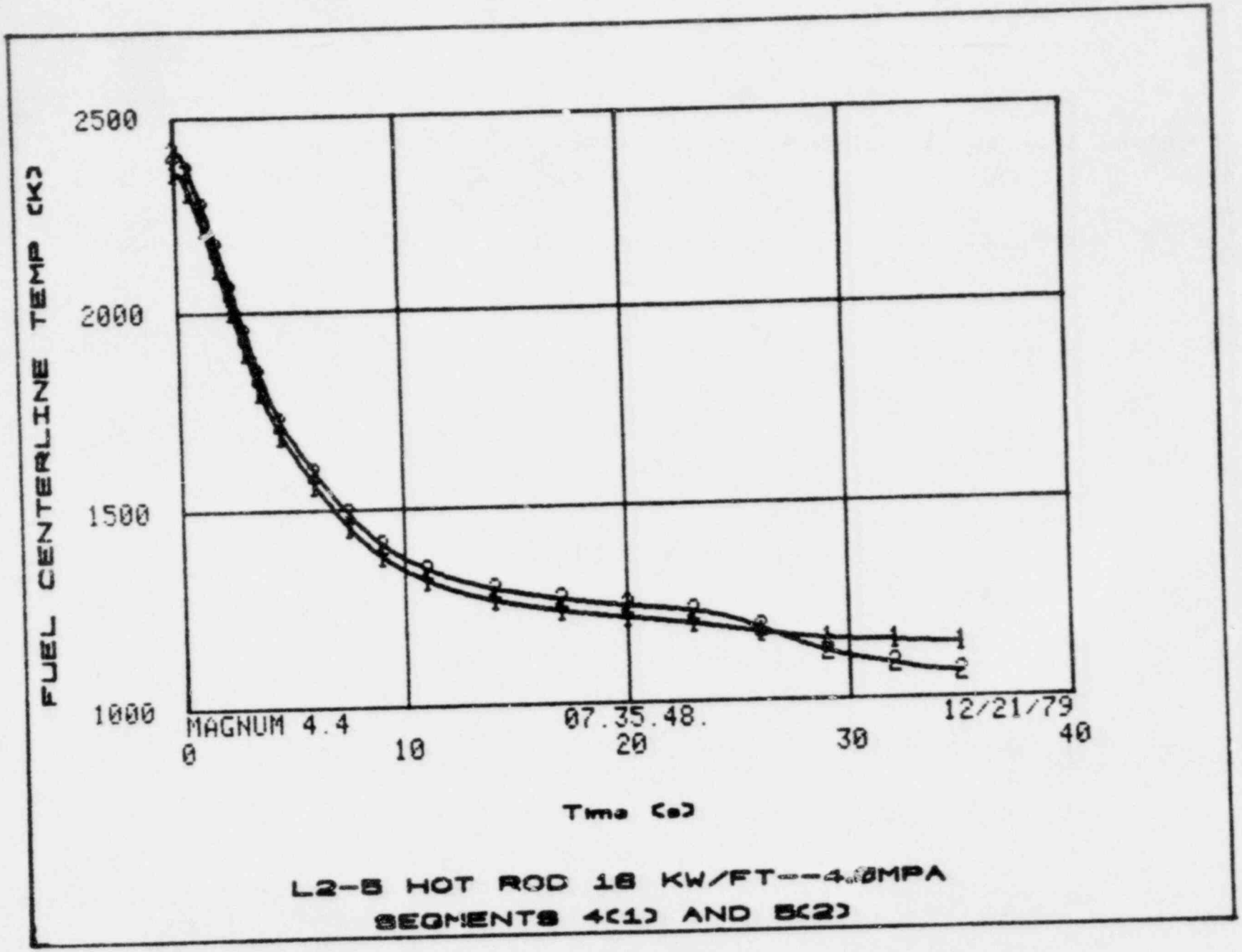

FIG. 43 Fuel centerline temperature with 52.5 kW/m initial power and 4.0 MPa pressurization

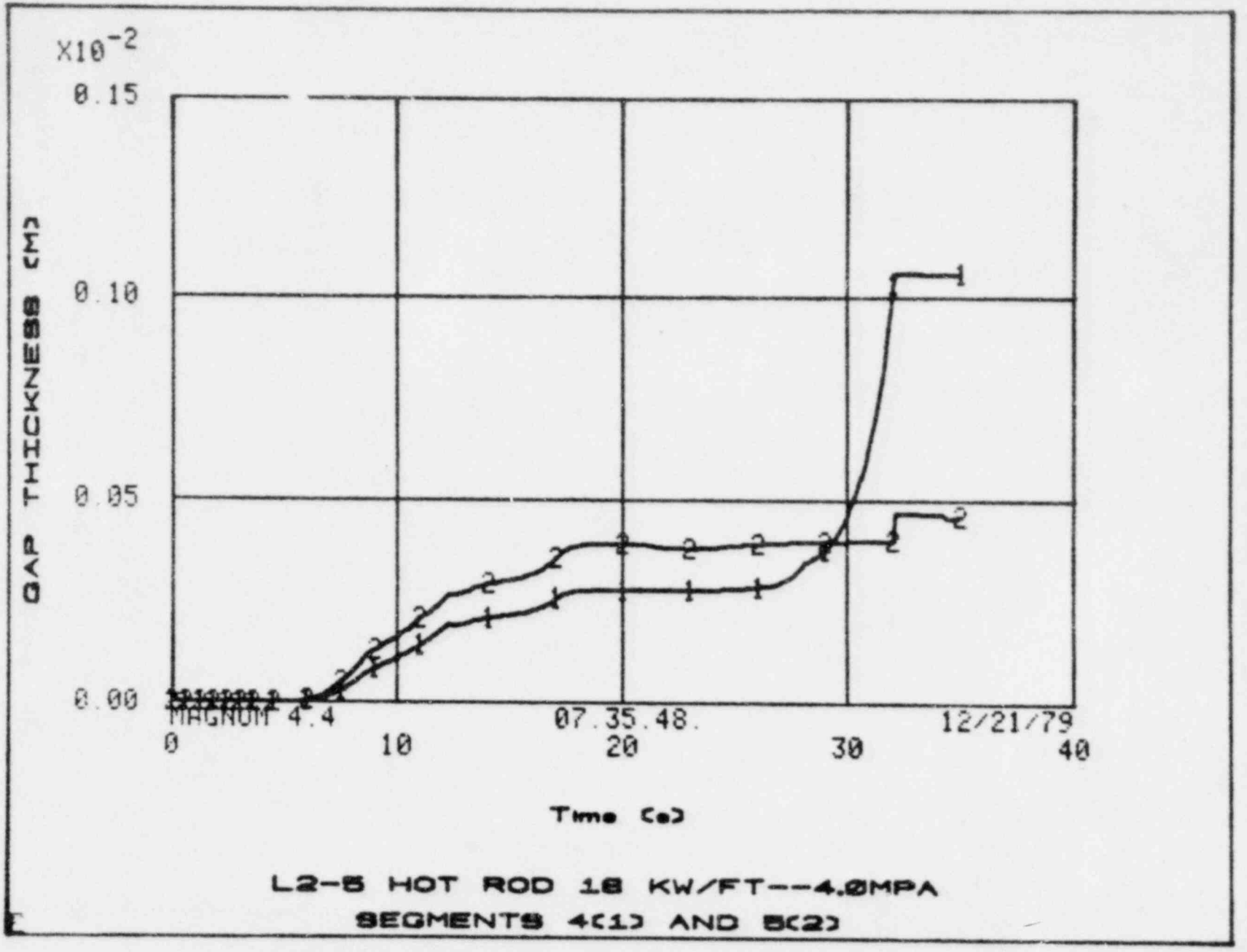

FIG. 44 Fuel-to-clad gap width (radial) with 52.5 kW/m initial power and 4.0 MPa pressurization

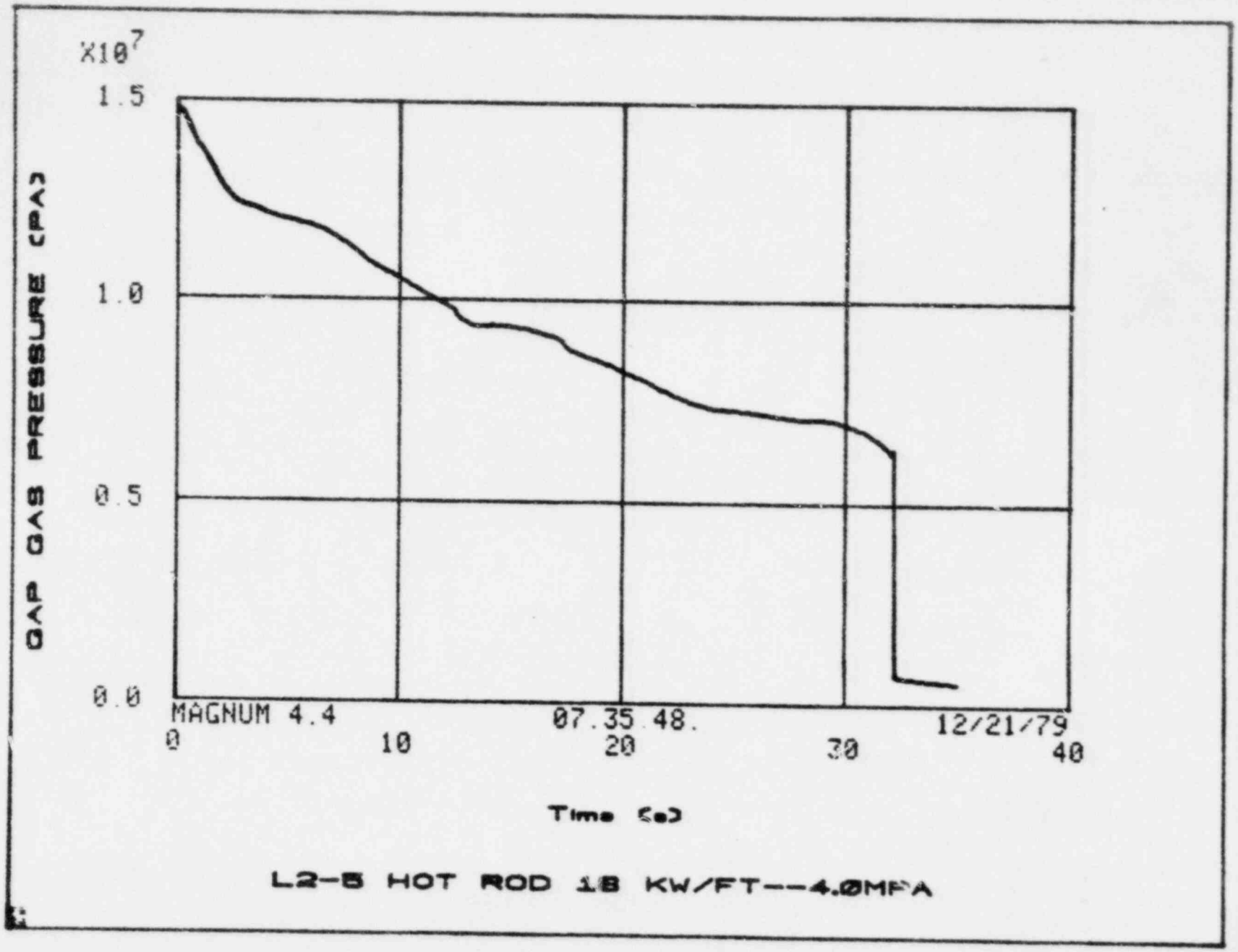

FIG. 45 Rod internal gas pressure with 52.5 kW/m initial power and 4.0 MPa pressurization

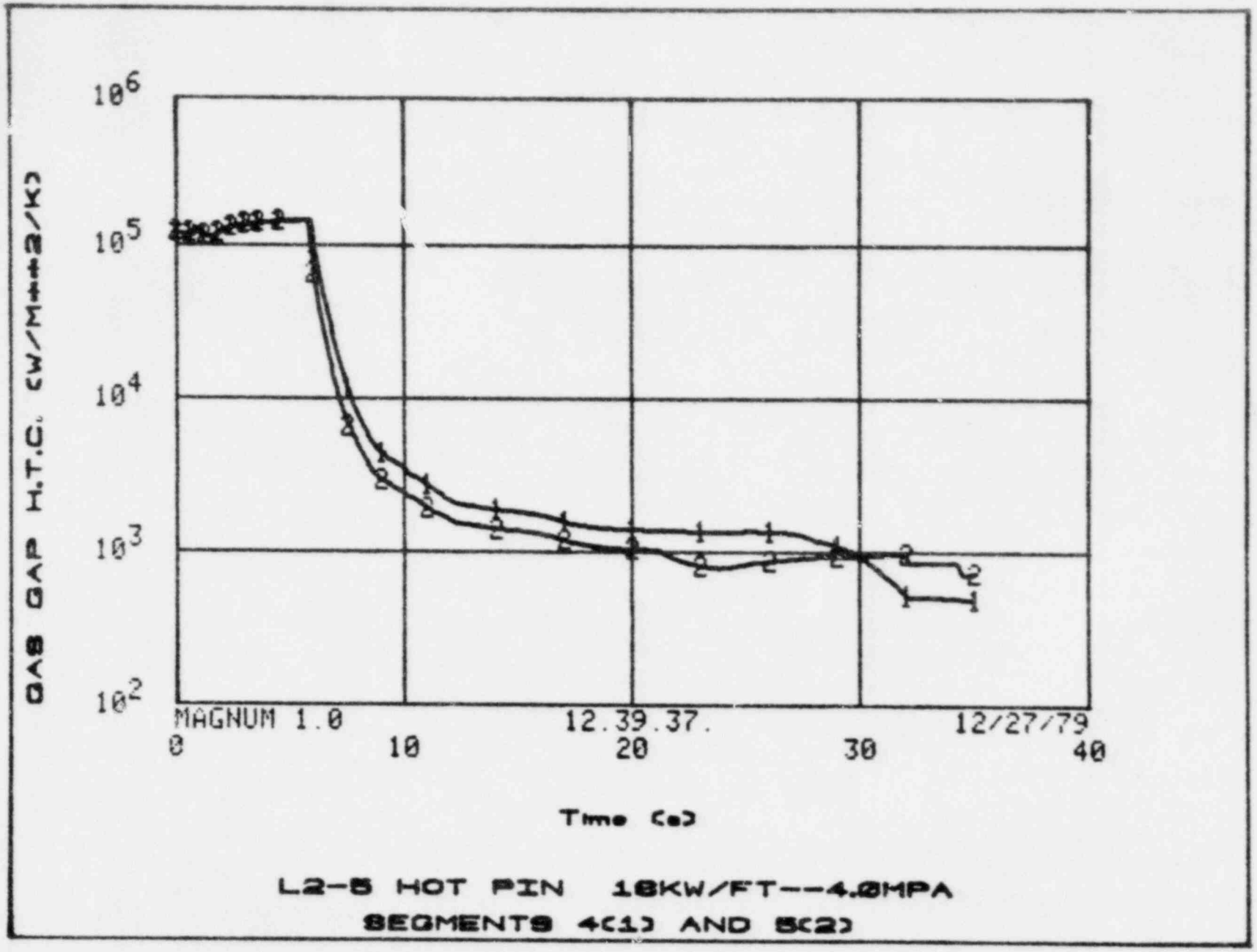

FIG. 46 Fuel-to-clad gap heat transfer coefficient with 52.5 kW/m initial power and 4.0 MPa pressurization

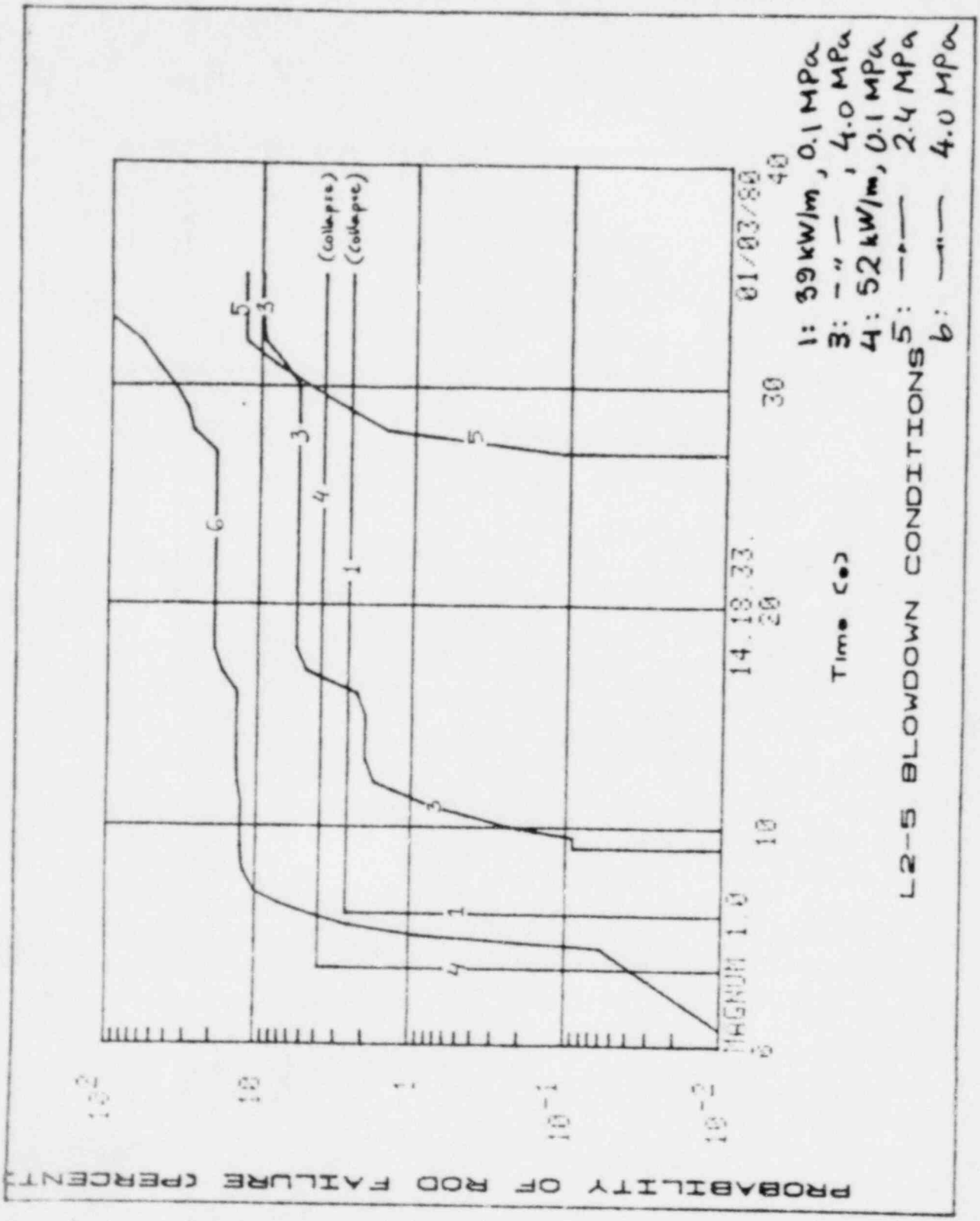

FIG. 47 Probability of rod failure

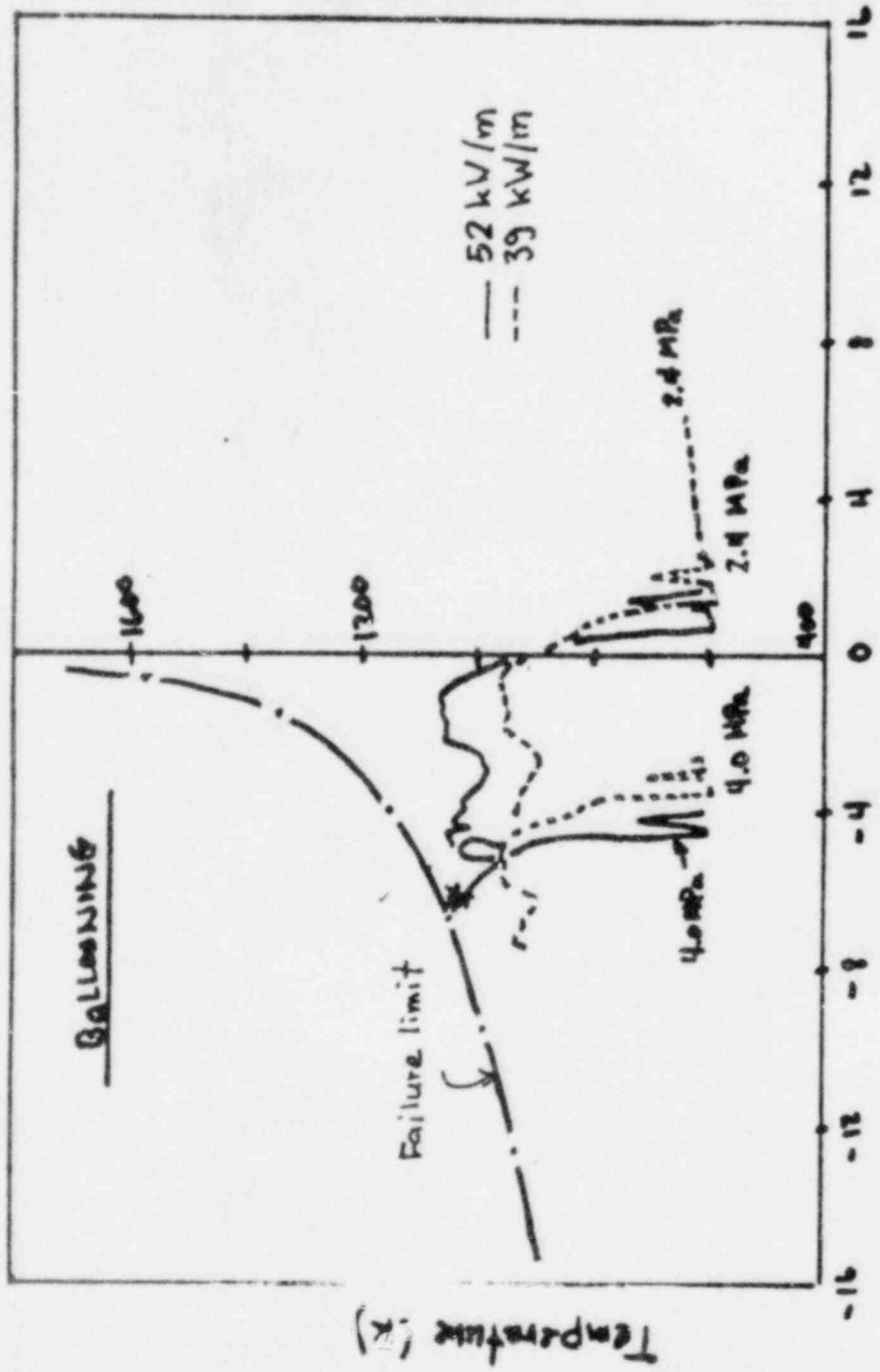

FIG. 48 Calculated response of the rod under L2-5 conditions with different assumptions